# DELFT UNIVERSITY OF TECHNOLOGY

Modelling, control and stability analysis of the COBRAcable project integrated in the Dutch transmission system: Evaluation of the performance of the controllers

Aristeidis Karaolanis

**Master of Science Thesis**

**Electrical Engineering – Electrical Sustainable Energy Track**

**Intelligent Electrical Power Grids**

Delft, September 2017

**FACULTY OF ELECTRICAL ENGINEERING, MATHEMATICS AND COMPUTER SCIENCE**

*Thesis Committee:*

| | |
|---|---|
| Prof. Ir. Mart A. M. M. Van der Meijden | TU Delft, chair |
| Dr. A. (Armando) Rodrigo Mor | TU Delft, external member |
| Dr. Ir. Jose L. Rueda Torres | TU Delft, thesis supervisor |
| Alex Alefragkis | TenneT TSO B.V, daily supervisor |
| Arcadio Perilla Guerra | TU Delft, daily supervisor |

*Excellence is an art won by training and habituation. We do not act rightly, because we have virtue or excellence, but we rather have those because we have acted rightly. We are what we repeatedly do. Excellence, then, is not an act but a habit.*
"Aristotle"

# *Acknowledgements*

I would like to express my special gratitude to Dr.ir. Jose L. Rueda Torres who gave me the opportunity to work on such an interesting and challenging topic. Exceptionally, I would like to thank Alex Alefragkis and Kees Koreman who gave me the chance to continue working at TenneT TSO B.V for my MSc thesis project. I would like to thank especially Alex for the patience he showed on technical and operational problems related to the COBRAcable project. I learnt a lot from him and I am grateful for that.

Moreover, I would like to thank Arjen A. Van der Meer, for the guidance he gave me concerning the FORTRAN modeling in PSSE and for always being a good teacher.

The project is made under the sincere guidance of Arcadio Perilla, my daily supervisor in TU Delft. I would like to thank him for his interest in the success of this thesis and all the valuable lessons that he taught me. He has been always open and committed to give me the right guidance for the success of the MSc project. I would also like to thank Professor Mart A. M. M. Van der Meijden and Dr. A. (Armando) Rodrigo Mor for being the reviewers of my thesis.

I would like to thank my parents, my brother and sister, for always believing in me. I would like to thank my friends (Anastasia, Marina, Maya, Kallirroi, Dimitris, Dimitris, Mike, Alex and Haris) for making my life a better place.

And finally, I would like to thank Nadia for her constant love and trust, whom without her nothing would be possible. I hope that I fixed you the way you fixed me!

# *Summary*

The COBRAcable project is one of the major interconnectors being constructed in the North Sea, connecting the Netherlands with Denmark. It is a 325 km submarine cable which will have the ability to transfer 700 MW. The importance of the interconnector is manifold: to facilitate the exchange of renewable energy coming from the onshore Danish power system. Since electricity demand and supply of wind energy is geographically spread an adequate transmission capacity is essential for the growth of renewable energy. The link will also provide a strong connection that will enhance the security of supply in the Northwestern European region. That is in line with the ambitions of the EU for a stronger interconnected European electricity transmission grid and it will be a backup in case of breakdowns.

Moreover, it will enhance the internal European electricity market. COBRAcable will contribute to the development of the internal European electricity market and specifically contribute to the further investigation of the Northwest European electricity market. Lastly, COBRAcable has been granted a European subsidy for researching and developing activities necessary for the connection of wind farms to the cable.

The main focus of the present thesis is to create a RMS model of the COBRA cable project in PSSE software. The starting point of the master thesis project was a basic model of a VSC station which consisted of the basic VSC converter controllers: the active power controller, the reactive power controller, the AC voltage controller and the DC voltage controller. Gradually, the active and reactive power controllers were upgraded in order to support the special functions of the COBRAcable project. Also, an equation regarding the injection of reactive current was added to implement the fault ride through capability of the converter. In the end, the responses of the final model created throughout this master thesis project were compared against the responses of the model built in Powerfactory, which was created in more detail and was already compared against the results of the EMT model in PSCAD.

The modelling framework for VSC – based HVDC transmission system was initially developed and tested in a benchmark system consisted of two areas. Both areas had three buses connected in a meshed configuration and the performance of the controllers mentioned above was evaluated there. Following the benchmark system, the modelling framework was then tested with a reduced model of the Dutch power system around the Eemshaven region.

Different tests were defined in order to evaluate the suitability of the model and in more details to evaluate the performance of the controllers. To evaluate the performance of the active power controller several cases were introduced associated with the special functions of the COBRAcable regarding the regulation of active power. The reference of the reactive power was changed and the performance of the reactive power controller was tested while using different ramping rates. Moreover, the voltage at the point of common coupling was changed in order to assess the performance of the AC voltage controller. Finally, the equations regarding the injection of reactive current were used to evaluate the fault ride through capability of the converter.

From the simulation results, it was observed that the active and reactive power controllers were able to follow the changes of the reference power quite stably regardless the different ramping rates that were used. The reference changes created a dynamic behavior regarding the performance of the AC voltages of the

buses in the Dutch power system. The investigation regarding the AC voltage controller led to the conclusion that there is a limit on how much you can increase and decrease the voltage at the PCC. The equations associated with the fault ride through capability have shown that the converter is actually trying to inject reactive power when the voltage has dropped below certain levels. In the end, the creation of a user – written model of the COBRA cable project in PSSE added an increased level of complexity. The absence of block diagrams with their respective signals as well as the required knowledge of the software made the translation of the control structure of the VSC station from the Powerfactory model difficult.

# Table of Contents

# List of Acronyms

| | |
|---|---|
| AC | Alternative current |
| DC | Direct current |
| FRT | Fault ride through |
| GSVSC | Grid side voltage source converter |
| GTO | Gate turn off thyristor |
| HVDC | High voltage direct current |
| IGBT | Insulated gate bipolar transistor |
| PCC | Point of common coupling |
| PI | Proportional integral controller |
| PLL | Phase locked loop |
| PWM | Pulse width modulations |
| TSO | Transmission system operator |
| VSC | Voltage source converter |
| RMS | Root mean square |
| EMT | Electromagnetic transients |

# List of Figures

# List of Tables

# Chapter 1: Introduction

## 1.1 Motivation

The COBRAcable is a joint project of TenneT and Energinet. The interconnector will provide an electricity connection between Endrup (Denmark) and Eemshaven (The Netherlands). It consists of a 325 km long subsea cable with a projected capacity of 700 MW and creates the first direct link to Denmark (Figure 1). The purpose of this project is to allow the transportation of more renewable energy into the European power grid through the Dutch and Danish system and also to increase the competition of the northwest European electricity markets.
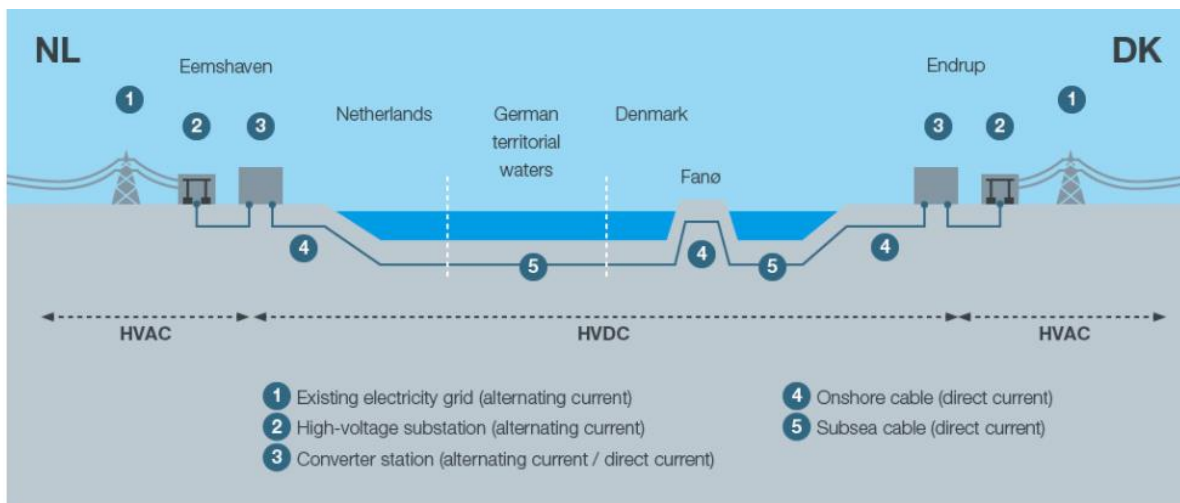


*Figure 1 - COBRA cable project[1]*

The COBRAcable consists of a 320 kV HVDC MIND/XLPE cable with two converter stations of 700 MW. Both converter station will be using HVDC plus voltage source converters with a multi – modular converter arrangement which will converter the AC to DC and vice versa. In comparison with the line – commutated technology (LCC), the HVDC plus system operates with IGBT, thus the commutation processes in the power converter run independently of the grid voltage. The fast control and protective capabilities of the converters provide stability in the transmission system, which help to reduce the grid faults and disturbances in the three – phase AC network.

The key objectives of COBRAcable are [1]:

1.  To facilitate the transport of renewable energy. The generation and demand of energy is volatile.

---

[1] https://www.tennet.eu/our-grid/international-connections/cobracable/

Therefore, the need for adequate transfer capacity is essential. Moreover, the connection of offshore wind farms in the COBRAcable is also foreseen.

2. The creation of a bigger, stronger, interconnect European electricity grid.
3. Enhancing the security of supply in the Northwest European electricity market which will create an alternative connection in case of breakdowns and will be a balancing tool for the volatile renewable energy.
4. To boost the playing field of the European electricity market. The COBRAcable project will connect the northwest European electricity market and further develop the internal European electricity market.

The benefits of COBRAcable will contribute to the improvement of the European electricity market with an increased efficiency of the available generation capacity and socioeconomic welfare, as well as achieving the objectives of the EU climate and sustainability policy, while ensuring security of supply and technical resilience of the system. The following specific benefits, can be identified [1]:

➢ The congestion revenues comprise the revenues directly generated by allocation of the transfer capacity of COBRAcable to market participants, either directly through an explicit auction or indirectly by applying market coupling through power exchanges.
➢ Increases the socioeconomic welfare by providing adequate transfer capacity so that the electricity markets can trade power in a more economically efficient manner, thus increasing the total surplus in the connected countries.
➢ Increase security of supply and help the system provide and/or safeguard an adequate and secure supply of electricity under ordinary conditions.
➢ Supports the integration of renewable energy resources by allowing the connection of new renewable energy and unlocks the existing and future green generation thus minimizing curtailments.
➢ Reduces the $CO_2$ emissions by increasing dispatch of generation with lower carbon content.
➢ Resilience and safety of the equipment and the system so that it can withstand increasingly extreme system conditions.
➢ Offers flexibility in order to be used in different future development paths or scenarios, including trading or balancing services.

## 1.2 Research objectives

The focus of this master thesis project is to obtain a RMS model of the COBRAcable project in PSSE. The features of the COBRAcable project will be tested in order to check the accuracy of the features designed in PSSE with the real operational needs of the project. The model created in PSSE will be compared against the model created in PowerFactory with the same aggregated network that represents the Eemshaven region and with the same generic CIGRE model for the control schemes of the VSC stations. Moreover, the extra features that are included in the COBRAcable project will be also compared to ensure that the results obtained are close to reality. Since accuracy refers to the closeness of a measured value to a standard or known value, it is important to see whether the results of the PSSE model are close enough with the ones obtained from the PowerFactory model.

## 1.3 Research approach

The research procedure was initiated in January 2017 with the literature review about the VSC – HVDC technology and the control structure of VSC stations. Simultaneously, a learning procedure had been started in order to get familiar with the modelling capabilities and also with the graphical interface of Siemens PTI PSSE package, the simulation tool that was used throughout this project.

The next step was to get acquainted in a better way with the modelling procedure in PSSE and how it was possible to create a user written model of a VSC – HVDC station. For that reason, an existing model of a VSC – HVDC station written in FORTRAN was used as the reference for research, which have been previously developed within a master thesis project at TU Delft in [2]. These models have been further upgraded to the real needs of the COBRAcable project with all the extra functions.

Special features regarding the active power regulation have been modelled in order to simulate the actual regulation of the active power once the link will be in operation. A reactive power controller which offer the ability to ramp the reactive power based on the needs of the system is also introduced in this project. Last but not least, a fault ride through capability is being offered in this project in order to see how the VSC station provides reactive current in order to boost the AC voltage of the system that it is connected to.

In order to proceed into the final stage, the models will be compared iteratively once they are completed. For that reason a comparison process will take place by implementing the models into the aggregated Dutch system representing the Eemshaven region. The comparison process will be performed by the author of this master thesis project and the PhD candidate Arcadio Perilla who is also an active member of the COBRAcable project. To compare, two different software were used: PSSE and PowerFactory. A test matrix was created in order to ensure that the operation of the controllers is correct and represent the real operation of the controllers of the COBRA cable project.

## 1.4 Expected results

The ultimate goal of this master thesis project is to create the COBRAcable project into PSSE software and investigate the effects of the link once the interconnector is in operation. For this to become a reality, a working model of the HVDC link will be created in PSSE software and a special focus will be given for the extra features of the control structure of the station so that the model will be able to represent the reality of the system.

Once the model has been established, a test matrix, to evaluate the performance of the controllers will be used. The test matrix will reveal valuable information regarding the performance of the active power controller, reactive power controller, AC voltage controller and also the fault ride through capability, referring to the capability of the converter to support the AC voltage by injecting reactive power during faults. The results will demonstrate the behavior of the controllers and also the reaction of the Dutch system while performing the contingencies described in the test matrix.

Lastly, the comparison process will reveal the accuracy of the two models. Keeping in mind the assumptions made for both models, the results will provide a better insight on the differences between the two models.

## 1.5 Thesis contribution

The contribution of the present thesis is to create a dynamic model of the COBRAcable project into PSSE software that could be used in the future for stability analysis problems regarding the issues that the interconnector could create when it will be in operation. In more specifics, the thesis shows the performance of the controllers while being subjected to active power regulation, reactive power regulation, AC voltage performance and fault ride through capabilities. Also, the current model could be used a starting point for the creation of extensions of the control structure of the VSC station.

The present thesis could also be of use for studies regarding the implementation of user – written models in PSSE. For that reason, a detailed guide of how the current project was executed using the necessary software will be given in the Appendix B. The guide will help the reader to get familiar with the software and also give an insight of the difficulties of creating a model.

## 1.6 Thesis outline

The report is organized in 6 chapters. Chapter 2 gives an overview regarding the HVDC technology up to date. Chapter 3 introduces the models that were created in FORTAN and their interaction with each other. Moreover, a detailed analysis of the controllers used in the project is given. Also, a short overview of the steps followed for the implementation and the execution of the simulations is given. Chapter 4 describes the system and the case studies that were investigated in the project. Chapter 5 evaluates the performance of the controllers using two different software. Final conclusions are drawn in Chapter 6.

# Chapter 2: High Voltage Direct Current Transmission

## 2.1 Introduction

The use of power electronics in the HVDC technology facilitates an efficient and flexible method to transmit a vast amount of power over long distances either with overhead lines or underground/submarine cables. It offers also the possibility to connect two different systems, when the AC connection cannot be used. Until recently, the HVDC technology was based on thyristors called classic HVDC or traditional HVDC and was used to convert the AC to DC and vice versa.

However, new implementations into power electronics helped create a new type of HVDC. It uses a more advanced semiconductor technology instead of thyristors. The semiconductors are Insulated Gate Bipolar Transistors (IGBTs), the converters are called Voltage Source Converters (VSC) and they operate in high switching frequencies (1-2 kHz) using pulse width modulation (PWM). The VSC – based HVDC technology has several advantages over the classic HVDC transmission, such as independent control of active and reactive power and reverse the power flow without changing the polarity of the DC voltage.

## 2.2 Converter arrangements

The bridges and the cables of the HVDC converter can be arranged into different configurations for effective utilization. The bridges can be either monopolar or bipolar as shown in Figure 2 and described below:
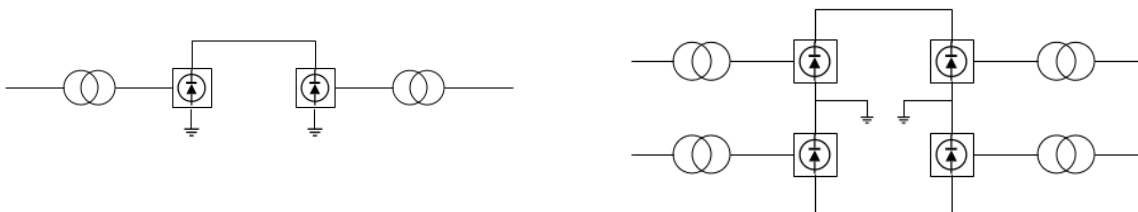


*Figure 2 – Monopolar (a) and bipolar (b) connection of HVDC bridges*

1. Monopolar HVDC system

In this configuration, two converters are used which are represented by a single pole line and a positive or negative DC voltage is used. In Figure 2(a), one transmission conductor exists and the ground is used as the return path for the current.

2. Bipolar HVDC system

It is the most common configuration used in a HVDC power transmission system. In Figure 2(b), the bipolar circuit link has two conductors that are used as plus and minus poles. If the neutral is grounded, then the two poles can be used independently. This increases the transfer capacity. In normal operation the currents flowing through each conductor are equal and there in no ground current. However, in case of a fault one the two poles can continue transmitting while the other is blocked thus increasing the reliability of the system.

The selection of the configuration of the HVDC systems depends on the function and the location of the converter stations. Several schemes and configuration for the systems exist and are shortly described below [3]:
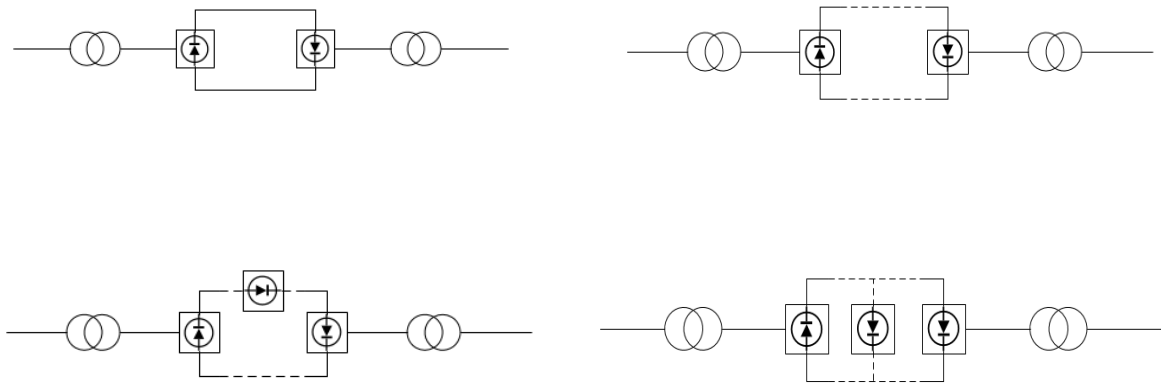


*Figure 3 - Arrangements of HVDC systems. (a) Back – to – Back HVDC system, (b) Two terminal HVDC system, (c) Series multi – terminal HVDC system and (d) Parallel multi – terminal HVDC system*

1. Back – to – back HVDC system

In this cases the converter stations are located in the same area but no line or cable is required to connect the converter bridges. The connection could be either monopolar or bipolar. A block diagram of a back – to – back system is shown in Figure 3(a). The two AC systems that are interconnected may have the same or different nominal frequency.

2. Transmission between two substations

This configuration is used when there are economic incentives to transmit electric power through a DC transmission from on location to another, as seen in Figure 3(b). Power is being transferred from one terminal called a rectifier to the other terminal operating as an inverter. This is the most typical configuration of HVDC transmission systems.

3. Multi – terminal HVDC transmission system

The use of three or more HVDC substations connected with transmission lines or cables then the HVDC transmission system is called multi – terminal as shown in Figure 3(c) (d). Multi – terminal DC systems are more difficult to justify economically due to the cost of the additional substations.

## 2.3 Classic HVDC transmission

### 2.3.1 Configuration of classic HVDC systems

A classic HVDC system, shown in Figure 4, consists of AC filters, shunt capacitor banks or other reactive – compensation equipment, converter transformers, converters, DC reactors, DC filters and DC lines or cables [4].
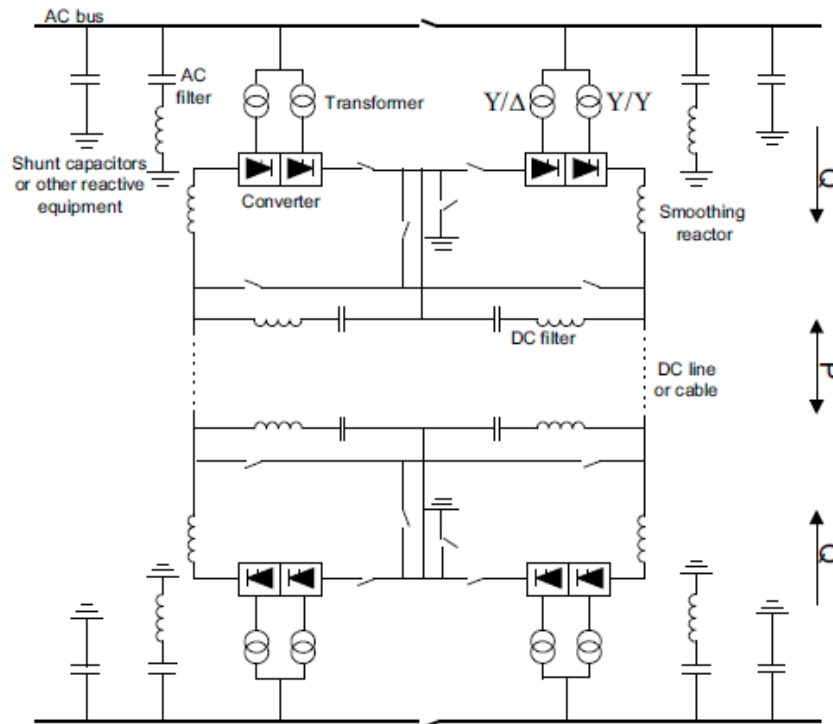


*Figure 4 - Configuration of a classic HVDC system [7]*

The valve type in the classic HVDC converter is the thyristor. Thyristors are able to conduct high currents and can block high voltages [5]. In the classic HVDC, a 6 – pulse bridge is the basic converter unit which can be used both as a rectifier or inverter. To create a 12 – pulse bridge, two 6 – pulse bridges can be connected either in parallel or in series. The bridges consist of a specific amount of thyristors connected in series. They are connected in the AC system through converter transformers in Y-Y and in Y-Δ winding configurations. By doing so, the 5th and 7th order harmonic currents through the transformers are in opposite phase which helps reduce the distortion in the AC system [6].

The converters are the most vital part of the HVDC system. Their purpose is to convert the power from AC to DC at the rectifier station and from DC to AC in the inverter station. Moreover, the converters are connected to the AC side in the point of common coupling with a converter transformer. The converters used in the classic HVDC transmission are the Current Source Converters (CSC). On the AC side, the CSC acts as a constant voltage source. It requires a capacitor as an energy storage device, large AC filters for the harmonic elimination and a reactive power supply for power factor correction. On the DC side, the CSC

acts as a constant current source. In this case, the CSC requires an inductor as its storage device and DC filters that provide appropriate fault current limiting features.


## 2.4 Design and operation of VSC HVDC


### 2.4.1 Configuration


The configuration of a VSC – HVDC system is shown in Figure 5. It consists of AC filters, transformers, converters, phase reactors, DC capacitors and DC cables. A short description about the components is given below [7]:
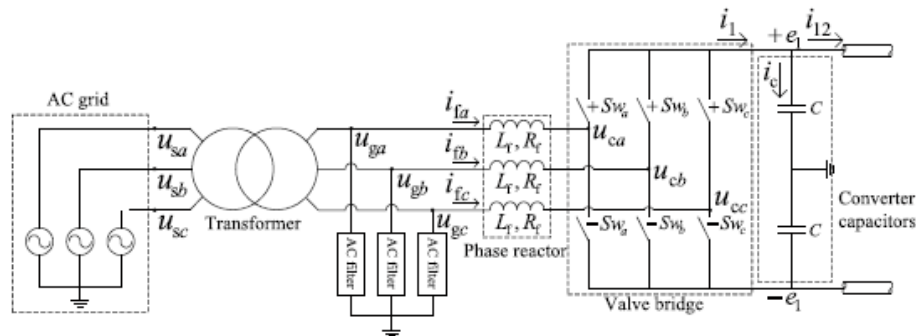


*Figure 5 - Configuration of a VSC - HVDC station [24]*

*Converters*

The converters are VSCs employing IGBT power semiconductors, one operating as a rectifier and the other one as an inverter. The converters are connected either back – to – back or through a cable depending on the application. The DC link capacitances are connected in parallel to the bridges which maintains the DC voltage level constant [8].

*Transformers*

The converters are connected to the AC system via transformers. The most important function of the transformers is to transform the voltage of the AC system to a voltage value suitable to the converter. They also provide a galvanic barrier between AC and DC sides. This is important since some faults in the AC system create overvoltages in the healthy phases.

*Phase reactors*

A phase reactor is connected in each phase. The main contributions of the phase reactor are the following: reduce the high – frequency harmonics in the AC current, provide independent control of active and reactive power by controlling the current that flows through the reactor and limit the short – circuit currents.

*AC filters*

The constant switching of the power electronics (IGBTs) induce harmonic components in the AC voltage. If these harmonics are neglected they could create problems with the AC equipment or create telecommunication disturbances. To avoid that, high – pass filter branches are installed in order to take care

of the higher order harmonics.

*DC capacitors*

On the DC side there are two capacitor stacks of the same size. The objective of the DC capacitor is primarily to provide a low inductive path for the current and an energy storage to be able to control the power flow. The capacitor also reduces the voltage ripple on the DC side. Disturbances in the system will cause DC voltage variations. The ability to limit these voltage variations depend on the size of the DC capacitors.

## 2.5 VSC modelling

The representation of a VSC model can be performed either in detail or by using an average model. If chosen to create a detailed model, then the semiconductor components present in the VSC station must be included as a single unit and be represented in the model. Using a detailed model is significant to study lower level control of the VSC station such as PWM switching and sub modules arm voltage control. The drawback using a detailed model compared to an average model is simulation time, thus an average model has been used throughout this master thesis project. Moreover, in an average model, a controllable AC voltage source is connected to the AC side and a controllable current source is connected to the DC side [9]. The AC and DC side representation can be shown by using Figure 6 [10].
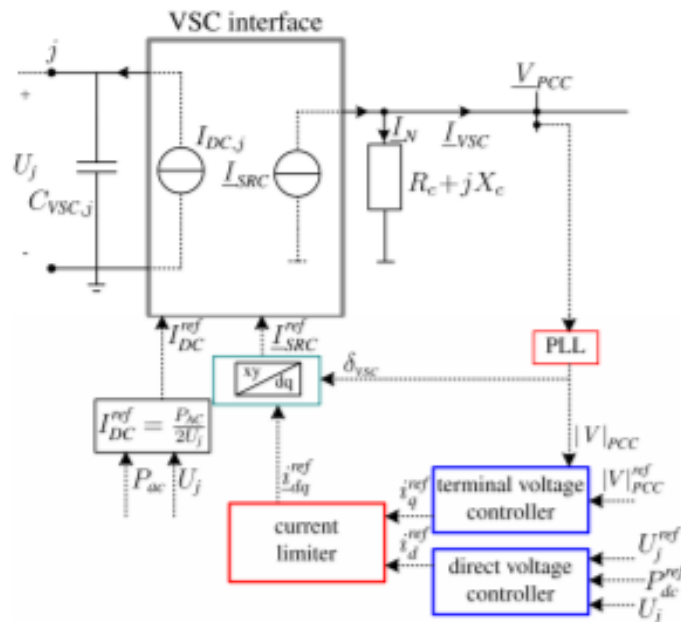


*Figure 6 - VSC dynamic model for transient stability simulations [10]*

In PSSE, an averaged VSC model is used [10]. The DC side is represented by a varying current source and the AC side by a time varying Norton current injection. Since the majority of the VSCs connected to AC systems use vector control, the terminal voltage of the VSC is controlled in such a way that the VSC behaves as a current source. The Norton current injection is given by [10]:

$$I_{SRC} = \frac{V_{PCC}}{R_C + jX_C} + i^{ref}{}_{VSC,dq} e^{j\delta_{PLL}} \quad (2.1)$$

where $I_{SRC}$ is the current injection of the converter, $V_{PCC}$ is the voltage at the point of common coupling, $i^{ref}{}_{VSC,dq}$ is the vector containing the d and q axis components of the current.

Because of the symmetrical nature of the AC network model, the distribution of power among the poles of the DC side of the VSC is equal. For this reason, a monopolar representation of the DC scheme is used to save computational power. At the DC side, the VSC exhibits current source behavior due to the control scheme and the connected phase reactors. Therefore, the AC/DC interaction of the VSC is governed by the active power balance as [9]:

$$I_{DC,j} = \frac{P_j}{2U_j} = -\frac{P_c - P_{loss}}{2U_j} \quad (2.2)$$

where $P_c$ is the VSC terminal power, $P_{loss}$ are the switching losses.

## 2.6 Operating principle of VSC – HVDC system

The operation of VSC – HVDC can be explained by considering each terminal as voltage source connected to the AC transmission network via series reactors and transformers. The two terminals are then connected via a DC link as shown in Figure 7.
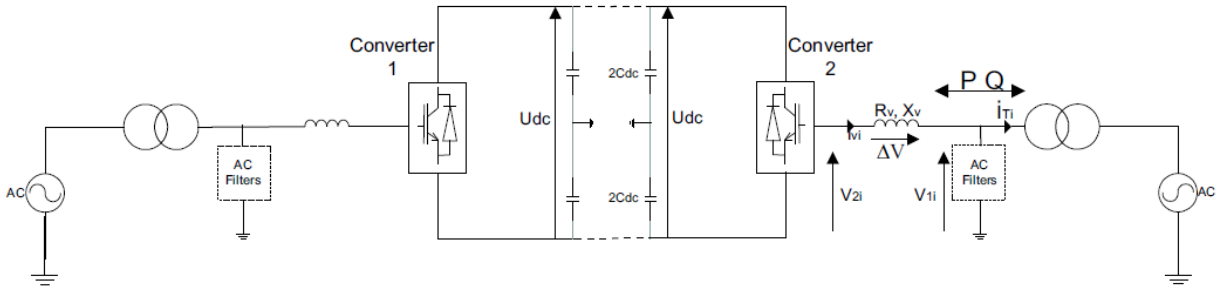


*Figure 7 - Topology of a VSC - HVDC connection [7]*

The converter can be represented on the AC side as an AC voltage source where the phase, frequency and amplitude can be controlled independently from each other. This means that the bridge of the VSC can be seen as a very fast controllable synchronous machine with the voltage ($V_{2i}$ in Figure 7) as described by the following equation:

$$V_{2i} = \frac{1}{2} U_{DC} m \sin(\omega t + \varphi) + harmonic\ terms \quad (2.3)$$

where m is the modulation index which is defined as the ratio of the peak value of the modulating wave and the peak value of the carrier wave, ω is the fundamental frequency, φ is the phase shift of the output voltage depending on the position of the modulating wave. The VSC controller can change the variables m and φ independently, resulting in various combinations of voltage magnitude and phase shift in respect with

the fundamental frequency voltage in the AC system. This means that the voltage drop which is present across the reactor can be used to control the active and reactive power flow.

The active power flow between the converter and the network can be controlled by changing the phase angle ($\varphi$) between the fundamental frequency voltage generated by the VSC ($V_{2i}$) and the voltage on the bus ($V_{1i}$). The power is calculated according to equation (2.4).

$$P = \frac{V_{1i}V_{2i}\sin\varphi}{X} \quad (2.4)$$

The reactive power flow is determined by the amplitude of $V_{2i}$. The reactive power is calculated according to equation (2.5).

$$Q = \frac{V_{2i}(V_{2i} - V_{1i}\cos\varphi)}{X} \quad (2.5)$$
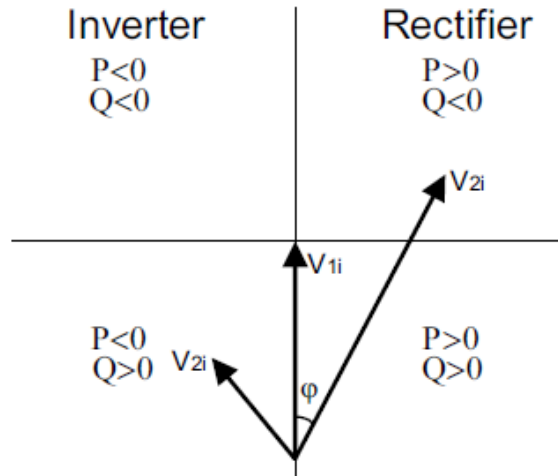


*Figure 8 - Phasor diagram*

The phasor diagram in Figure 8 demonstrate how the signs of the active and reactive power depend on the phase and the amplitude of the voltage generated by the converter assuming that the voltage at the bus remains constant. For example, if the voltage at the bus is leading the voltage of the converter, then active power flows from the AC network to the converter.

In VSC – HVDC connections, the active power flow on the AC side and DC side if the losses are disregarded. It is possible to achieve this, if the one of the two converters is in active power control mode and the other one in DC voltage control mode. The generation and the consumption of the reactive power of the converter can be used to satisfy the needs of the connected network. In Figure 9, the active and reactive power capability of the converter can be seen. The VSC – HVDC is able to operate at any point inside the circle, while the circle represents the power ratings of the converter in MVA [11]. The reactive power capabilities of the converter can be used to control the AC voltages of the networks connected to the converters or to support the network during faults. Moreover, the active power can be transmitted bidirectional only to be limited by the rating of the converter.
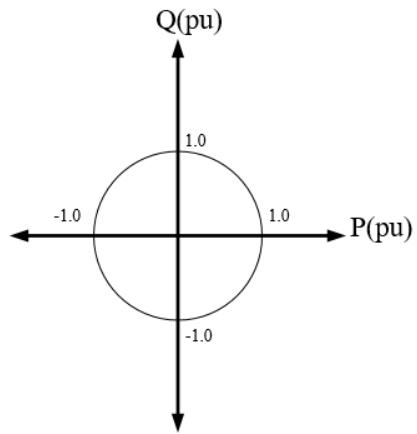
*Figure 9 - PQ characteristics of a VSC – HVDC*

# Chapter 3: Dynamic model and control system of a VSC – HVDC network

## 3.1 Introduction

In the first part of this chapter a schematic model of the VSC is given. The common approach to represent a VSC model in power system stability studies is by using an average phasor model [12]. As for the HVDC cables a $\pi$ – equivalent circuit modeled has been adapted as it is the most common approach to model HVDC cables in stability studies [13] [14]. The second part of this chapter describes the control structure of the VSC. A detailed overview of the controllers used in this thesis is given, which was based on [15]. The last part of this chapter describes the user – written models that were created in order to simulate a VSC – HVDC system.

## 3.2 Generic VSC – HVDC model

The VSC – HVDC converter is connected to the AC system through a phase reactor and a transformer. In Figure 10 the building blocks of the VSC – HVDC transmission system are introduced. The converter utilizes the IGBTs to create the three phase sinusoidal voltage waveform. The transformer changes the AC voltage of the converter to the AC voltage of the system at the point of common coupling. The phase reactor is used to reduce high order harmonic contents of the current that are created by the switching of the IGBTs. The AC harmonic filter which is located between the phase reactor and the transformer is used to suppress high – frequency harmonics into the AC side of the VSC station.
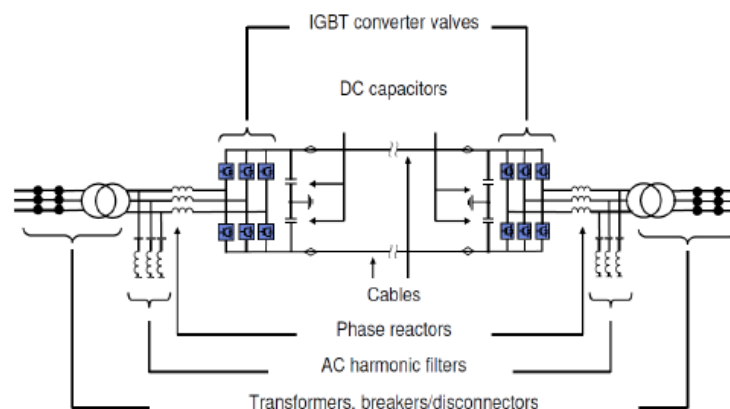


*Figure 10 - Blocks of the VSC - HVDC transmission system [16]*

From the DC side of the converter station there is a DC capacitor connected to the terminal of the HVDC cable. The main functionality of the DC capacitor is to lower the voltage ripple in the DC side and help maintain the direct voltage constant.

A schematic representation of the system can be seen in Figure 11.
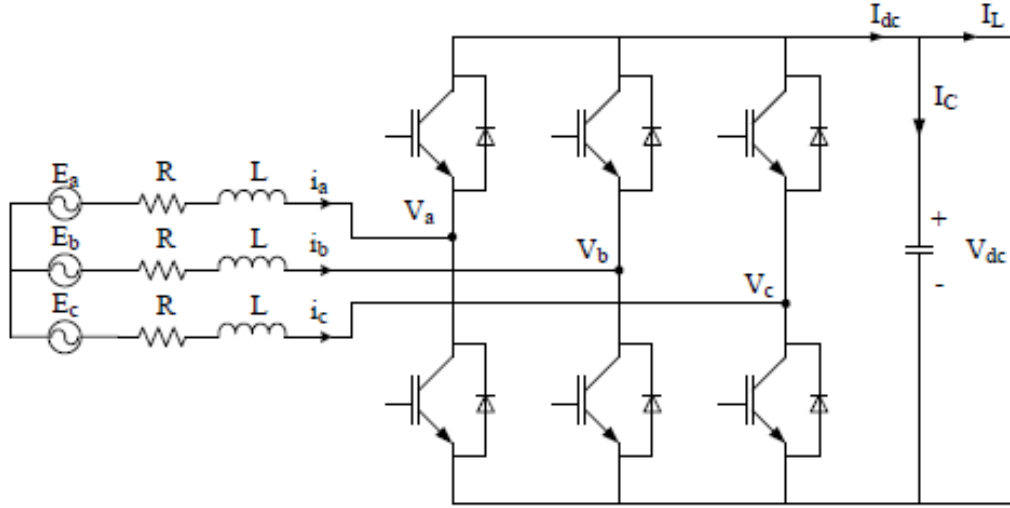


*Figure 11 – Schematic representation of the VSC – HVDC system*

For stability studies, it is common to represent the converter module by controlled phasor average models. To analyze the system connected to the grid in Figure, standard Kirchhoff's voltage law is used, thus the voltage at the gird side of the converter can be described as:

$$E_{abc} = L\frac{d}{dt}i_{abc} + v_{abc} + Ri_{abc} \quad (3.1)$$

where $v_{abc}$ are the converter input voltages, $i_{abc}$ are the grid side currents, $E_{abc}$ are grid voltages, R and L are the resistance and inductance respectively between the converter and the grid.

However, in most power system studies a dq reference frame is adapted due to the advantages it offers to the calculations.

To successfully transform the abc quantities [29] [30] to the dq reference frame, Park's transformation is used (see Appendix A). After deriving the Park's matrices and neglecting the zero component, equation (3.1) can be transformed into the dq reference frame.

By neglecting the zero component the following equations are derived:

$$E_d = v_d + Ri_d + L\frac{d}{dt}i_d - \omega_s Li_q \quad (3.1)$$

$$E_q = v_q + Ri_q + L\frac{d}{dt}i_q + \omega_s Li_d \quad (3.2)$$

By using equation (3.1) inside the αβ reference frame the following equation is obtained:

$$E_{\alpha\beta} - V_{\alpha\beta} = L\frac{d}{dt}i_{\alpha\beta} + Ri_{\alpha\beta} \quad (3.3)$$

The equation that allows the transformation from the αβ reference frame to the dq reference frame is given by:

$$x_{\alpha\beta} = x_{dq}e^{j\omega t} \quad (3.4)$$

The angle ωt is provided from the phase locked loop (PLL). The PLL is the control system that acts upon the phase difference between the reference signal and the input, such that, the phase of the output is locked to the phase of the reference.

$$E_{dq}e^{j\omega t} = V_{dq}e^{j\omega t} + Ri_{dq}e^{j\omega t} + e^{j\omega t}L\frac{d}{dt}i_{dq} + j\omega Le^{j\omega t}i_{dq} \quad (3.5)$$

By dividing the equation (3.9) with $e^{j\omega t}$ the differential equations of the AC circuit of the VSC in the dq reference frame are obtained.

$$E_d = v_d + Ri_d + L\frac{d}{dt}i_d - \omega Li_q \quad (3.6)$$

$$E_q = v_q + Ri_q + L\frac{d}{dt}i_q + \omega Li_d \quad (3.7)$$

## 3.3 DC cable equivalent model

The equivalent model that represents the DC cable for the transient stability studies is shown in Figure 12. Applying time domain circuit laws, the differential equations are [16]:
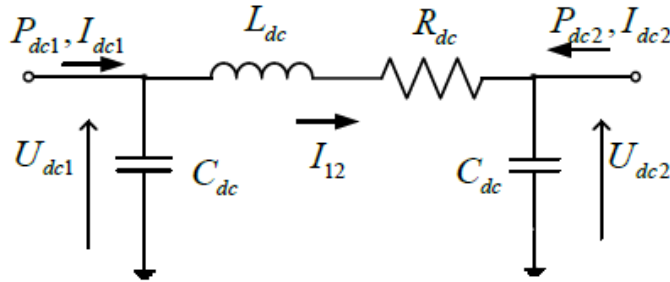


Figure 12 - DC cable equivalent model [16]

$$C_{DC}\frac{dU_{DC1}}{dt} = I_{DC1} - I_{12} \quad (3.8)$$

$$C_{DC}\frac{dU_{DC2}}{dt} = I_{DC2} + I_{12} \quad (3.9)$$

$$L_{DC}\frac{dI_{12}}{dt} = U_{DC1} - U_{DC2} - R_{DC}I_{12} \quad (3.10)$$

By rearranging the above equations, it is possible to obtain the state space representation of the DC cable as showed in equation (3.15). It is also worth mentioning that the DC capacitor of the VSC station is included and modelled within the DC cable capacitance. Thus, the DC cable capacitance is a sum of the VSC capacitance and the $\pi$ – equivalent cable model capacitance.

$$\frac{d}{dt}\begin{bmatrix} U_{DC1} \\ U_{DC2} \\ I_{12} \end{bmatrix} = \begin{bmatrix} 0 & 0 & -\dfrac{1}{C_{DC}} \\ 0 & 0 & \dfrac{1}{C_{DC}} \\ \dfrac{1}{L_{DC}} & -\dfrac{1}{L_{DC}} & -\dfrac{R}{L_{DC}} \end{bmatrix}\begin{bmatrix} U_{DC1} \\ U_{DC2} \\ I_{12} \end{bmatrix} + \begin{bmatrix} \dfrac{1}{C_{DC}} & 0 \\ 0 & \dfrac{1}{C_{DC}} \\ 0 & 0 \end{bmatrix}\begin{bmatrix} I_{DC1} \\ I_{DC2} \end{bmatrix} \quad (3.11)$$

## 3.4 Control system of the VSC station

The control system of the VSC – HVDC is based on a fast inner current control loop which controls the AC current. The references for the AC current are calculated by the outer controllers which generate a reference value that goes in the inner current control loop. These controllers are: the active power controller, the reactive power controller, the DC voltage controller and the AC voltage controller. The reference value for the active current can be derived from the active power controller and the DC voltage controller whereas the reference value for the reactive current can be derived from the reactive power controller and the AC voltage controller. With this delegation, it can be concluded that the outer controllers are used to facilitate the control of the active and reactive power flows as well as the AC and DC voltage of the VSC. The reference value is fed to the inner current controller which calculates the voltage drop on the phase reactor that will lead to the desired current.

The majority of the control methods implemented in the VSC – HVDC system are based on vector control. Basically all the controllers are using PI (proportional – integral) controllers. It is obvious that not all of the aforementioned controllers can be used simultaneously. The choice of the different controllers to calculate the reference values will depend on the application and the power system study. For example in Figure 13, the active power from/to the converter can be controlled by the active power controller, the reactive power controller can control the reactive current and the AC voltage controller can control the AC voltage. It is important to note that the active power inside the DC link must be balanced which means that regardless the losses, the active power that comes inside the DC link must be equal to the active power of the network. The purpose of the DC voltage controller is to control the active power balance and ensure its stability in all cases.

The inner current controller as well as the outer controllers used in the master thesis project were modelled based on the [14] and will be described in detail in this chapter. The performance of the controllers will be evaluated in the following chapters.
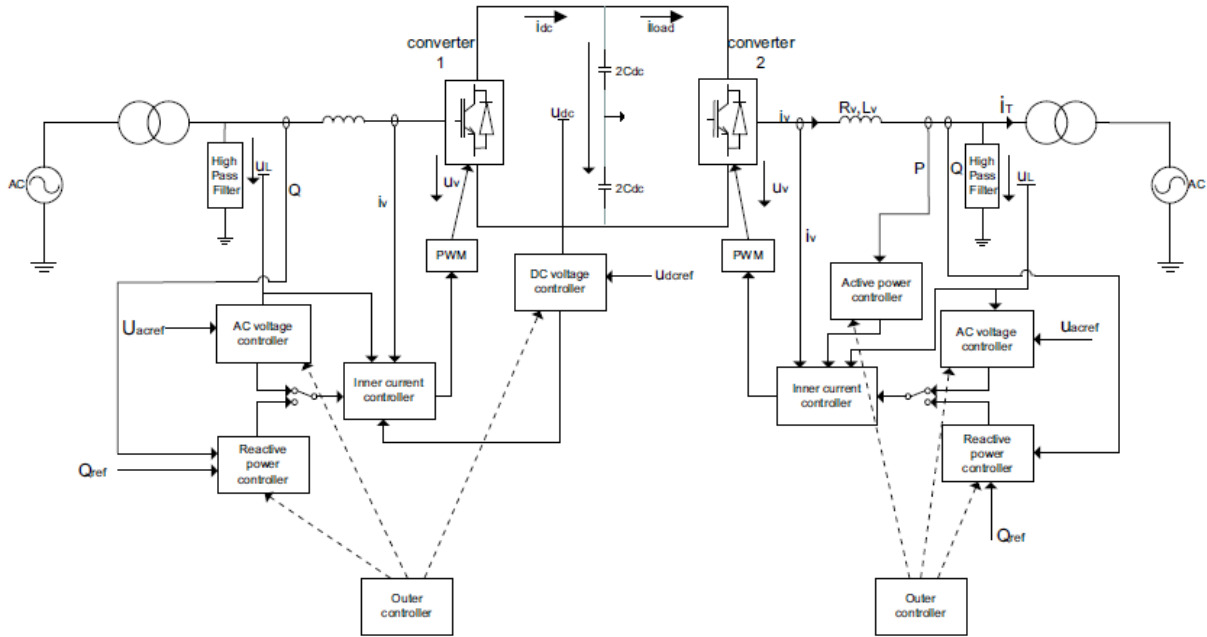
*Figure 13 - Overall control structure of the VSC – HVDC [7]*

## 3.5 Controllers used in the VSC

### 3.5.1 The inner current controller

The voltage across the phase reactor is evaluated by the inner current controller and the desired AC current is produced without violating the maximum current of the converter.

Usually, the currents and the AC three phase voltages are transformed from the abc system to the rotating dq coordinate system, which will then be synchronized with the AC network through the phase lock loop (PLL). The converter voltage references will be determined by the control system in the dq framework and then they will be transformed back to the abc quantities before they are provided to the converter's PWM control.

For the VSC – HVDC schematic presented in Figure 11 it is possible to write:

$$E_d = v_d + Ri_d + L\frac{d}{dt}i_d - \omega Li_q \quad (3.12)$$

$$E_q = v_q + Ri_q + L\frac{d}{dt}i_q + \omega Li_d \quad (3.13)$$

Rearranging the equations (3.16) and (3.17) and transforming them to the Laplace domain the following equations are obtained:

$$E_d - v_d = Ri_d + Lsi_d - \omega Li_q \Rightarrow i_d = \frac{E_d - v_d + \omega Li_q}{R + Ls} \quad (3.14)$$

$$E_q - v_q = Ri_q + Lsi_q + \omega Li_d \Rightarrow i_q = \frac{E_q - v_q - \omega Li_d}{R + Ls} \quad (3.15)$$
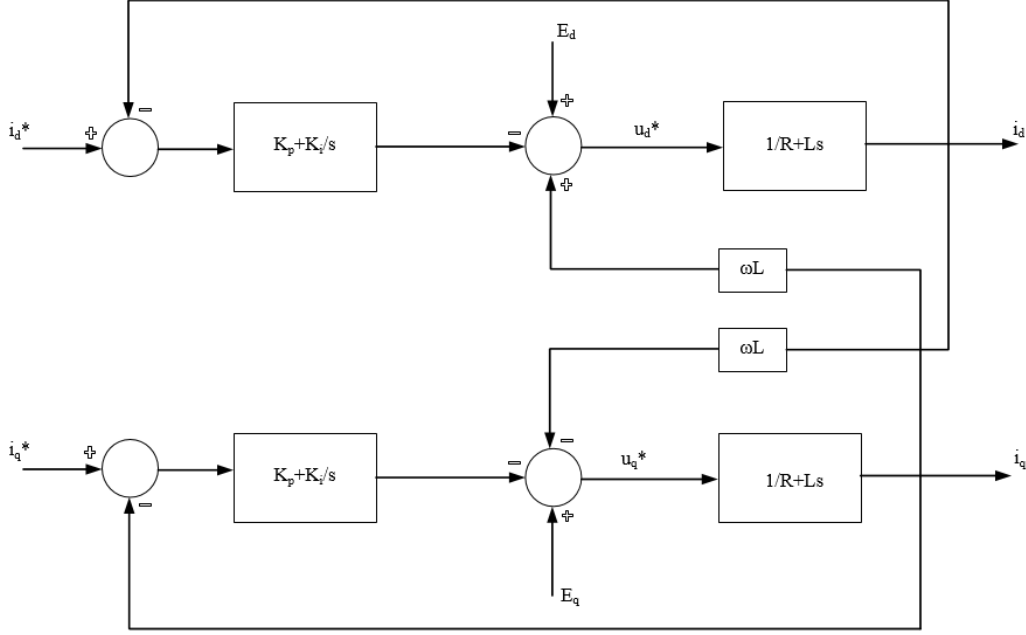


*Figure 14 - Inner current controller block diagram*

From the above, it is clear that the purpose of the inner current control is to provide the voltage references values to the VSC for any given reference current given from the outer controller. The current reference value is the output of the outer controllers which will be described in the following paragraphs.

$$v_d = E_d + \omega Li_q + \left(k_p + \frac{k_i}{s}\right)(i_d{}^* - i_d) \quad (3.16)$$

$$v_q = E_q - \omega Li_d + \left(k_p + \frac{k_i}{s}\right)(i_q{}^* - i_q) \quad (3.17)$$

The algebraic and differential equations described above need to be utilized in case a dynamic user written model is developed in PSSE software package. Every dynamic model in PSSE is separated into modes. Each mode represents a different stage in the dynamic simulation. For more information regarding the creation of user written models and the description of each phase see Appendix B.


### 3.5.2 Outer controllers


The outer controllers are responsible for generating the reference values for the active and reactive component currents and provide them to the inner current control. In this thesis two different controllers

are being used for each case: for the generation of the reference of the active current component the active power controller and the DC voltage controller is used whereas for the generation of the reference of the reactive current component the reactive power controller and the AC voltage controller is used.

In an VSC – HVDC system where a point to point connection is in operation one of the two stations is operated as an inverter thus controlling the active power of the link and the other station is operated as a rectifier being responsible for the balance of the DC voltage of the link. The control of the active and reactive power of the station can be performed independently from each other. This can be achieved by using a proper vector control method. The principle behind it is to align the d – axis of the dq rotating reference frame with the synchronously rotating vector of the system voltage.
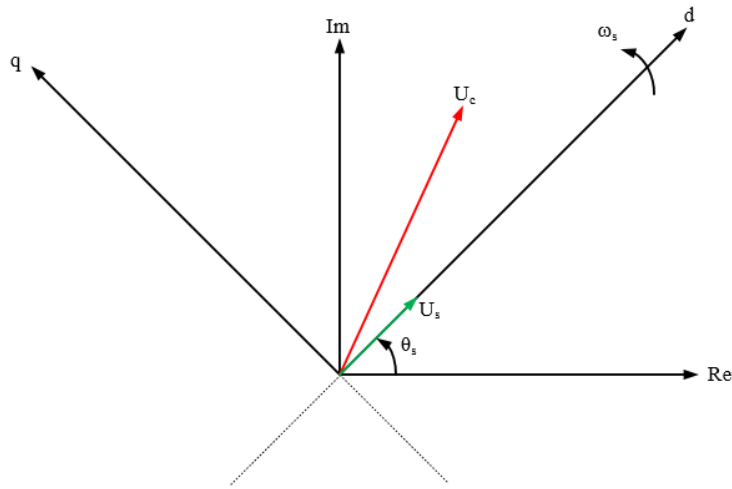


*Figure 15 - Phasor diagram for vector control*

In Figure 15 the phasor diagram of the VSC connected to an infinite base can be seen. It can be observed that when the synchronously rotating vector of the system voltage $U_S$ is aligned with the synchronously rotating reference frame then there is no q – axis component of the system voltage $U_S$ while the d – axis component is equal to the voltage amplitude.

$$|\widetilde{U_s}| = \sqrt{U_d^2 + U_q^2} \xrightarrow{U_q=0} |\widetilde{U_s}| = U_d \quad (3.18)$$

The apparent power in the αβ reference frame is given by [27]:

$$S_{\alpha\beta} = P_{\alpha\beta} + jQ_{\alpha\beta} = V_{\alpha\beta}i_{\alpha\beta}^* = (U_a + jU_\beta)(i_a - ji_\beta)$$

$$P_{\alpha\beta} = U_a i_a + U_\beta i_\beta \quad (3.19)$$

$$Q_{\alpha\beta} = U_\beta i_a - U_a i_\beta \quad (3.20)$$

By using the equations (3.19) and (3.20), the active power can be given from the αβ reference frame to the dq reference frame by:

$$y_\alpha = y_d cos\omega t - y_q sin\omega t \quad (3.21)$$

$$y_\beta = y_d sin\omega t + y_q cos\omega t \quad (3.22)$$

$$P_{dq} = (U_d cos\omega t - U_q sin\omega t)(i_d cos\omega t - i_q sin\omega t) + (U_d sin\omega t + U_q cos\omega t)(i_d sin\omega t + i_q cos\omega t)$$

Finally,

$$P_{dq} = U_d i_d + U_q i_q \quad (3.23)$$

And the reactive power, respectively from:

$$Q_{dq} = (U_d sin\omega t + U_q cos\omega t)(i_d cos\omega t - i_q sin\omega t) - (U_d cos\omega t - U_q sin\omega t)(i_d sin\omega t + i_q cos\omega t)$$

Finally,

$$Q_{dq} = U_q i_d - U_d i_q \quad (3.24)$$

Eventually, introducing the proper vector control method described in equation (3.18), it is possible to decouple the control of the active and reactive power. The final form of the active and reactive power are given by:

$$P_{dq} = U_d i_d \quad (3.25)$$

$$Q_{dq} = -U_d i_q \quad (3.26)$$

### 3.5.3 Active power controller

The active power controller is responsible for the active power injection of the VSC to the AC bus it is connected to. As mentioned before, by applying a proper vector control it is possible to decouple the active and reactive power. The active power in the dq reference frame is given by equation (3.25).

From this equations it is clear that by controlling the active current id, it is possible to control the active power of the VSC. By inserting a PI controller, it is possible to create a feedback loop which will control the active power of the inverter. In Laplace domain the active power controller is given by:

$$i_d{}^* = \frac{P^*}{V_{ac}} + \left(k_p + \frac{k_i}{s}\right)(P^* - P) \quad (3.27)$$

Regarding the active power, two special functions will be discussed. The special functions regarding the active power regulation are called Absolute Power Control (AREG) and Delta Power Control (DREG). The first one, the AREG, can be applied to regulate the HVDC link to a power transmission in a point of reference that equals the set absolute final value, gradient and absolute direction. So, this means that, in order to use AREG a new set point for the active power must be given and also a direction as well as a gradient, a rate of change of the active power, must be given. The second one, the DREG, can be applied to command additional power to the transferred power. DREG can be applied in addition to the AREG, meaning that both can be in operation. The power change is being determined by the delta final value, gradient and delta direction. This means that when AREG is in operation, a set point for that function has

already been given. DREG requires another set point of its own operation, without obstructing the operation of AREG. When DREG has reached its own set point, AREG is again enabled and will continue its operation of reaching the final set point of active power. Of course, this means that DREG can be enabled multiple times in order to achieve the final set point of the AREG faster.

The regulation must cease when the final value is attained or if a command to stop regulation is received, if a new regulation is received during an ongoing regulation the new regulation must take over the regulation. The results of the performance of the active power controller will be given in the following paragraphs.
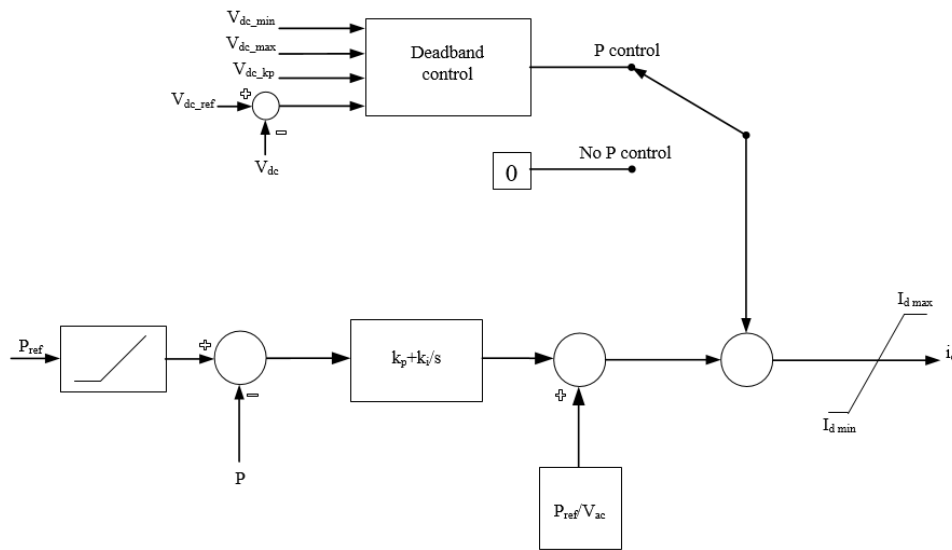


*Figure 16 - Active power controller block diagram*

In Figure 16, the complete structure of the active power controller based on [14] is presented.

### 3.5.4 Direct voltage controller

The direct voltage controller is responsible for controlling the voltage at the terminal of the DC line of the VSC. The DC voltage is determined by the charging power of the capacitor which is the difference between the input active power to the VSC and the DC load power. In Figure 17, the equivalent circuit that demonstrates the way the AC and DC part of the VSC are coupled is shown.
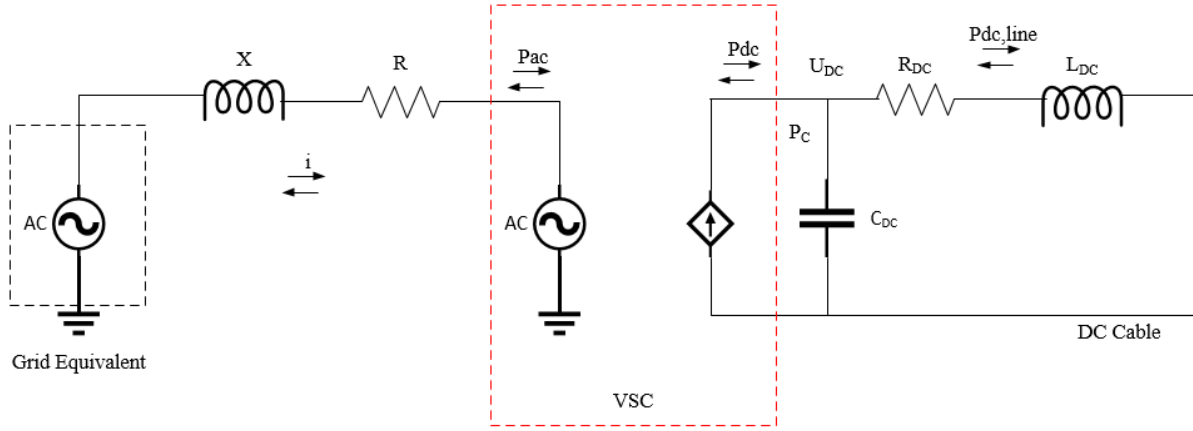
*Figure 17 - Equivalent circuit of the AC and DC side of the VSC*

The converter behaves as a controlled voltage source from the AC side and modelled as a DC current injection from the DC side [17]. The active power balance creates a dependency between the AC and DC side, while the losses are not considered in this case. In reality the VSC has active power losses, but for this study it is modelled as a lossless station. For that reason, the DC power is equal to the AC power:

$$P_{DC} = P_{AC} \Rightarrow U_d i_d + U_q i_q = I_{DC} U_{DC} \quad (3.28)$$

In addition, the DC power balance at the terminal where the DC capacitor is located is given by:

$$P_{DC} - P_{DC,line} = P_c = \frac{dW_c}{dt} = \frac{d\left(\frac{1}{2} C_{DC} U_{DC}^2\right)}{dt} \quad (3.29)$$

By substitution of the equation (3.28) into (3.29):

$$P_{AC} - P_{DC,line} = \frac{1}{2} C_{DC} \frac{d}{dt}(U_{DC}^2) \quad (3.30)$$

From equation (3.30), it can be concluded that the AC active power control is linked with DC voltage. This means that, by controlling the active power injection of the VSC at a specific AC bus, it is also possible to control the power balance of the DC capacitor thus the DC voltage at the terminal of the DC line.

In this way, another control loop is introduced in the direct axis component of the current reference:

$$i_d^* = \frac{P^*}{V_{ac}} + \left(k_p + \frac{k_i}{s}\right)(U_{DC} - U_{DC}^*) \quad (3.31)$$

The control loop compares the reference DC voltage with the actual DC voltage measured at the DC terminal. The error is fed to a PI controller. In that way, it is possible to control the DC voltage of the VSC.

It is important to note that the VSC station in order to provide the reference for the direct axis component of the current reference, can operate either in DC voltage control mode (rectifier) or in active power control mode (inverter).
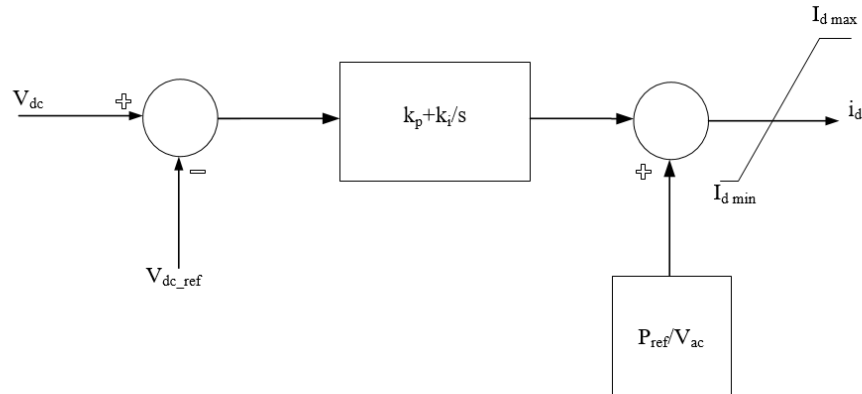
*Figure 18 - VDC controller block diagram*

### 3.5.5 Reactive power controller

The control of the reactive power is also an important capability of a VSC. To achieve independent control of the active and reactive power, the same vector control method should be used as in the case of the active power controller. Reactive power in the dq reference frame is given by equation (3.26)

From that equation, it can be seen that by controlling the reactive current $i_q$, it is possible to control the reactive power. Therefore the reactive controller is given by:

$$i_q^* = -\frac{Q^*}{V_{ac}} + \left( k_p + \frac{k_i}{s} \right)(Q - Q^*) \quad (3.32)$$

Given a reactive power reference, the controller will regulate the injection of the reactive power at the point of common coupling.

The inherent reactive power capability must be possible to be continuously controlled, although transfer of active power have higher priority than reactive power in normal operation as well as voltage in its steady state region. The reactive power must also be possible to control when no active power is transferred on the link irrespective if no power is being transmitted due to demand of zero, cable outage or station outage. The reactive power control commands must be able to be executed independently in any of the converter stations.

When operating in Q control mode, it is possible to change the current active set point of the reactive power to a new set point with a specific ramp. The set points of the stations should be between zero and +/- the maximum converter reactive power rating. The performance of the reactive power controller will be given in the following paragraphs.
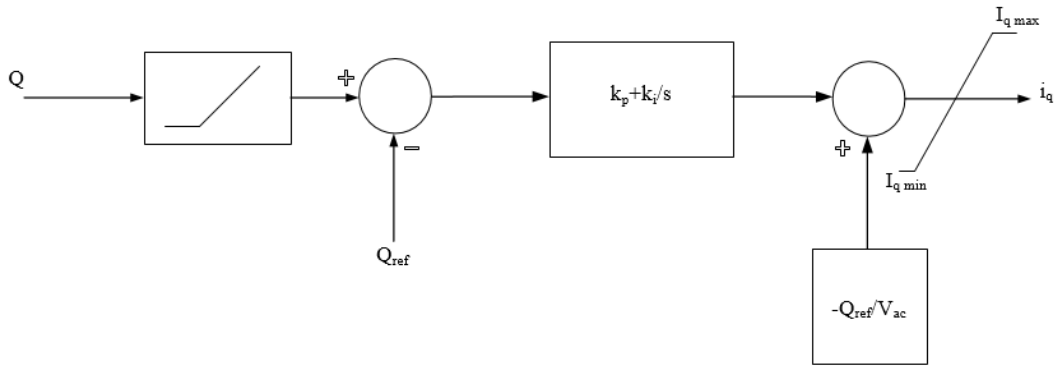
*Figure 19 - Reactive power controller block diagram*

### 3.5.6 AC voltage controller

The objective of the AC voltage controller is to regulate the AC voltage at the point of common coupling at a specific reference by modifying the current reference of the q – axis. In this way, the VSC can support the point of common coupling with reactive power contributing to the AC voltage stability.

$$i_q{}^* = -\frac{Q^*}{V_{ac}} + \left(k_p + \frac{k_i}{s}\right)(V_{ac} - V_{ac}{}^*) \quad (3.33)$$

The main function of the controller is to control the q – component of the current, based on the AC voltage level, thus controlling the reactive power injection.
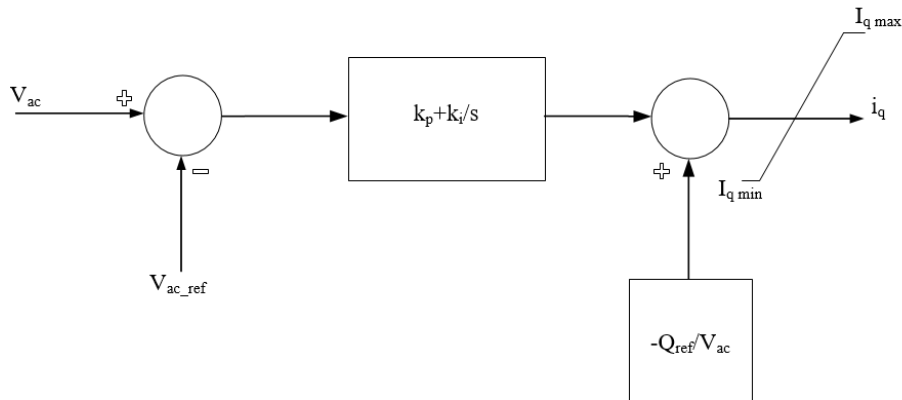


*Figure 20 - AC voltage controller block diagram*

### 3.5.7 Fault ride through capability controller

As stated in [22] and [31], the HVDC station must stay connected and provide maximum voltage support by supplying a controlled amount of reactive power so as to ensure that the HVDC link helps to stabilize the voltage within the desired framework. In moments like this, reactive current has higher priority than the active power in order to maximize the reactive power contribution. Two different equations were used in order to evaluate the fault ride through capability of the converter:

$$i_q = -\frac{100}{35}V_{ac} + \frac{85}{35} \quad (3.34)$$

$$i_q = \frac{12}{7} - \frac{\sqrt{5}\sqrt{20V_{ac}^2 - 20V_{ac} + 28alpha + 5}}{7} - \frac{10V_{ac}}{7} \quad (3.35)$$

where $V_{ac}$ is the AC voltage of the point of common coupling, $i_q$ is the reactive current injection and $alpha$ is a variable which creates different variations of equation (3.35). In Figure 21, the two equations in respect to the AC voltage of the point of common coupling can be observed.
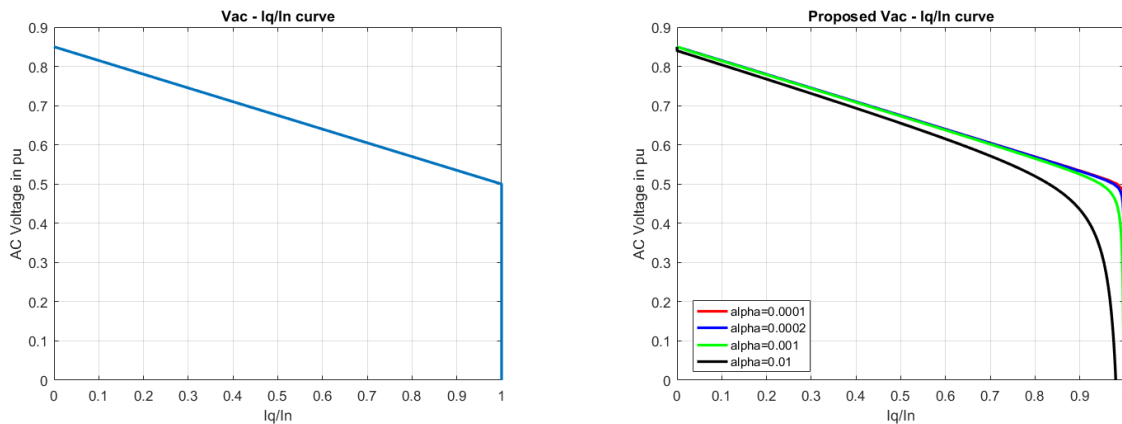


*Figure 21 - FRT equations. (a) Equation (4.1) and (b) Equation (4.2) with different values of alpha*

Overall, it can be seen that when the voltage at the point of common coupling has been dropped below 0.85 pu then the fault ride through capability controller is being activated and bypasses the operation of the reactive power controller or the AC voltage controller. In more details, in Figure 21(a) it can be observed that when the AC voltage drops below 0.5 pu then there is an immediate injection of the reactive current equal to the nominal current of the converter. On the other hand, in Figure 21(b), the immediate injection of the reactive current does not follow the same steep performance as in the previous figure but there is a more smooth transition of the injection of the current. It is also clear that reducing the value of alpha it is possible to approximate the original reactive current contribution given by equation (3.34). In this master thesis, both equation (3.34) and equation (3.35) with alpha equal to 0.0001.

## 3.6 User written models for implementation in PSSE

In this master thesis project, PSSE simulation package has been used in order to study the interaction between the AC and DC power systems. As it has already been mentioned, the creation of a user – written model for the VSC station was imperative in order to match the behavior of the station with the real operational needs. For that reason, a script describing the control structure of the station was created in FORTRAN. Moreover, in order to facilitate the DC side behavior of the VSC – HVDC system, thus a script was also modeled in FORTRAN. After the creation of these two models a dynamic link library was created by using PSSE's environment manager. The environment manager compiles the scripts created in FORTRAN and creates a library which is then possible to import in PSSE, thus being able to use the user defined model in the simulations like any other model of the PSSE library.

Furthermore, in order to initialize the proposed models and coordinate the whole simulation process, several scripts were created in PYTHON programming language. For that reason, a sequential AC and DC power flow script has been created in order to initialize the AC and DC quantities of the system. On top of that, several other scripts were created [18].

For any case, in order to run a dynamic simulation in PSSE, the existence of a .dyr, describing the dynamic behavior of the components of the system is required. For that reason, a script that is able to create a .dyr file in addition to the already existing one was created in PYTHON, so that the dynamic behavior of the VSC station, meaning the control structure of the system, can be used. The script reads an excel file which contains all the essential information regarding the parameters of the controllers and then creates the .dyr file, ready to be imported into the PSSE case. Another PYTHON script creates the dynamic conditions for each case. Through that, it is possible to create different dynamic events, like bus faults, trip branches, disable generators and run the simulation. It is all possible to express which of the output channels would be visible by the user or not.

From the things that were described previously, it is important to note, that for the completion of this master thesis, proper knowledge of the environment of the PSSE simulation software, FORTRAN programming and PYTHON programming, was essential. More information regarding this process will be given in APPENDIX B.

To let the reader understand how this whole process works, a detailed overview of the essential steps required to run the simulation is given:

1. The creation of the control structure of the VSC station in FORTRAN script. Inside that script, all the necessary algebraic and differential equations regarding the controllers mentioned in the previous paragraphs are implemented. For that reason, proper knowledge of the creation of models in PSSE is required and was obtained throughout this master thesis project (see APPENDIX B).
2. The creation of the DC cable in FORTRAN script is also important in this step. As in the previous case, the script contains all the equations required.
3. The compilation of the two scripts with the PSSE's environment manager for the creation of the dynamic link library (.dll).
4. The creation of the excel file which contains the information about the VSC station related parameters and the DC cable data.

5. The execution of the PYTHON scripts that contain the information regarding the power flow simulation and the dynamic simulation.
6. Plotting the results in MATLAB.

It has been mentioned that the VSC – HVDC dynamic model is developed into several modules. The following modules are included:

- Grid side voltage source converter (GSVSC) model
- A DC network model
- Current limiter model
- A DC network load flow script
- Several other scripts regarding the operation of the simulation

The assumptions made in the master thesis project are the following:

- AC network quantities like voltages and currents are represented by time – varying phasors in system per unit vales.
- Generator modules like the VSC stations are modeled current sources. This is the typical approach that PSSE adopts for dynamic simulations.
- Only the fundamental frequency is taken into account. This means that higher harmonics are not present and do not influence the dynamic behavior of the system.

## 3.6.1 GSVSC model

The dynamic models of generation units in PSSE are represented by a Norton equivalent current source [19]. This means that the equivalent model of the VSC need to be transformed to a current source equivalent. In order not to confuse the reader, this does not mean that the VSC is now a current source converter but it is more of an interpretation for the software in order to handle the dynamic simulations. In Figure 22 the two equivalent AC models can be seen.
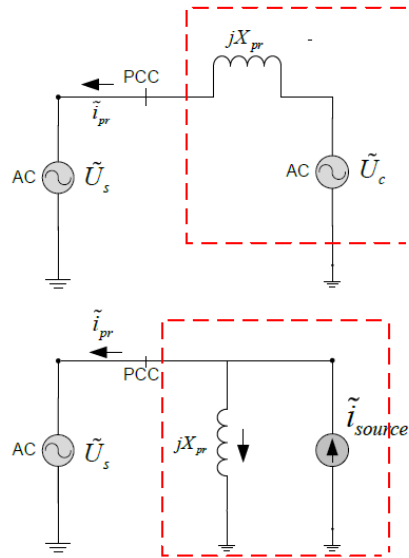
*Figure 22 - (a) VSC model represented as a voltage source. (b) VSC model represented as a Norton equivalent current source*

An important simplification that has been developed in the PSSE model of the GSVSC which reduces the number of states and improves the cost of calculation is that the GSVSC does not have a sophisticated inner current controller. This means that the converter reaches the current reference given by the outer controllers instantly.

The inner current controller used in this master thesis project is just a proportional gain and it is equal to 1. This means that the output of the outer controllers, which is the reference current of the $d$ – axis component and the $q$ – axis component is directly fed to the inner current controller, which is the same as the output of the outer controllers. In this way the direct and quadrature axis component current is reached almost instantly.

### 3.6.2 DC network model

In paragraph 3.3, a description about the state space equations for the HVDC cable has been given. The input signals for the DC network script is the vector of the DC current injections at the nodes where the VSC is present. The DC current injections are calculated from the GSVSC model.

As previously mentioned, the user written define models that have been created require a correct initialization in order to conduct dynamic simulations. For that specific reason, a sequential AC – DC power flow is being utilized in order to determine the operational points of the two VSC stations both from the AC and DC side [10] [20].

In more details, in the AC side, the GSVSC stations are modelled as PV buses. First, the active and reactive power is being set for both stations and then the AC power flow needs to be executed. However, this does not mean that a DC power flow can be run directly from PSSE, since PSSE does not have this capability.

Moreover, in order to correctly initialize the DC network, there must be a coordination between the power feed from the GSVSC stations from the AC side. In order to solve that problem, an external PYTHON script has been modeled that contains the DC power flow solution. With the use of PYTHON, the PSSE variables that contain the AC power injection from the VSC station at the specific buses can be accessed. These values are the set points of the VSC station introduce in the AC power flow.

In the DC side, one bus is always considered as a slack bus being responsible for the losses while the other bus is always considered as a constant power node. When the DC power flow has converged, the calculated voltages and currents now represent the initial states of the state space model of the DC network. In Figure 23, an overview of the whole approach described above can be seen.
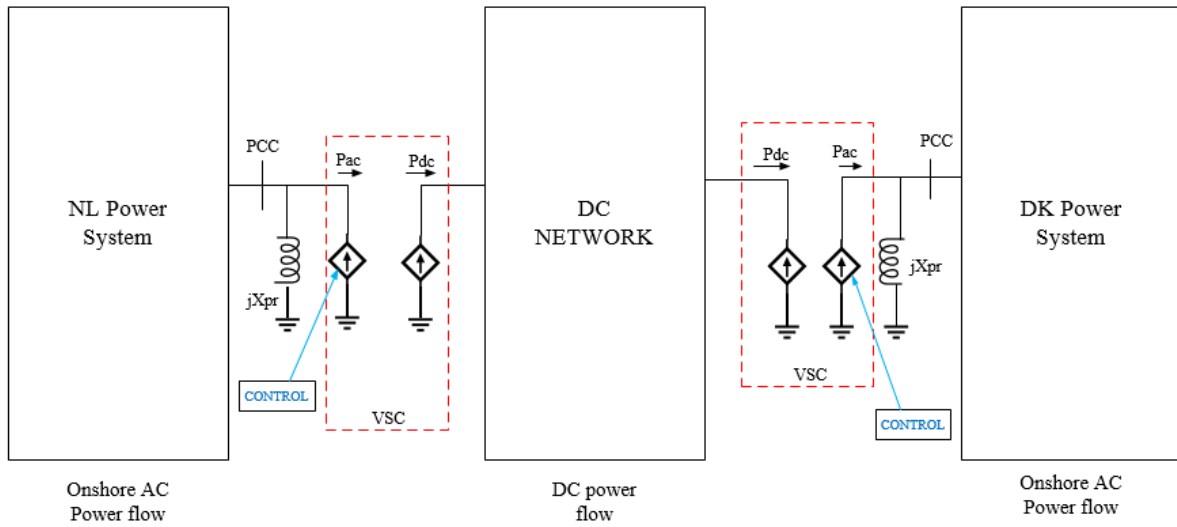


*Figure 23 - AC and DC power flows in the VSC - HVDC system*

Now that the initial points of the DC network have been established, the points need to be written in dynamic model file (.dyr) in PSSE. Thus, when the DC power flow has converged, the dyr file is created which can be used to correctly initialize the DC network dynamic model. The same method applies for the GSVSC stations. Similar to the DC model, the initial states of the VSC stations are introduced in PSSE via a dyr file as described in paragraph 3.6. Once the system is correctly initialized it is possible to run the dynamic simulations for the VSC – HVDC system.

### 3.6.3 DC power flow equations

A quick analysis of the equation regarding the DC grid power flow will be given in this paragraph [18] [20]. The analysis will be performed for the case of n nodes that are present in the DC grid. The nodal voltages and the current injections for each node in the DC network can be written as:

$$U_{DC} = \begin{bmatrix} U_{DC}{}^1 & U_{DC}{}^2 & \cdots & U_{DC}{}^{N-1} & U_{DC}{}^N \end{bmatrix} \quad (3.36)$$

$$I_{DC} = \begin{bmatrix} I_{DC}{}^1 & I_{DC}{}^2 & \cdots & I_{DC}{}^{N-1} & I_{DC}{}^N \end{bmatrix} \quad (3.37)$$

It is possible to calculate the network admittance matrix $Y_{DC}$, given the DC cable resistances. The admittance matrix is given as:

$$Y_{DC}{}^{NxN} = M \begin{bmatrix} \dfrac{1}{R_1} & 0 & 0 & 0 \\ 0 & \dfrac{1}{R_1} & 0 & 0 \\ 0 & 0 & \ddots & \dfrac{0}{1} \\ 0 & 0 & 0 & \dfrac{1}{R_1} \end{bmatrix} M^T \quad (3.38)$$

The current injections are not calculated prior to the DC power flow solution. Also, the DC power injections are known as a results of the AC power flow solution except for the DC slack bus. Moreover, the DC voltages are known only for the DC slack bus whereas the other nodes the voltages are defined by the DC power flow solution.

The unknowns are:

$$X = \begin{bmatrix} U_{DC}{}^1 \\ \vdots \\ U_{DC}{}^{N-1} \\ P_{DC,slack} \end{bmatrix} \quad (3.39)$$

The non – linear algebraic equation to be solved is given by:

$$F(U_{DC}) = Y_{DC}{}^{NxN} U_{DC} - \begin{bmatrix} \dfrac{P_{DC}{}^1}{U_{DC}{}^1} & & & \\ & \dfrac{P_{DC}{}^1}{U_{DC}{}^1} & & \\ & & \ddots & \dfrac{P_{DC}{}^1}{U_{DC}{}^1} \end{bmatrix} = 0 \quad (3.40)$$

In order to solve the non – linear equation, the Newton – Raphson method has been used. The Jacobian matrix is defined as:

$$J = \frac{\partial F}{\partial U_{DC}} = Y_{DC}{}^{NxN} + \begin{bmatrix} \dfrac{P_{DC}{}^1}{U_{DC1}{}^2} & & & \\ & \dfrac{P_{DC}{}^2}{U_{DC1}{}^2} & & \\ & & \ddots & \dfrac{P_{DC}{}^1}{U_{DC1}{}^N} \end{bmatrix} \quad (3.41)$$

And the DC voltages are given in each iteration by:

$$U_{DC}{}^{k+1} = U_{DC}{}^k - J^{-1} F(U_{DC}{}^k) \quad (3.42)$$

### 3.6.4 Current limiter model

The switching devices that are present in the VSC have limited rating for the current that can pass through them. In order to avoid higher currents than the voltage source converter can tolerate a current limiting has been adopted.

The current limiter model compares the reference currents that are obtained from the outer controllers of the VSC with the maximum permitted value of the current. If the reference currents are above the allowed ones, then the reference currents will be equal to the maximum allowed currents. The magnitude of the reference current is given by:

$$|i| = \sqrt{i_d^{*2} + i_q^{*2}} \quad (3.43)$$

There are three current limiting strategies applicable for the VSC [21]. The first strategy gives priority to the d – axis component of the current and thus priority to the active power, thus giving the converter the possibility to produce more power. The second strategy gives priority to the q – axis component of the current and thus priority to the reactive power, thus giving the converter the possibility to increase the reactive power support equal to its rating during voltage dips. The third strategy performs equal scaling of the d – axis and q – axis current. In Figure 24, the three limiting strategies can be observed. The role of the current limiter to the participation of the VSC at faults and to reactive power support will be discussed in the following chapters.
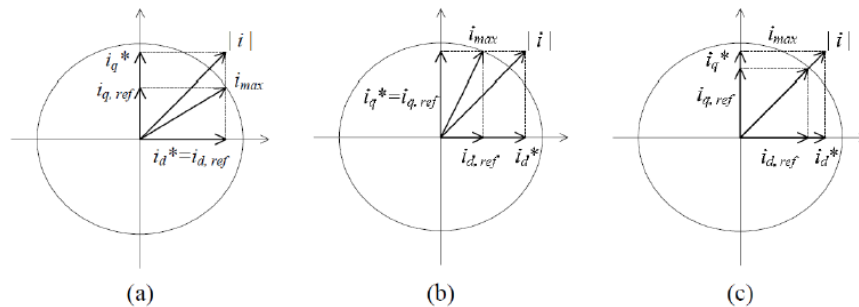


*Figure 24 - Current limiting strategies [16]*

# Chapter 4: Test system and simulation results

## 4.1 Introduction

As mentioned in the previous chapter, the controllers used in this master thesis project were based on [14]. Moreover, active controller, reactive controller were further developed in order to meet the minimum requirements of the COBRAcable project. In order to investigate the performance of the controllers Dutch transmission system and the Danish transmission system. In the end, several important conclusions regarding the operation of the COBRAcable and its effect in the Dutch transmission system have been drawn.

## 4.2 Benchmark system for the Dutch and Danish side

The benchmark system used for the representation of the Dutch transmission system and the Danish transmission system can be seen in Figure 25. The Dutch transmission system is represented by a reduced AC network for the Eemshaven region. As it can be seen, the Dutch transmission system is consisted of eight buses, five of them at 380 kV, two of them at 220 kV and one at 23 kV. It consists of three generators, one of which is used to represent the COBRAcable, one to represent the Dutch equivalent network, and the last one is a generator located in the area. The generator representing the Dutch equivalent network is represented with a 7th order generator model and it is equipped with an excitation system, turbine governor system and a power system stabilizer. The generator connected to the 23 kV bus is also equipped with an excitation system and a turbine governor. The generator used to represent the COBRAcable will be used in order to implement the FORTRAN script containing the necessary information about the control structure and operation of the VSC station.

On the other side, the Danish transmission system is a standard benchmark model of three buses and two generators, one representing the Danish equivalent system and one for the COBRAcable. The three buses are at 400 kV and the line parameters are as seen in Table 1 below:

| R | 0.014375 (pu) |
|---|---|
| X | 0.140625 (pu) |

*Table 1 - Line parameters for the Danish transmission system*

The line parameters were selected in that way so that the short – circuit impedance at the point of common coupling, meaning the point where the COBRAcable is connected to the system, is equal to 156.6349 Ohms. The generator representing the Danish equivalent network is represented by a 7th order generator model and is equipped with an excitation and a turbine governor system.

Power flow simulations were performed in order to match the ratings of the stations. The station located in Eemshaven region is operated as an inverter and it is in P control mode and Q control mode, obtaining 600

MW and injecting 180 MVAr, whereas, the station located in Endrup is operated as a rectifier and it is in DC voltage control mode and Q control mode, delivering 600 MW and injecting 230 MVAr.

In the following paragraphs, a detailed analysis of the behavior and performance of the controllers used in the system will be given.
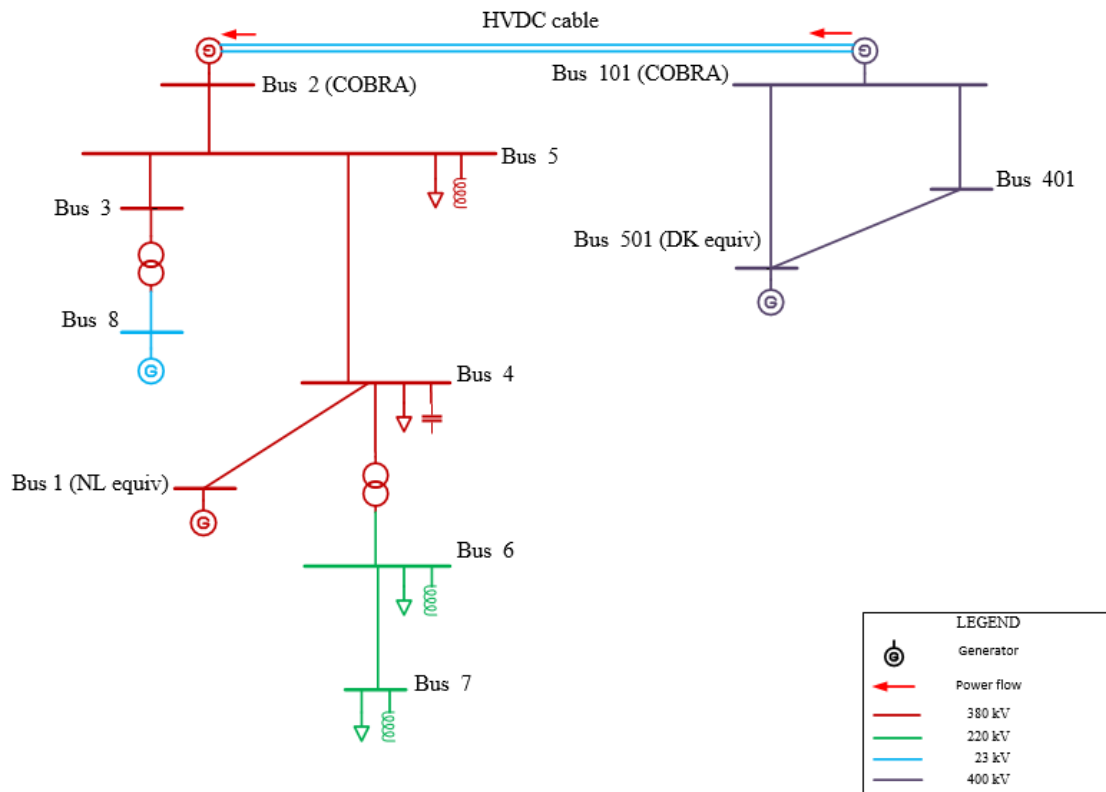


*Figure 25 - Dutch and Danish transmission system*

## 4.3 Active power controller performance

In this paragraph, a detailed analysis of the case studies regarding the performance of the active power controller will be discussed. For the active power controller, it is assumed that the inverter station is operating in P control mode obtaining 600 MW. This means that on the other end, the rectifier station is always working in DC voltage control mode delivering 600 MW plus the losses of the DC cable. While the inverter is operated in P control mode, four different cases will be analyzed. For each of these cases, two different control modes for the q – axis component will be used. Firstly, the inverter will be in Q control mode operation and for the last part the inverter will be operated in AC voltage control mode. The cases are listed in Table 2.

| First case | Active power response while decreasing from 600 to 550 MW |
|------------|----------------------------------------------------------|
| Second case | Active power response while increasing from 600 to 650 MW |
| Third case | Active power response while decreasing from 600 to 400 |
| Fourth case | Active power response while performing a power reversal |

*Table 2 - Active power response cases*

### 4.3.1 First case: Active power response while decreasing from 600 to 550 MW in Q control mode and AC voltage control mode

At 5 seconds, an order has been issued that the active power reference point should be changed from 600 MW to 550 MW. This regulation of the active power will be assisted by the special function AREG. AREG function is enabled at 5 seconds, while using different ramping rates of 100 MW/min, 500 MW/min and 999 MW/min. The total duration of the simulation is 20 seconds. The active power regulation stops when the new active power reference has been achieved, as it has been described in the COBRA cable specifications.
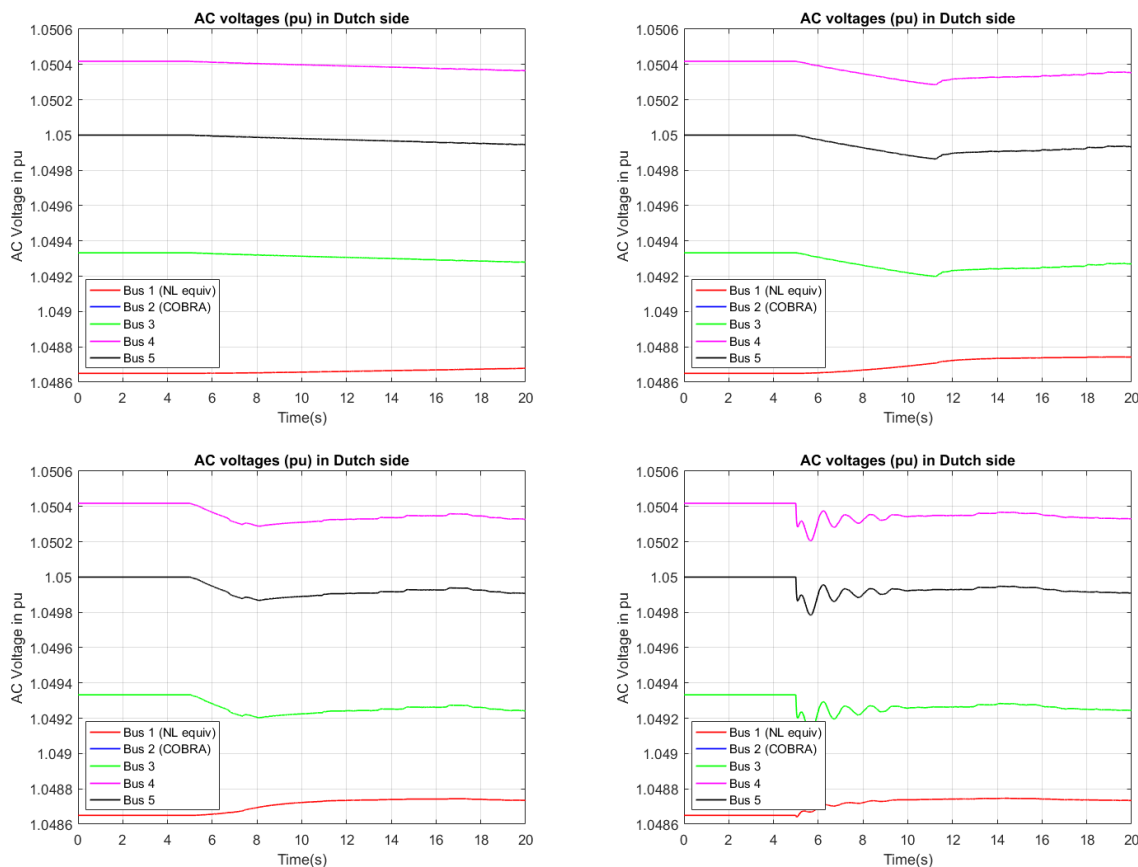


*Figure 26 - AC voltages of the Dutch transmission system while reducing active power from 600 MW to 550 MW. (a) AC voltages for 100 MW/min, (b) AC voltages for 500 MW/min, (c) AC voltages for 999 MW/min and (d) AC voltages for a step input in Q control mode*

In Figure 26, the AC voltages in the Dutch transmission system are affected by the decrease of active power that is being transmitted through the HVDC link after the 5 second mark. In more details, the bus that the

COBRA cable (see blue curve) is connected is a PV bus and with the absence of an excitation system during in the point of common coupling the decrease of active power will result a decrease in the AC voltage of the bus [25]. The buses 3 (green curve), 4 (pink curve) and 5 (yellow curve) in Figure 25, experience the same behavior. However, the bus that the equivalent of the Dutch network is connected, has an excitation system and since there is a decrease in active power it will immediately sense that and will try to increase the voltage slightly.
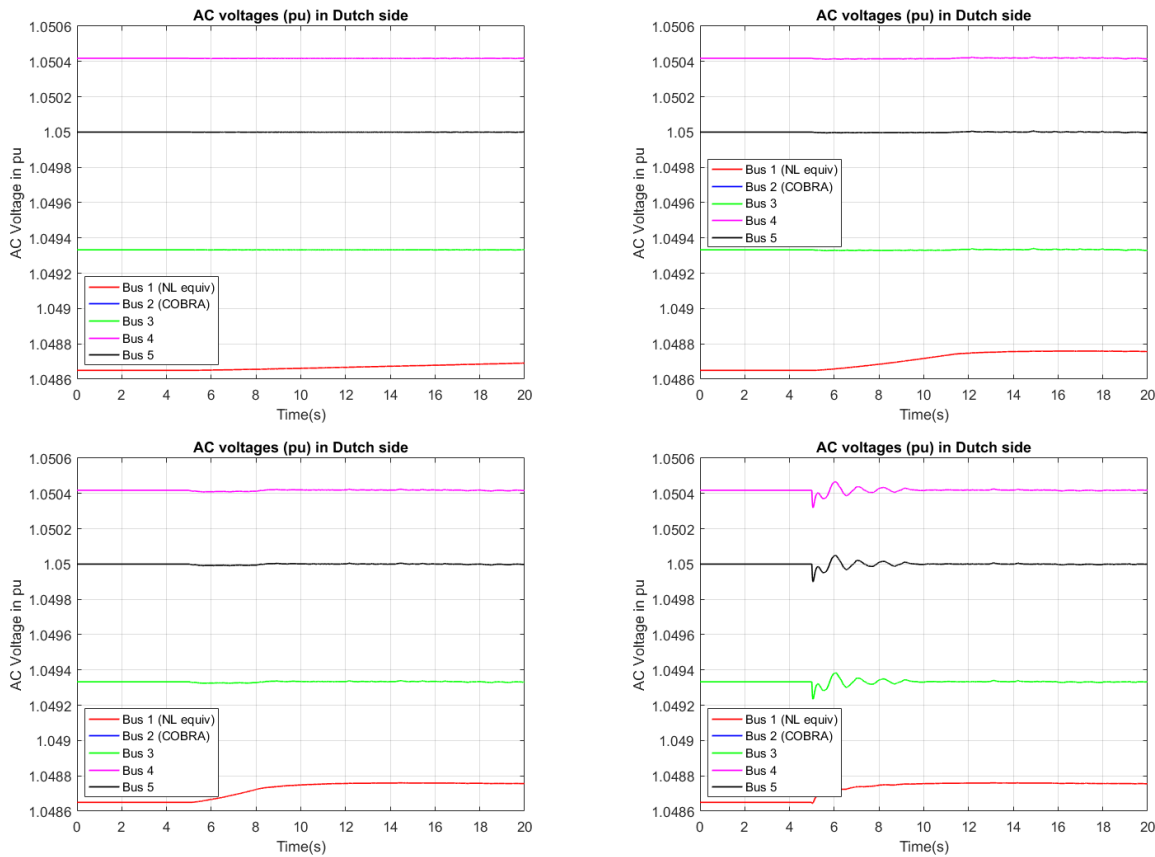


*Figure 27 - AC voltages of the Dutch transmission system while decreasing active power from 600 MW to 550 MW. (a) AC voltages for 100 MW/min, (b) AC voltages for 500 MW/min, (c) AC voltages for 999 MW/min and (d) AC voltages for a step input for AC voltage mode*

On the other hand, in Figure 27, the q – axis component of the current is controlled by the AC voltage controller. The difference between the two control modes (Q and AC voltage control) is immediately observed. While operating in Q control mode the AC voltages of the buses are affected by the decrease of the active power. In this case, the AC voltages of the system remain stable throughout the simulation time and for all the different ramping rates used. Even for the worst case scenario, which is a step input, the AC voltages oscillate around their steady state value.

Since the changes in the active power affect the d – axis component of the current there are some changes at the DC voltage at the beginning of the AREG operation. In Figure 28 (b) (c) and (d), there is a slight increase of the DC voltage which is happening till the new reference point has been achieved. It is also visible that the by changing the ramping rate of the active power, the response of the DC voltage is also affected.

This is one of the limitations of the models that stem from the model itself. The model used for the evaluation of the controllers is an average model. Since there is no sophisticated representation of the capacitance of the VSC station, the rate of change of active power while regulating clearly affects the rectifier, which sole purpose is to keep the DC voltage constant at 1 pu. Another reason is that the model does not have an inner current control as mentioned in the previous chapter. The inner current control is just a proportional gain which means that no feedback loop is present in order to correct the error in each iteration. These two reasons create a deviation for the rectifier station but as it can be observed the deviation of the DC voltage of the rectifier station is almost zero and does not create any problems.
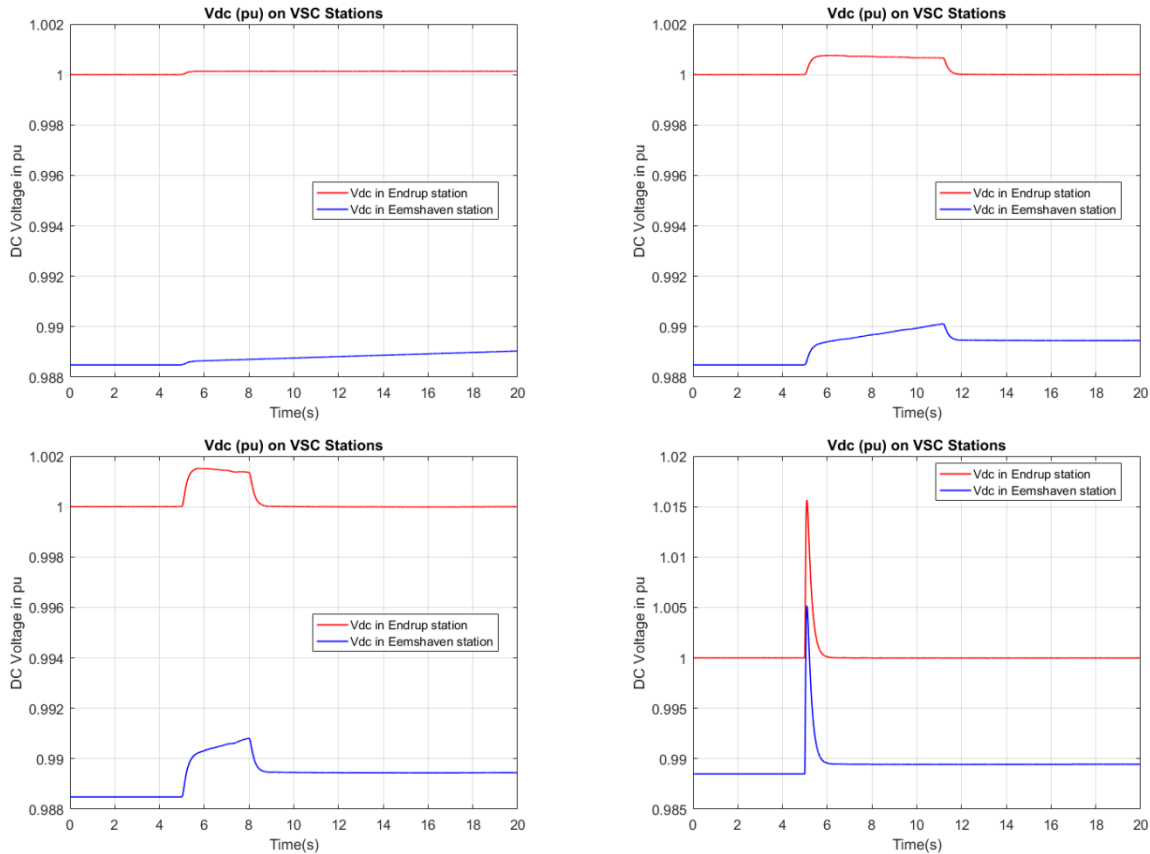


*Figure 28 - DC voltage response while reducing active power from 600 MW to 550 MW. (a) DC voltage for 100 MW/min, (b) DC voltage for 500 MW/min, (c) DC voltage for 999 MW/min and (d) DC voltage for a step input for both control modes*

From the simulations performed with the different ramping rates and also with a step input, it can be observed that the active power controller in the inverter station responds stably to the change of the active power reference as seen in Figure 29.
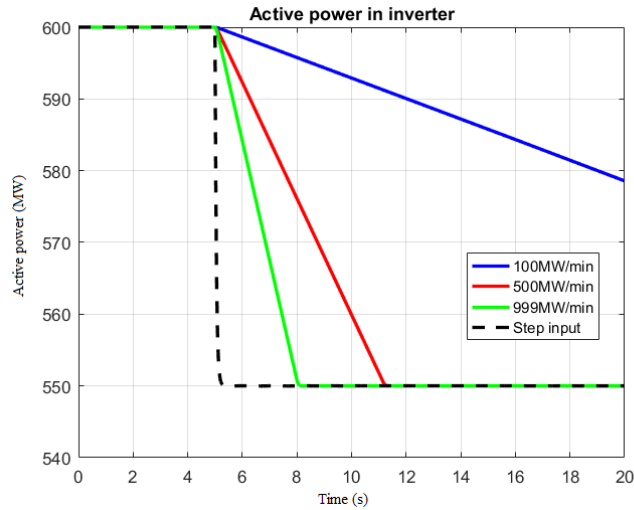
*Figure 29 - Active power response while decreasing active power from 600 MW to 550 MW with different ramping rates for both control modes*

## 4.3.2 Second case: Active power response while increasing from 600 to 650 in Q control mode and AC voltage control mode

In this case an order has been issued that the active power should be increased from the original set point of 600 MW to 650 MW with the same ramping rates as in the first case. Again the increment will be assisted by the AREG function. The function of AREG is again activated at 5 seconds while the simulation lasts 20 seconds.
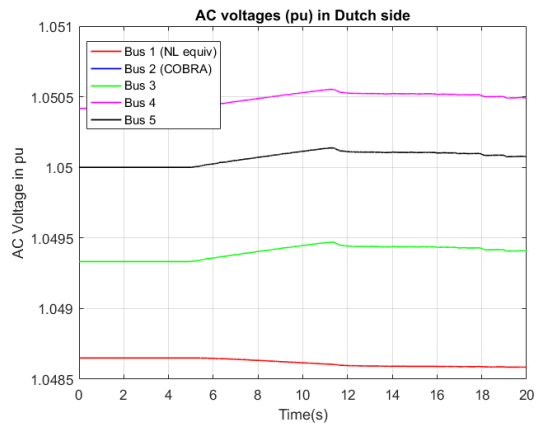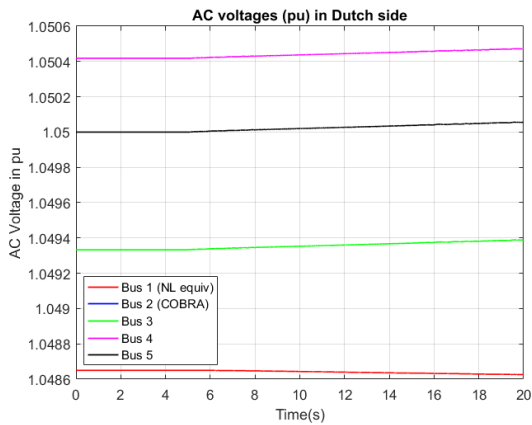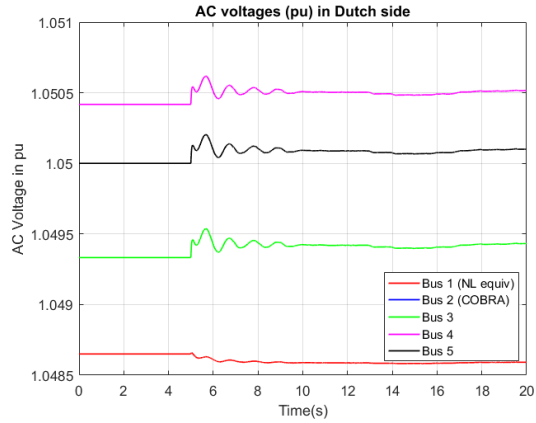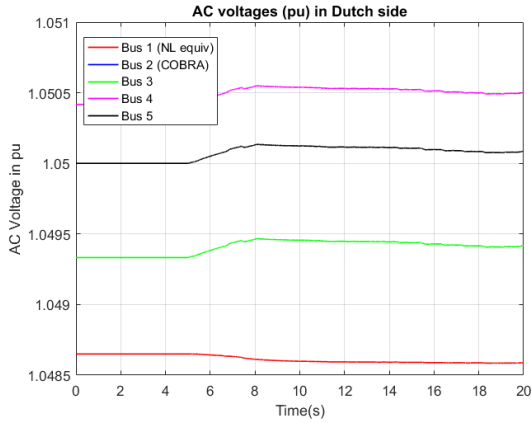
*Figure 30 - AC voltages for the Dutch transmission system while increasing active power from 600 MW to 650 MW. (a) AC voltages for 100 MW/min, (b) AC voltages for 500 MW/min, (c) AC voltages for 999 MW/min and (d) AC voltages for a step input in Q control mode*

The AC voltages in the Dutch transmission are again affected by the increase of active power as it can be seen in Figure 30. In more details, the buses of the Dutch network follow the increment of the power by increasing their voltage due to the absence of an excitation system in the buses nearby. The slack bus, where the generator that represents the equivalent Dutch network has an exciter that will try to maintain the voltage at a constant level. It is visible (red curve) that the exciter senses the increase in active power and tries to decrease the voltage at the bus to a new steady value.
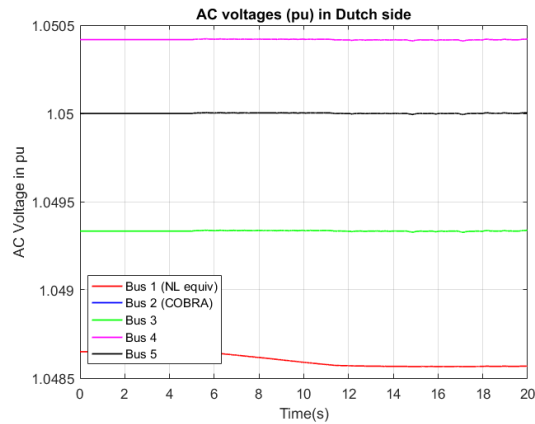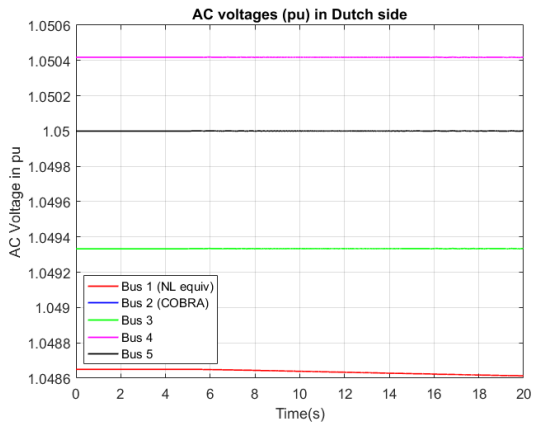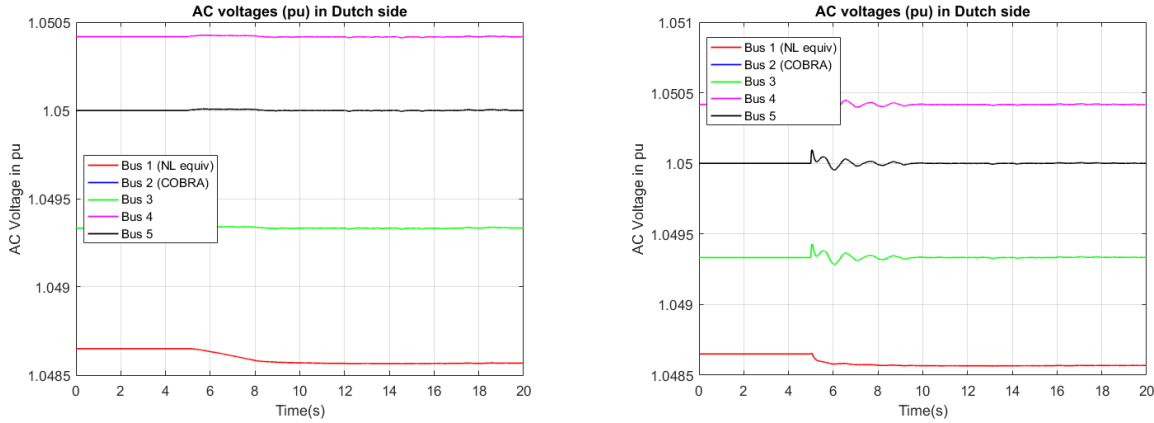
*Figure 31 - AC voltages of the Dutch transmission system while increasing active power from 600 MW to 650 MW. (a) AC voltages for 100 MW/min, (b) AC voltages for 500 MW/min, (c) AC voltages for 999 MW/min and (d) AC voltages for a step input in AC voltage mode*

Likewise in Figure 31, the AC voltages remain almost the same with the increase of the active power from 600 to 650 MW and only the bus where the generator with the excitation system (red curve) will sense the difference in active power thus decreasing the voltage slightly.

The DC voltage on the other hand are affected in the opposite way in respect with the first case. The increment of the active power has an immediate effect in the d – axis component of the current which will affect the DC voltage, meaning that the DC voltage will experience a drop until the active power has settled in the new active power reference point. The drop can be seen in Figure 32. Like in the previous case, the ramping rate affect the magnitude of the DC voltage.

The same reasoning as in the previous case can be used here regarding the reaction of the rectifier station. Since the inner current control is absent, meaning that it has no integral part, and that the capacitive behavior of the station is not modelled, the rectifier deviates from the constant value of 1 pu while the AREG is enabled.



56
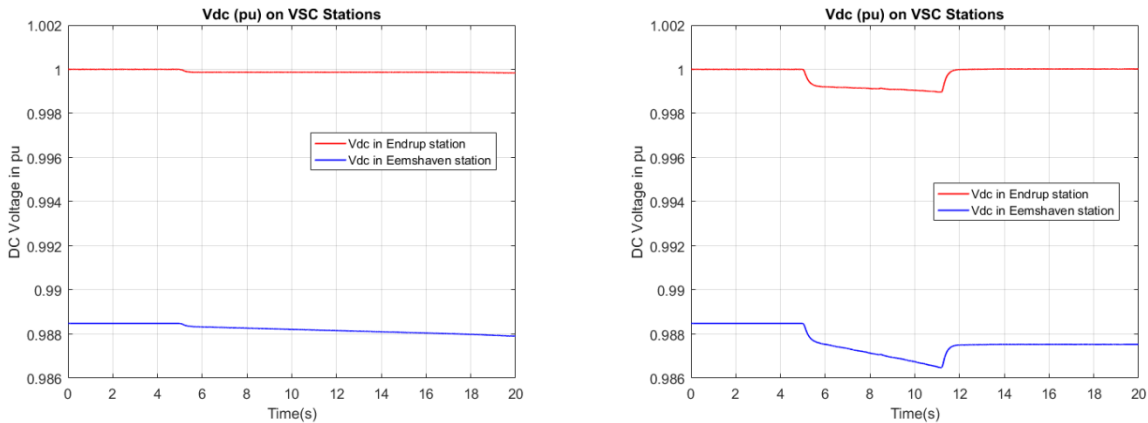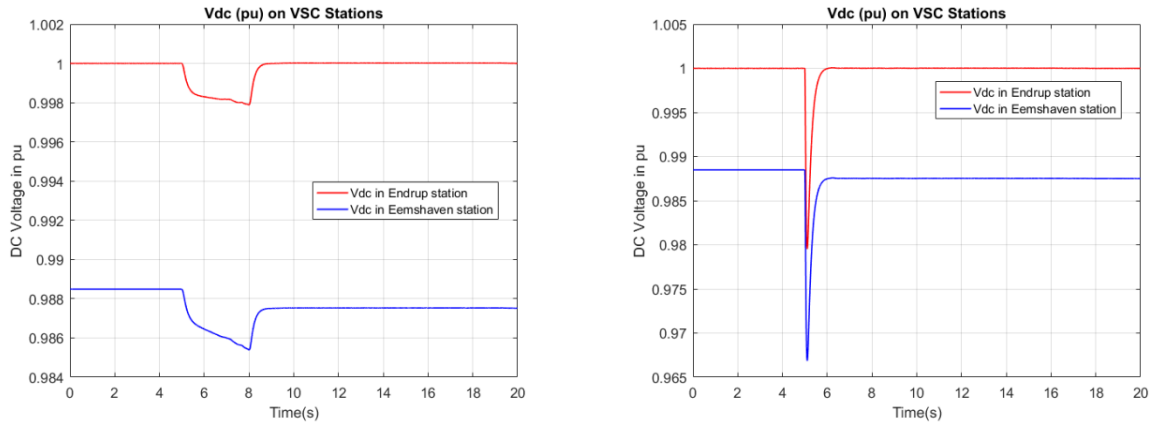
*Figure 32 - DC voltage response while increasing active power from 600 MW to 650 MW. (a) DC voltage for 100 MW/min, (b) DC voltage for 500 MW/min, (c) DC voltage for 999 MW/min and (d) DC voltage for a step input for both control modes*

As in the previous case, the active power controller can follow the change of the reference point while using different ramping rates without any oscillations in the active power. The performance of the controller can be seen in Figure 33.
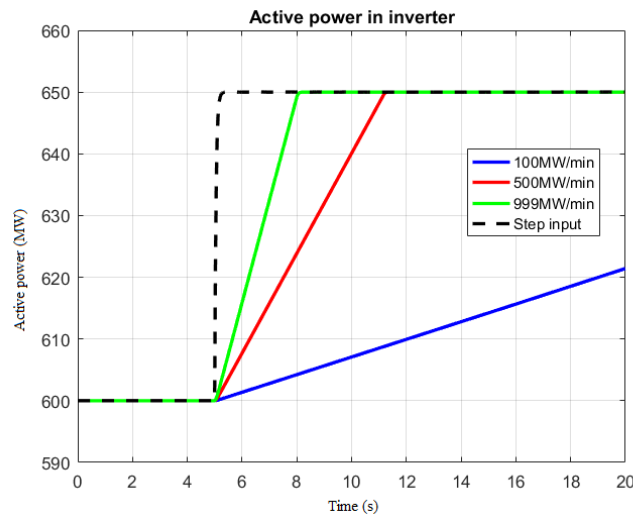


*Figure 33 - Active power response while increasing active power from 600 MW to 650 MW with different ramping rates for both control modes*

## 4.3.3 Third case: Active power response while decreasing from 600 to 400 in Q control mode and AC voltage control mode

In this case an issue has been order for the reduction of active power from 600 MW to 400 MW at 5 seconds. This time the active power regulation will not be performed solely from the AREG function but DREG function as well. The function of AREG is enabled at 5 seconds with a ramping rate of 500 MW/min and after 1 second the DREG function is enabled with the maximum ramping rate available. The total duration of the simulation is 20 seconds.
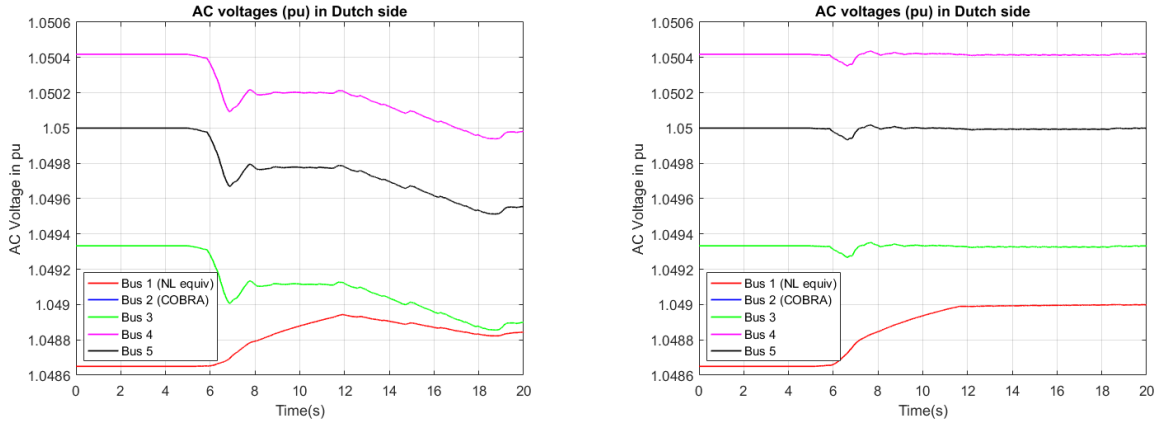
*Figure 34 - AC voltages of the Dutch transmission system while decreasing active power from 600 MW to 400 MW for both control modes*

In Figure 34, the AC voltages experience the same decrease as in the first case when the active power was decreased from 600 MW to 550 MW. The only difference here is the amplitude of the AC voltages which now encounters a bigger voltage dip than in the first case since the amount of power that is being reduced is bigger than in the first case.

After the control mode has been changed to the AC voltage control mode in the inverter station of the Dutch system, the voltages in that system will remain almost constant to their original value, not being affected by both functions (AREG and DREG). It is visible that at 5 seconds only the bus where the equivalent Dutch network is connected responds to the decrease of active power since it has an excitation system that is able to track the changes in active power.

Although the change in the active power reference and the differences in the AC voltages of the Dutch transmission cannot be associated for the long distance buses, it is clear that the bus where the equivalent network is, is affected by the change in active power when operating in the AC control mode, which is far away from the point of common coupling of the COBRA cable station.
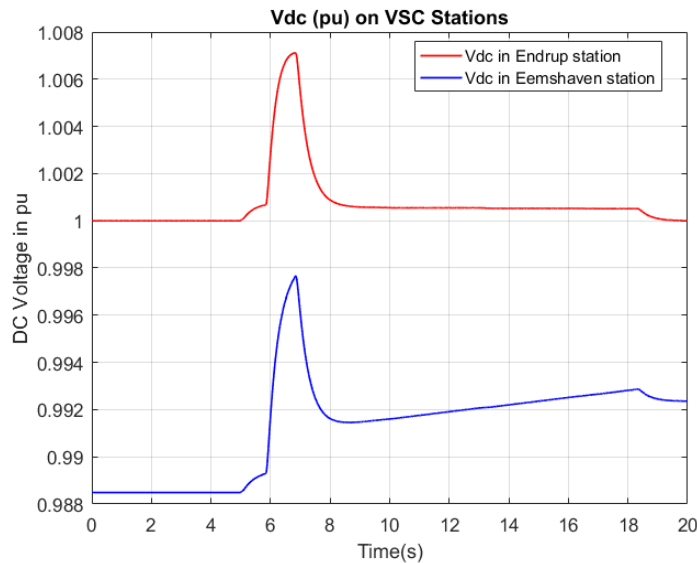


*Figure 35 - DC voltage response while decreasing active power from 600 MW to 400 MW for both control modes*

As it can be observed in Figure 36, the active power is starting to decrease with a ramping rate of 500 MW/min at 5 seconds. After 1 second, DREG is enabled and an order to reduce the active power transmission by 100 MW is given. When the order has been completed, DREG is deactivated, since the set point has been achieved, and then the active power follows the original set point of 400 MW with the ramping rate of AREG. This is why the active power response in the same figure has changes in its direction.

Since the d – axis component of the current is linked with the DC voltage, the reduction of the current has an opposite effect in the DC voltage behavior. In Figure 35, when AREG is enabled, the DC voltage experiences an increase in voltage, which after 1 second experiences an even steeper increase since the DREG has been enabled. It is clear now that depending on the ramping rate of the active power that have been chosen for the AREG and DREG operation the increase or decrease of the DC voltage can be determined.
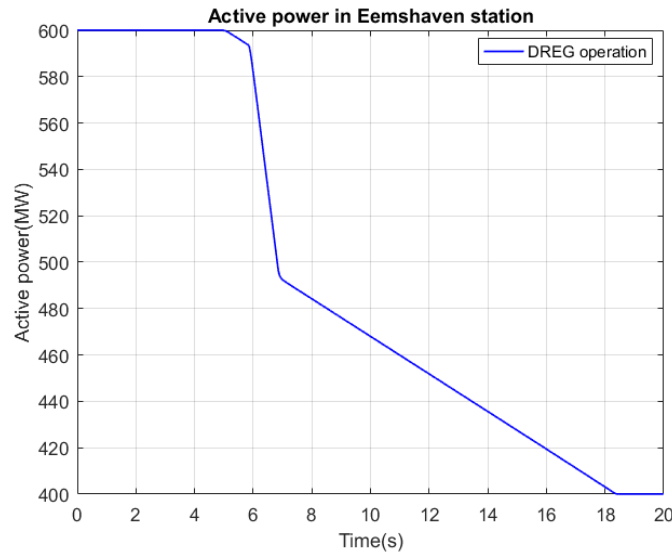


*Figure 36 - Active power response while decreasing active power from 600 MW to 400 MW for both control modes*

## 4.3.4 Fourth case: Active power response while performing a power reversal in Q control mode and AC voltage control mode

In the last case, a power reversal has been issued at 2 seconds. This means that the active power will be reversed from 600 MW to -600 MW with the highest possible ramping rate of 999 MW/min. The AREG function will assist with the power reversal and is being activated at 2 seconds. The total duration of the simulation is 50 seconds.
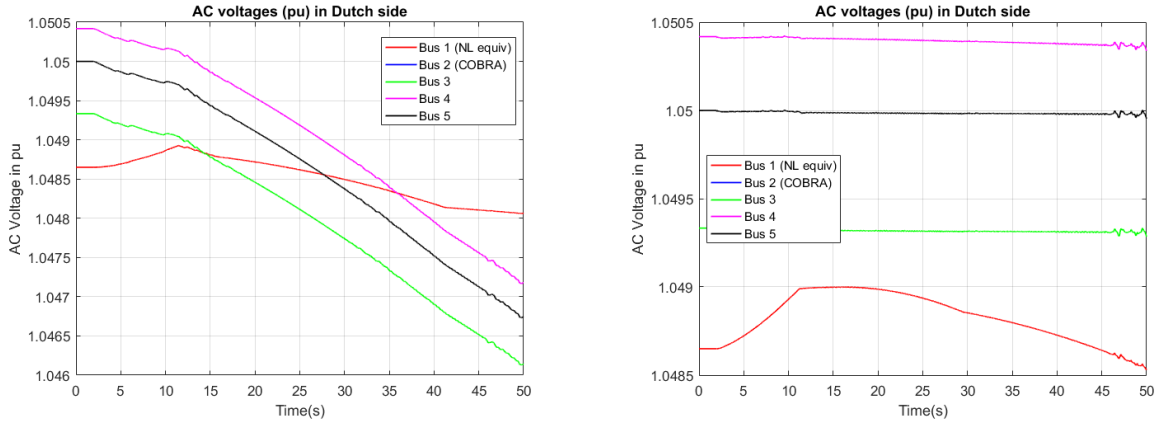
*Figure 37 - AC voltages of the Dutch transmission system while performing a power reversal from 600 to -600 MW for both control modes*

In Figure 37, the AC voltages of the Dutch network for both control modes can be observed. Comparing this graph with the graphs in the previous cases one might conclude that the power reversal created the biggest voltage dips for the buses of the Dutch network. However, when the inverter station is operated in the AC voltage control mode, it is capable of keeping the AC voltage of the buses of the Dutch transmission system almost constant and around their initial values.

The same reasoning behind the long distance buses applies here for the AC control mode. The bus where the equivalent network is connected is affected by the change of the active power reference and tries to react to the changes through an AVR.
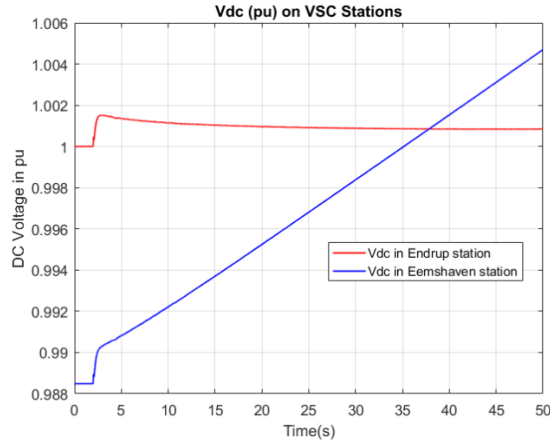


*Figure 38 – DC voltage response while performing a power reversal from 600 to -600 MW for both control modes*

To transmit power through the HVDC link, the DC voltages at both ends should be different. Since the rectifier controls the DC voltage around 1 pu, this means that the inverter station should have DC voltage less than 1 pu in order to secure the flow of active power from the rectifier station to the inverter station. While performing a power reversal, the DC voltage of the inverter station gradually rises towards the 1 pu. The behavior of the DC voltage can be seen in Figure 38. When the DC voltage of the inverter station reaches 1 pu, there is a point in time that the active power has reached zero as seen in Figure 39. After that point, the DC voltage rises above 1 pu and will reach a new stable point when the power reversal has been completed. Since the voltage of the inverter station has become more than 1 pu the active power flow has now changed and the transmission of the active power is now from the inverter station to the rectifier station.
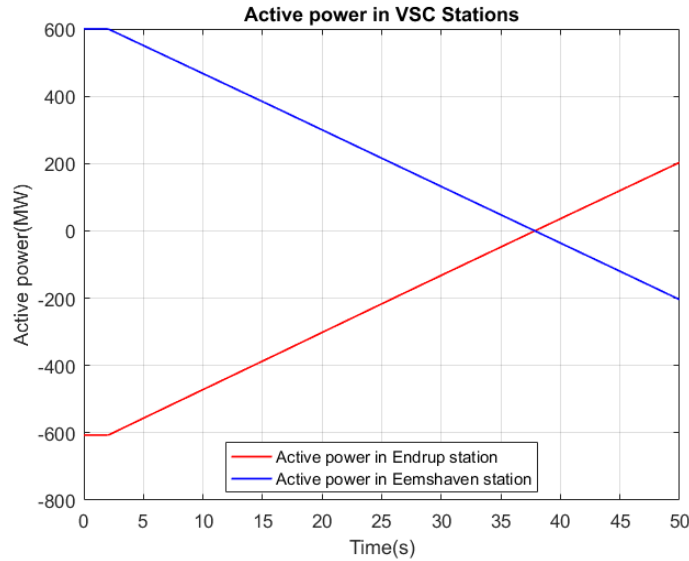
*Figure 39 - Active power response while performing a power reversal from 600 to -600 MW for both control modes*

## 4.4 Reactive power controller performance

To test the performance of the Q controller, an order has been issued to change the reactive power reference of the station is changed from 180 MVAr to 230 MVAr at 5 seconds, while using different reactive power ramping rates to achieve the new reference point. The ramping rates used in this paragraph are 50 MVAr/min, 200 MVAr/min and 350 MVAr/min. The activation of the ramping of the reactive power is happening at 5 seconds. The total time of the simulation is 20 seconds. When the new reference point has been reached, the ramping of the reactive power stops.
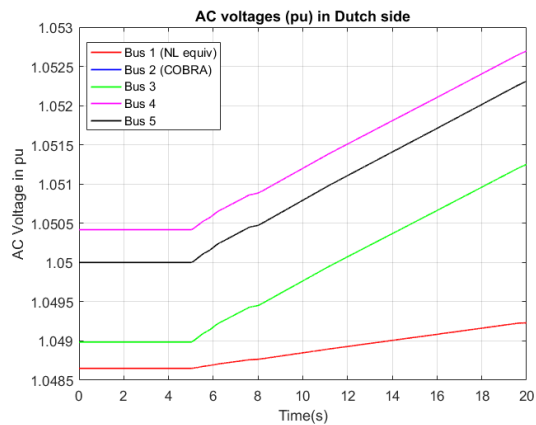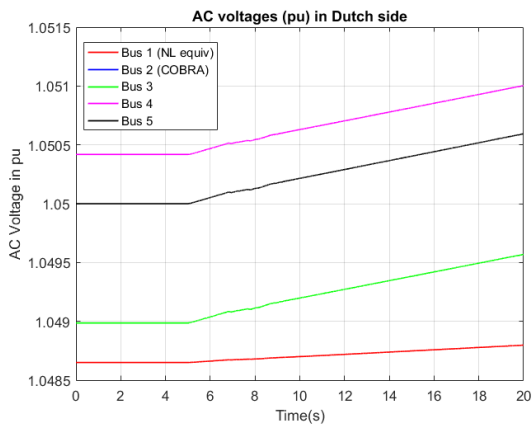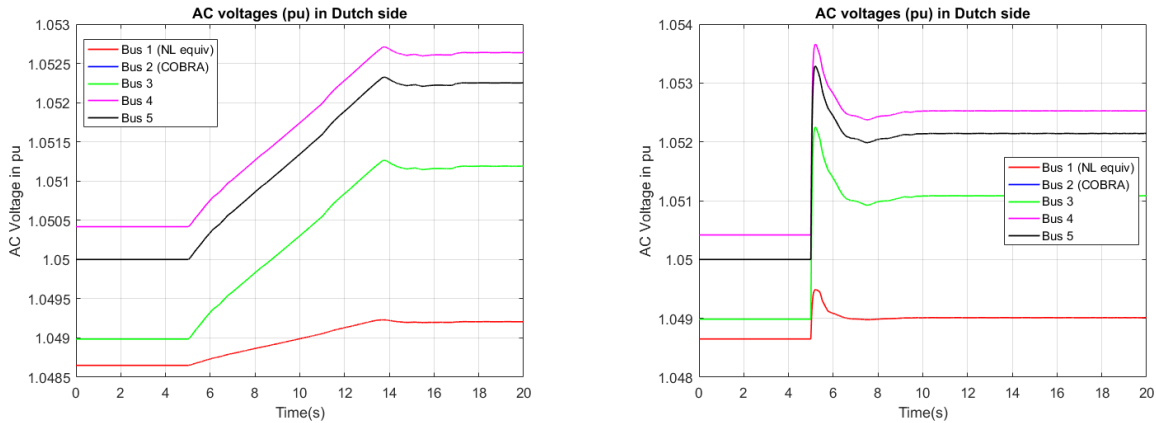
*Figure 40 - AC voltages of the Dutch transmission system while increasing reactive power from 180 MVAr to 230 MVAr. (a) AC voltages for 50 MVAr/min, (b) AC voltages for 200 MVAr/min, (c) AC voltages for 350 MVAr/min and (d) AC voltages for a step input*

It is clear that by ramping the reactive power up to 230 MVAr, the AC voltages of the buses will start to rise. However, this increment is not very extreme since the values did not deviate much from the original point of operation. For example, in Figure 40 (c), for Bus 2 (blue curve), which is the same as Bus 3 (yellow curve), the increment is only by 0.0022 pu.
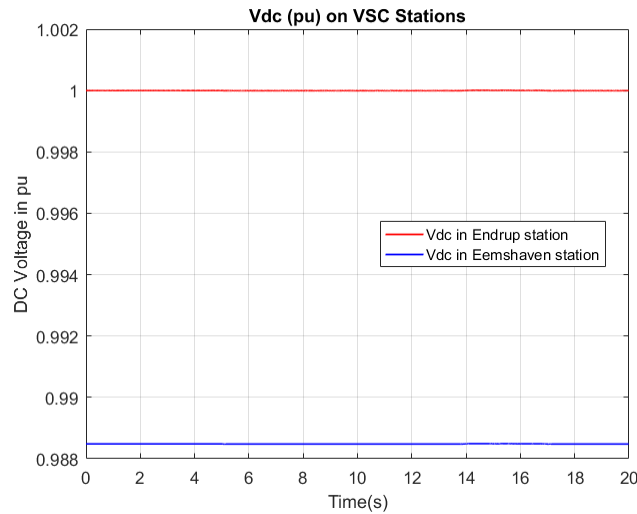


*Figure 41 - DC voltage response while increasing reactive power from 180 MVAr to 230 MVAr*

While AC voltages experience a small increase, in Figure 41, the DC voltage does not experience any change since it is linked with the d – axis component of the current. Furthermore, if there is no change in the active power transmitted through the link then there is no change in the DC voltage behavior.

In Figure 42, the response of the reactive power with different ramping rates can be seen. It is clear that the reactive power controller at the inverter station can follow the changes of the reference point while using different ramping rates without any oscillations.
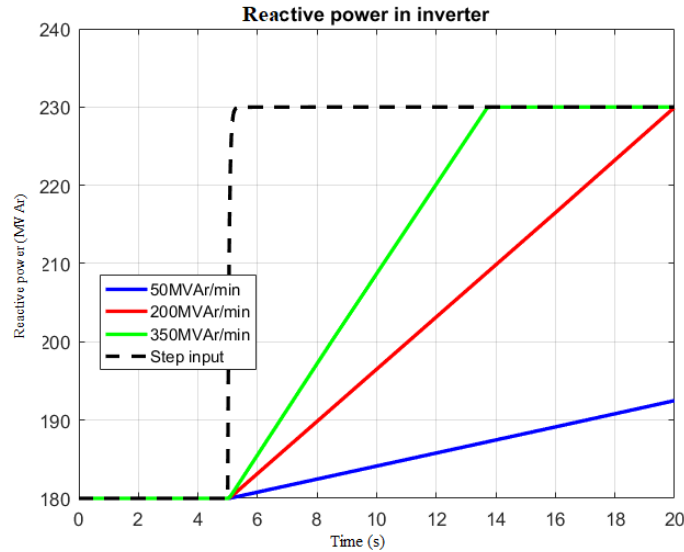
*Figure 42 - Reactive power response while increasing reactive power from 180 MVAr to 230 MVAr*

The AC voltages in the Dutch system are clearly affected by the rise of the reactive power injection of the converter station. Although buses 2, 4 and 5 (blue, magenta, yellow curves in Figure 40) experience a rise in the voltage due to injection, buses 1 and 3 (red and green curves in Figure 40) experience a rise as well. The buses are connected close to generators that are provided with an excitation system, able to track the change in the voltage. Since the injection has an immediate effect in the AC voltage (rise) these two buses should, by definition, reduce the AC voltages in their respective buses. This effect shows that the excitation system lacks of an integral part and provides only a proportional error and it is not able to track the changes in the voltage. That is why the sudden increase of the AC voltages in these two buses is happening.

## 4.5 AC voltage controller performance

Another case was observed regarding the performance of the AC voltage controller. For this case, the inverter station will be operated in AC voltage control mode. The voltage of the bus that COBRAcable is connected is equal to 1.05 pu and assuming that this is the 1 pu level, two responses was tested. The first one was to increase the voltage by 1% of the nominal voltage, meaning 1.06 pu and the second one to reduce the voltage by 1%, meaning 1.04 pu. For each of these cases, the AC voltage behavior of the Dutch system will be studied. The cases are listed in Table 3.

| First case | AC voltage increased by 1% |
|---|---|
| Second case | AC voltage decreased by 1% |

*Table 3 - AC voltage controller cases*

### 4.5.1 First case: AC voltage at point of common coupling increased by 1%

The voltage at the bus where the generator that represents the COBRAcable is connected to is 1.05 pu. Since the first case is about increasing the AC voltage by 1%, the new reference point for the AC voltage controller will be 1.06 pu. With the new reference point now, the performance of the AC voltage controller

will be evaluated. The change of the reference is issued at 5 seconds and the total duration of the simulation is 20 seconds.
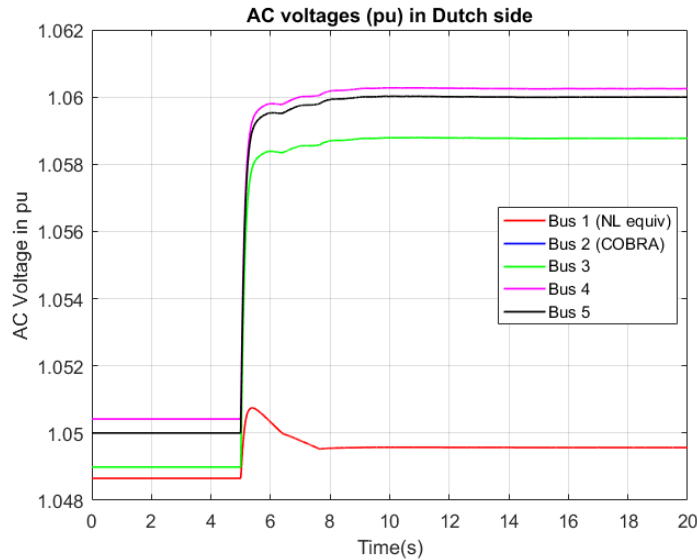


*Figure 43 - AC voltages of the Dutch transmission system for an increase of the AC voltage at the PCC by 1%*

From Figure 43, it is clear that the new reference point of 1.06 pu (see yellow and blue curve) has been achieved after 3 seconds. The change of the AC voltage at the PCC has created an immediate effect to the voltages of the other buses which they have been increased as well.

The reactive power of the station should be increased in order to compensate the increase of the AC voltage of the bus of the point of common coupling. In Figure 44, the reactive power injection of the inverter station can be seen. The converter station starts at 180 MVAr and at 5 seconds the injection starts to increase. After 12 seconds, the reactive power has been settled at a value around 445 MVAr which is above the rated reactive power capability of the converter and clearly violates the upper limit of 230 MVAr.

Like in this case, the increase by 1% of the AC voltage of the bus at the point of common coupling, which is a dynamic phenomenon, creates a reactive power injection that surpasses the rating of the converter. In order to increase the voltage by 1% while using the AC voltage controller, the reactive current must also increase (see equation 3.26). This increase of the reactive current will result in an increase of the reactive power injected by the converter station. Someone would expect that injection of the converter would be inside the capabilities of it, however in these case the solution of the space vector theory and the solution of the power flow solutions that are used (see above), do not match, thus this violation exists.
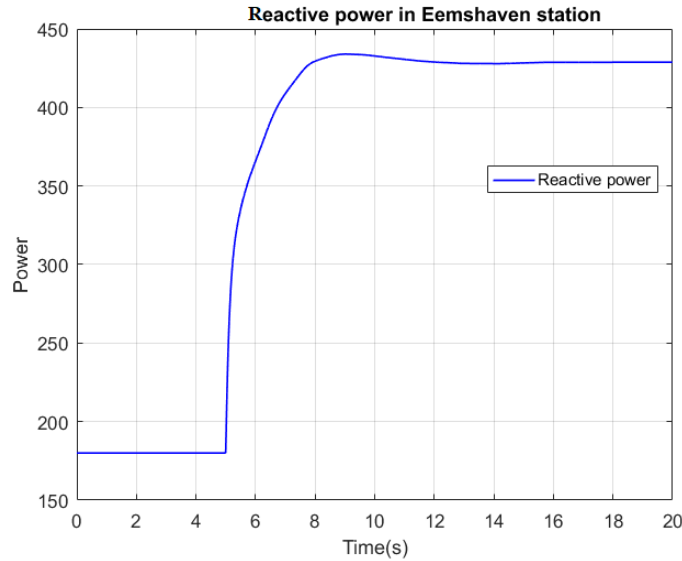
*Figure 44 - Reactive power of the inverter station for an increase of the AC voltage at the PCC by 1%*

### 4.5.2 Second case: AC voltage at point of common coupling decreased by 1%

On the other hand, in the second case, the AC voltage at the point of common coupling has been decreased to 1%. Since the voltage at the PCC is 1.05 pu, a decrease by 1% results the new reference point of 1.04 pu. The reference has been changed at 5 seconds and the total duration of the simulation is 20 seconds.
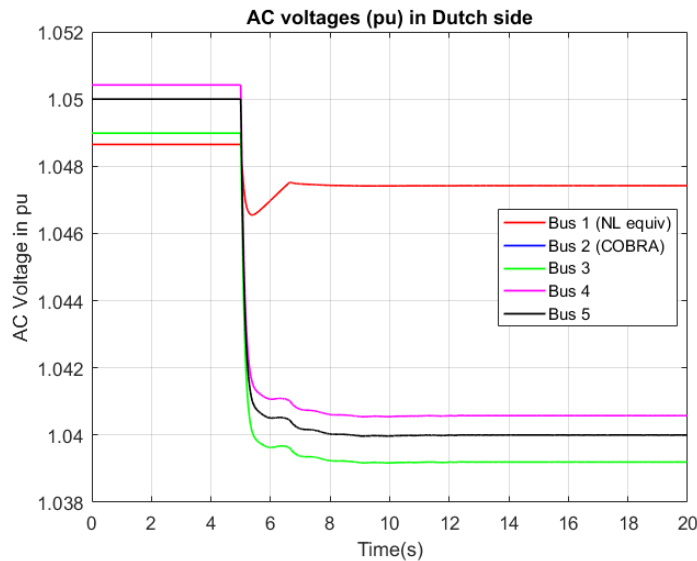


*Figure 45 - AC voltages of the Dutch transmission system for a decrease of the AC voltage at the PCC by 1%*

In Figure 45, the AC voltages of the Dutch transmission system can be seen. Since the AC voltage is being decreased so is the reactive power injection of the station. The new value of the reactive power injection is now – 75 MVAr. It is only natural that this drop of the reactive power will create a drop in the AC voltage

of the buses of the Dutch system, something that is observed in the aforementioned figure. The AC voltage at the PCC has settled in the new reference point at 8 seconds.
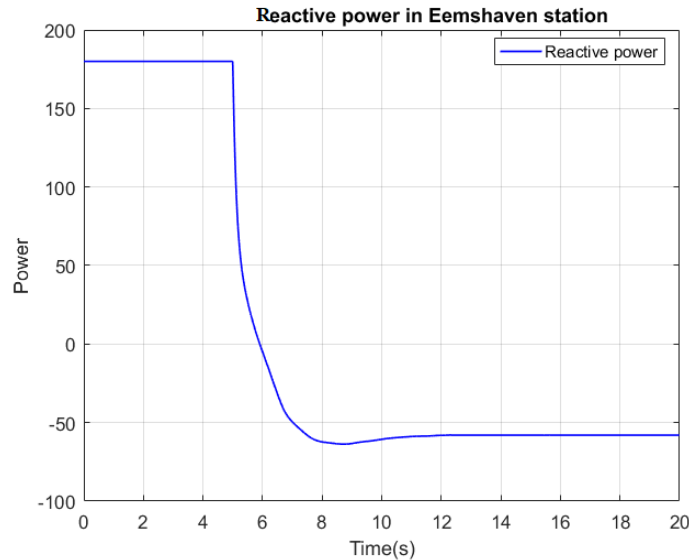


*Figure 46 - Reactive power of the inverter for a decrease of the AC voltage at the PCC by 1%*

The reactive power is trying to compensate the reduction of the AC voltage by changing the injection of the station. The behavior can be observed in Figure 46. When decreasing to the 1.04 pu, the violation does not exist anymore since the converter remains inside its capabilities due to the fact that the solution of the space vector theory and the power flow solutions match. A discussion about the capabilities of the converter are given in paragraph 4.7.

## 4.6 Fault ride through investigation

In this paragraph, the fault ride through (FRT) capability of the inverter station will be investigated. For that reason, three phase faults will be simulated across the system, in buses where no generation exists. The evaluation will be performed with both equations discussed in paragraph 4.2.3. The results of this investigation will determine how FRT capability helps to boost the voltage at the point of common coupling of the COBRAcable in the Dutch network.

| First case | Bolted fault and a high impedance fault at bus 3 |
|---|---|
| Second case | Bolted fault and a high impedance fault at bus 4 |
| Third case | Bolted fault and a high impedance fault at bus 5 |
| Fourth case | Bolted fault and a high impedance fault at bus 6 |
| Fifth case | Bolted fault and a high impedance fault at bus 7 |

*Table 4 - Fault ride through capability cases*

As mentioned earlier, three phase faults will be simulated in the Dutch transmission system, in buses, where there is no generation. As seen from Figure 25, there are five buses that meet this criteria. There are three buses at 380 kV level and two buses at 220 kV level. The duration of the fault will 200 ms whereas the total duration of the simulation will be 0.5 seconds. The fault starts at 0.1 seconds. The FRT capability will be

evaluated with the equations introduced in paragraph 3.5.7. The alpha variable for equation (3.35) in all the cases is 0.0001. The cases can be seen in Table 4.

### 4.6.1 First case: Bolted fault and a high impedance fault at bus 3

For the first case two instances are distinguished: a bolted fault (nominal voltage goes to zero) at bus 3 and a high impedance fault, which dips the voltage at 70% of the nominal voltage. In each case, the AC voltage of the point of common coupling of the COBRA cable will be evaluated as well as the performance of the FRT capability and the response of the DC voltage.
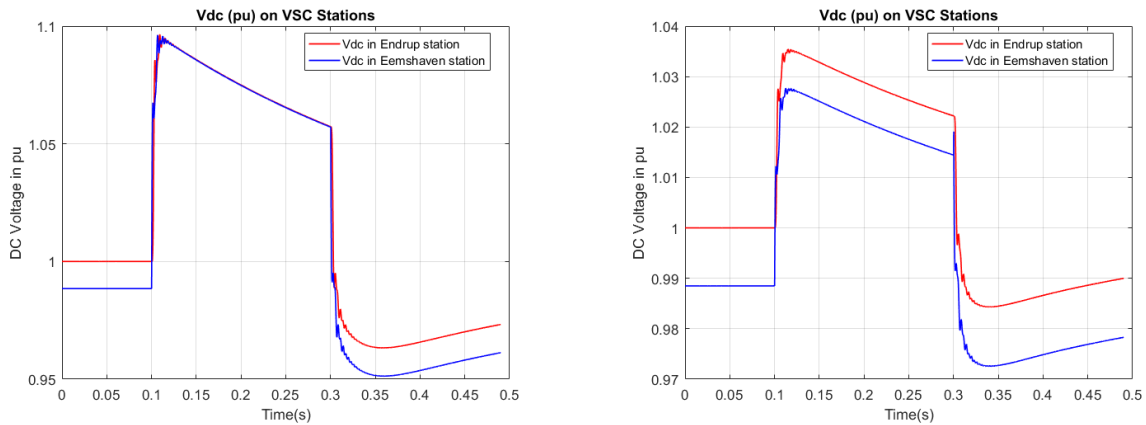


*Figure 47 - DC voltage response. (a) Bolted fault and (b) High impedance fault in bus 3*

For a bolted fault at bus 3, in Figure 47 (a), the DC voltage can be seen. The duration of the fault is 200 ms and it can easily be seen that the DC voltage peaks at around 1.1 pu resulting a rise of 10% of the nominal value while the lower part peaks at 0.95 pu of the nominal value. In this case the cable voltage limits are not violated by a fault of that magnitude. On the other hand, in Figure 47 (b), the case of a high impedance fault can be seen. The fault is not as severe as for the previous case and the DC voltage response is far away from the violation limits.
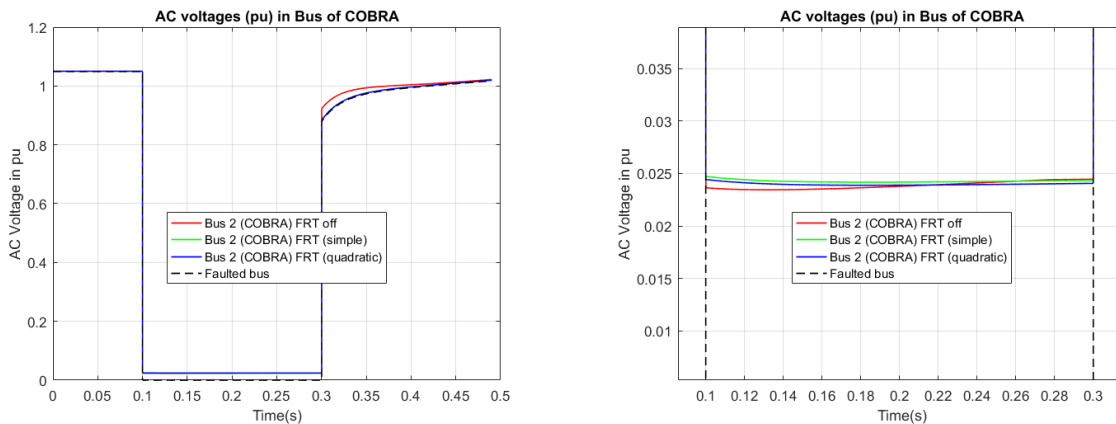


*Figure 48 - Contribution of the inverter station for a bolted fault in bus 3*

For a bolted fault at bus 3, the voltage goes directly to zero, thus resulting a dip in the voltage of the bus of the point of common coupling (red curve in Figure 48). By applying equation 4.1 (green curve), the inverter

station is able to boost the voltage of the bus of the point of common coupling to 0.0025 pu. Using the second equation (4.2), the voltage is again increased by almost the same value.
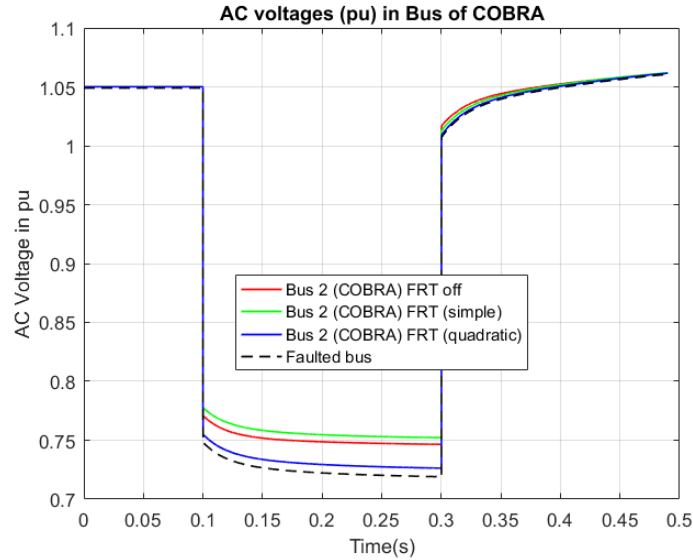


*Figure 49 - Contribution of the inverter station for a high impedance fault in bus 3*

A completely different behavior can be seen in Figure 49. Here the same equations are used. While using the equation 4.1, there is an increase of the voltage by 0.05 pu, whereas in the case of the equation 4.2, the voltage is kept below the case where there is no FRT contribution.

## 4.6.2 Second case: Bolted fault and a high impedance fault at bus 4

For the second case, a bolted and a high impedance fault is performed at bus 4 for a duration of 200 ms. The DC voltage response of the system as well as the contribution of the inverter station to the bus of the point of common coupling for the two faults will be analyzed here.
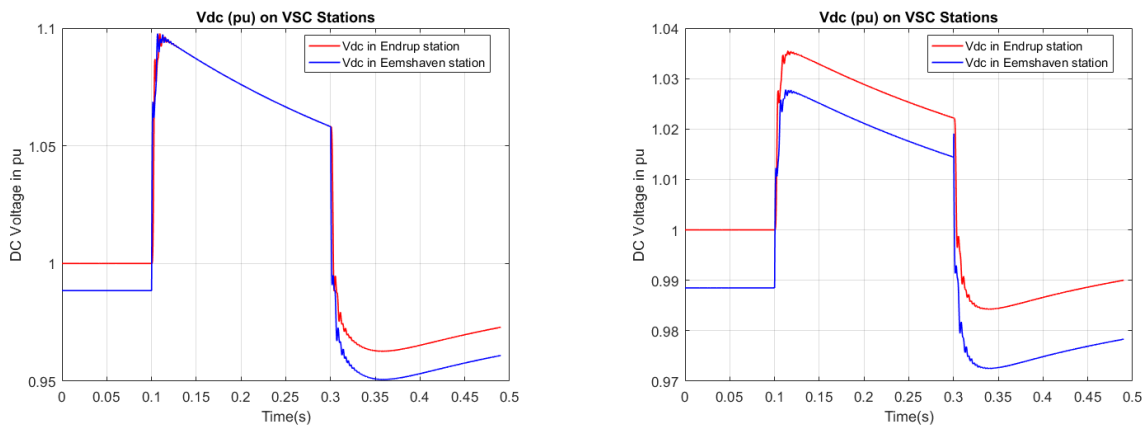


*Figure 50 - DC voltage response. (a) Bolted fault and (b) High impedance fault in bus 4*

The DC voltage response in this case is the same as in the first case for a fault at bus 3. In Figure 50, there is no violation of the upper and lower voltage limits of the DC cable. In Figure 51, the bus of the point of common coupling can be seen, in different instances. In red curve the voltage of the bus without the FRT capability enabled can be seen. Using both equations, the contribution in the voltage is pretty similar. The boost of the voltage is of the magnitude of 0.005 pu.
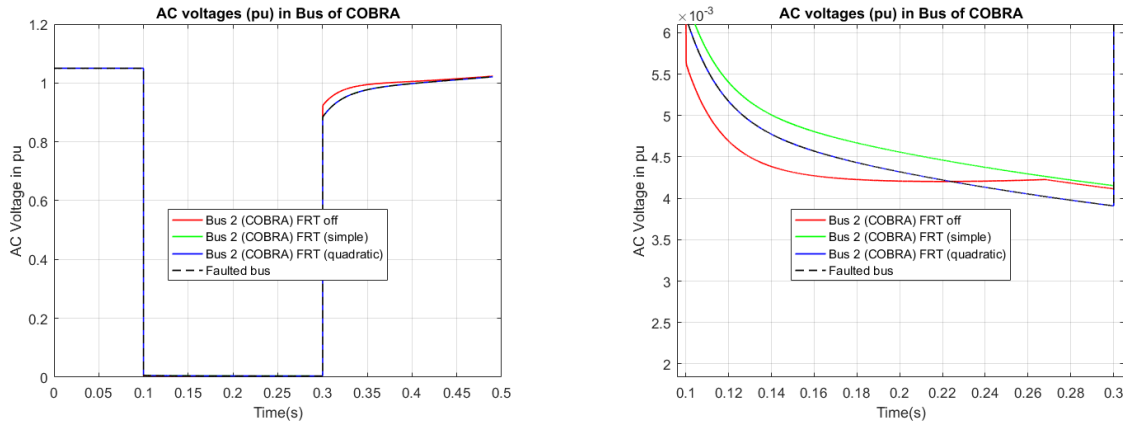


*Figure 51 - Contribution of the inverter station for a bolted fault in bus 4*

For a high impedance fault, the contribution of the two equations can be seen in Figure 52. Equation (4.1) offers a bigger contribution in voltage than equation 4.2.
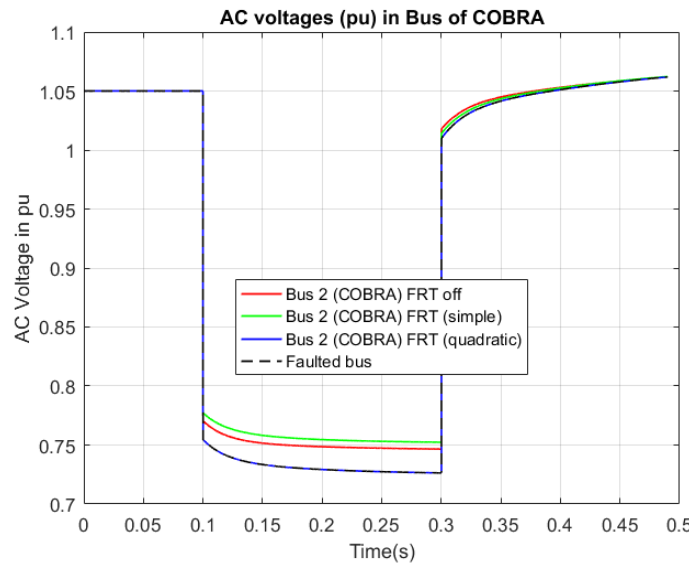


*Figure 52 - Contribution of the inverter station for a high impedance fault in bus 4*

### 4.6.3 Third case: Bolted fault and a high impedance fault at bus 5

Like in the two previous cases, a bolted and a high impedance fault is performed at bus 5 for a duration of 200 ms. The DC voltage response of the system as well as the contribution of the inverter station to bus of the point of common coupling for the two faults will be analyzed here.
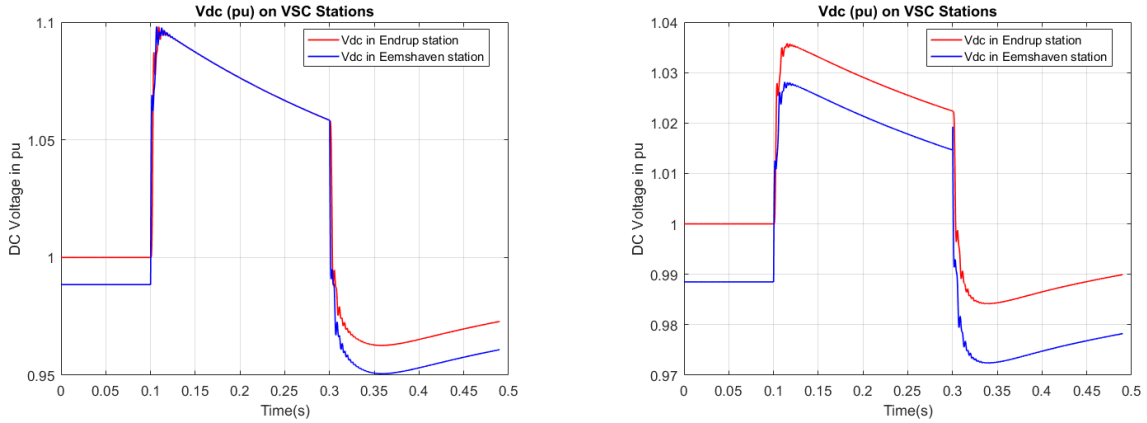
*Figure 53 - DC voltage response. (a) Bolted fault and (b) High impedance fault in bus 5*

As in the previous cases, the response of the DC voltage is almost the same. The fault is performed for 200 ms and for that period the DC voltage experiences two peaks, the first one at around 1.1 pu and the other one at 0.95 pu. In the case where there is a high impedance fault the severity of the fault is decreased which means that the effect in the DC voltage is also decreased as seen in Figure 53 (a) and (b).
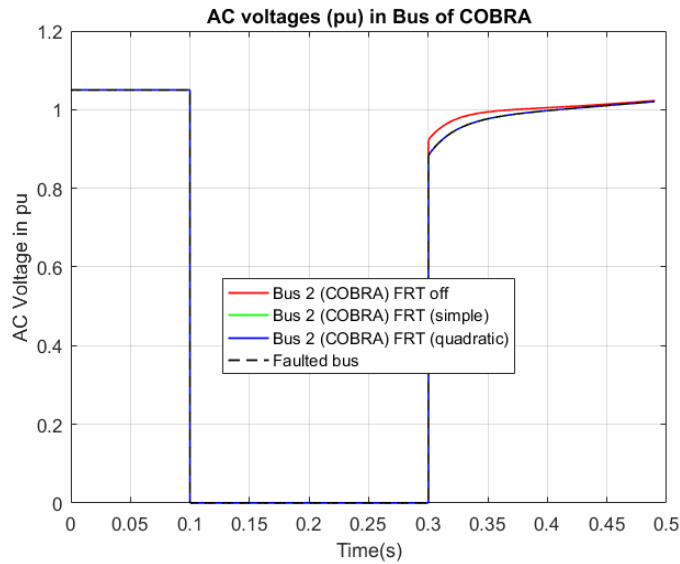


*Figure 54 - Contribution of the inverter station for a bolted fault in bus 5*

Due to the fact that the line connecting bus 5 and the PCC of the COBRAcable is really small, simulating a fault at bus 5 is like simulating a fault at the PCC. The contribution of the inverter station for both cases (bolted and high impedance fault) can be seen in Figure 54. It is clear that the fault is so severe that neither equation (4.1) or (4.2) can increase the voltage. In Figure 55, the contribution for a high impedance fault can be seen. Likewise, the behavior is the same as in the previous case of bus 4 where equation (4.1) is actually performing better than equation (4.2).
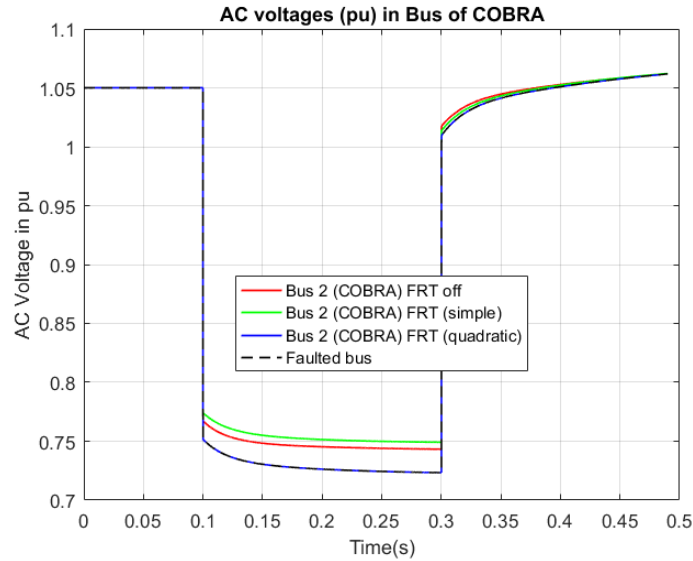
*Figure 55 - Contribution of the inverter station for a high impedance fault in bus 5*

### 4.6.4 Forth case: Bolted fault and a high impedance fault at bus 6

While the previous cases where in the 380 kV level, the fourth and fifth case are at 220 kV level. In the fourth case a bolted and a high impedance fault is performed at bus 6 for 200 ms. The results are listed below.
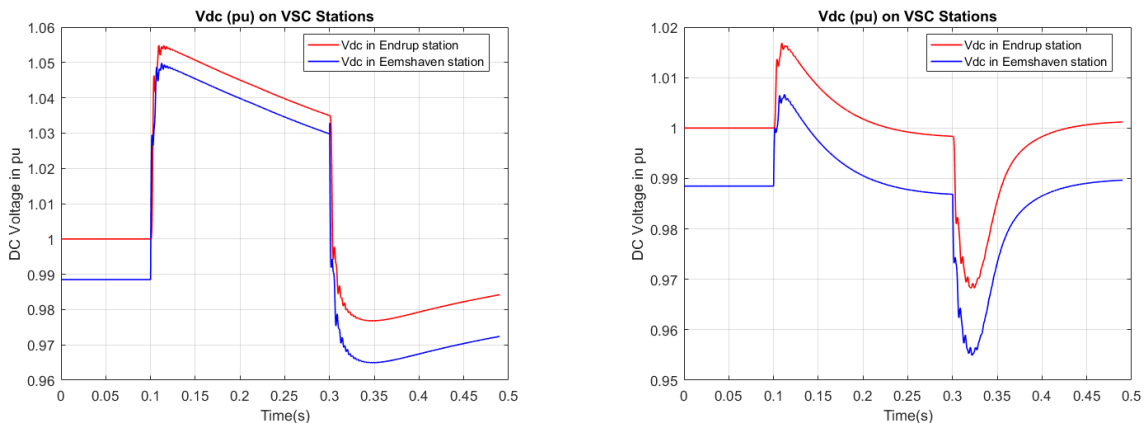


*Figure 56 - DC voltage response. (a) Bolted fault and (b) High impedance fault in bus 6*

The bolted and high impedance fault do not create any violation of the upper and lower limits of the DC voltage. In Figure 56 (a), the DC voltage does not rise more than 1.05 pu and not lower than 0.96 pu, whereas in Figure 56 (b), the voltage does not rise more than 1.01 pu and lower than 0.95 pu.

71
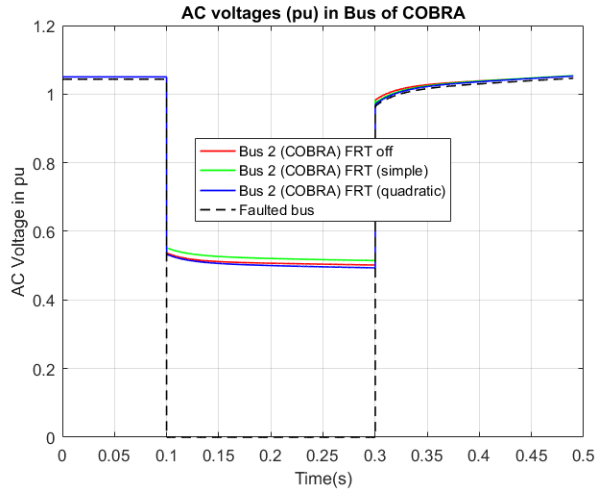
*Figure 57 - Contribution of the inverter station for a bolted fault in bus 6*

The AC voltages in Figure 57 are affected by the bolted fault in bus 6. Although the fault did not have a huge impact into the DC voltage, the AC voltage at the point of common coupling has been reduced to 0.5 pu. The green curve (equation 4.1) helps to boost the voltage, whereas, the blue curve (equation 4.2) increases the voltage slightly in respect to the red curve (FRT capability off).
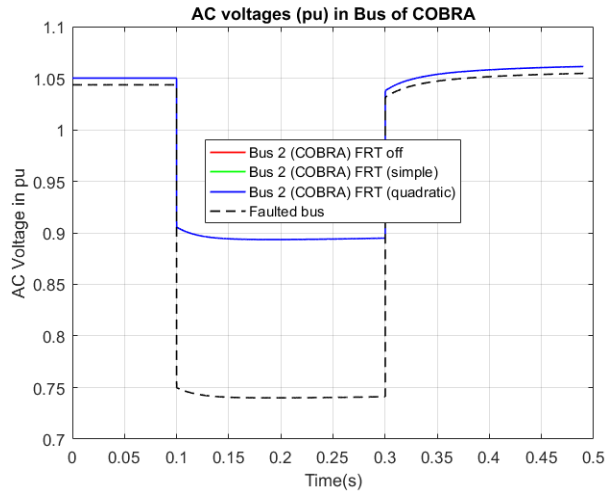


*Figure 58 - Contribution of the inverter for a high impedance fault in bus 6*

For a high impedance fault (Figure 58), the voltage at the point of common coupling is slightly affected. As mentioned in the paragraph 4.2.3, the activation of the equations regarding the fault ride through capability require that the voltage at the PCC is below 0.85 pu. Since this criteria is not satisfied, there is no contribution from the converter station.

## 4.6.5 Fifth case: Bolted fault and a high impedance fault at bus 7

In the last case, a bolted and a high impedance fault is performed at bus 7. The results of the fault can be seen in the following figures.
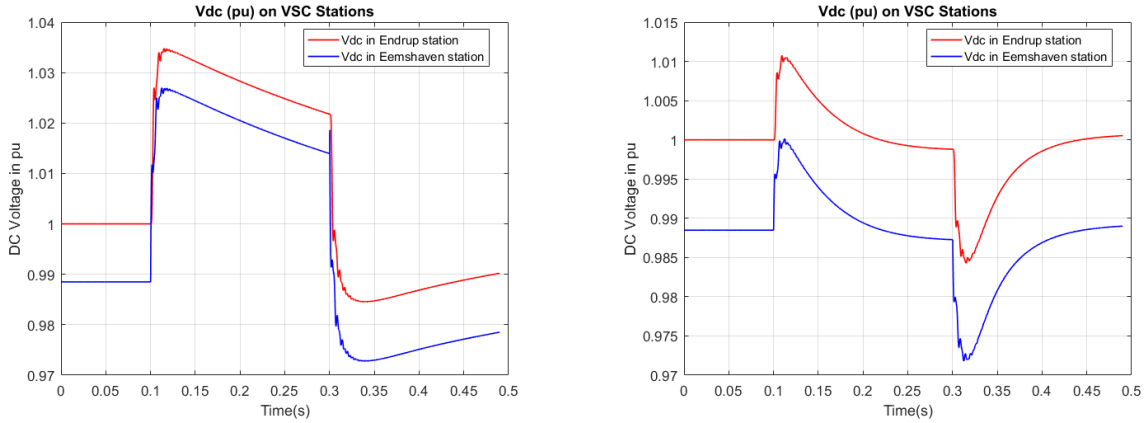
*Figure 59 - DC voltage response. (a) Bolted fault and (b) High impedance fault in bus 7*

Due to the fact that the fault is performed in a different voltage level (Figure 59), the severity is completely different than in the previous three cases. Even for a bolted fault the DC voltage does not rise more than 1.04 pu or 0.97 pu. For a high impedance the voltage does not rise more than 1.01 pu and 0.97 pu.
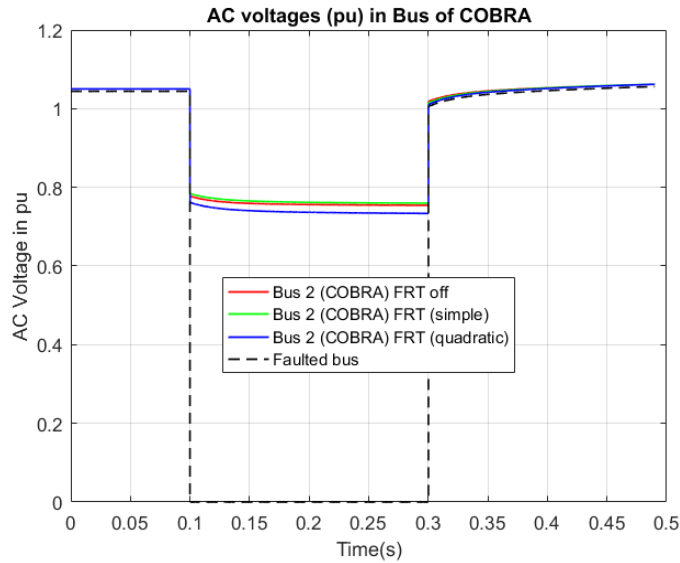


*Figure 60 - Contribution of the inverter station for a bolted fault in bus 7*

A bolted fault in bus 7 inflicts a dip in the voltage which affects the bus of the point of common coupling. Again, equation (4.1) performs better than equation (4.2), which fails to boost the voltage. In Figure 60, it can be observed that the blue curve (equation (4.2)) is below the red curve which is when the FRT capability is off.
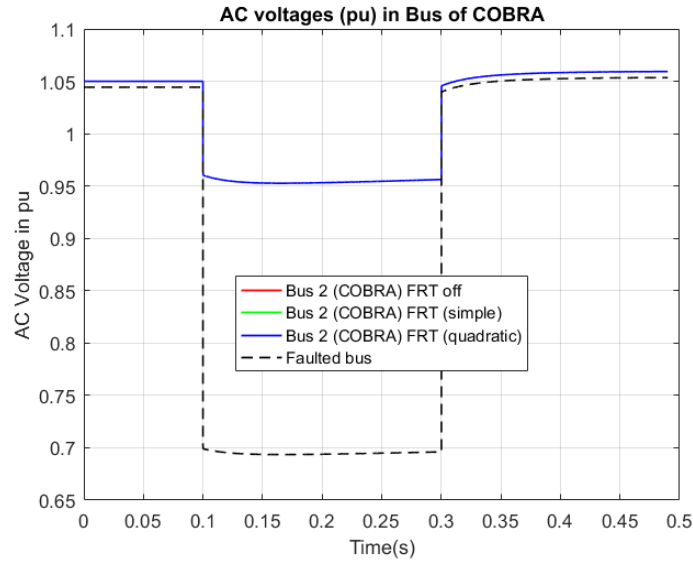
*Figure 61 - Contribution of the inverter station for a high impedance fault in bus 7*

The same reasoning can be applied for the case of a high impedance fault in bus 7. Since the voltage at the PCC has not been dropped below 0.85 pu, there is no contribution from the converter station. The results can be observed in Figure 61.

## 4.7 Conclusions

From the results, some conclusions can be drawn regarding the performance of the controllers. Regarding the active power controller, the controller is capable of following the changes of the active power reference with all the ramping rates discussed in the paragraph (4.3). The change in active power changes the reference of d – axis component of the current which affects the DC voltage through the HVDC link. The rate of change of the DC voltage is also linked with the ramping rates used. Higher ramping rates create a steeper response of the DC voltage. Moreover, the AC voltages of the buses in the Dutch network are affected by the changes in reference in active power. Increasing the active power results in an increase of the AC voltages whereas a decrease of the active power results a decrease of the AC voltages. However, as it can be observed from the figures in paragraph (4.3), the increment or decrease of the AC voltages is around the steady state values.

Regarding the DREG function, the controller is again able to track the changes of the ramping rate that are introduced by the AREG and DREG function. The set point of the active power has been set by AREG with a specific ramping rate. At a certain moment in time DREG is also enabled creating a different set point of the active power with the maximum ramping rate. The behavior is also depicted in the DC voltage. As said previously, changing the d – axis component of the current will change the DC voltage. It is important to note, that the model used to create the DREG function can be extended for multiple applications of DREG as it can be seen in Figure 62.
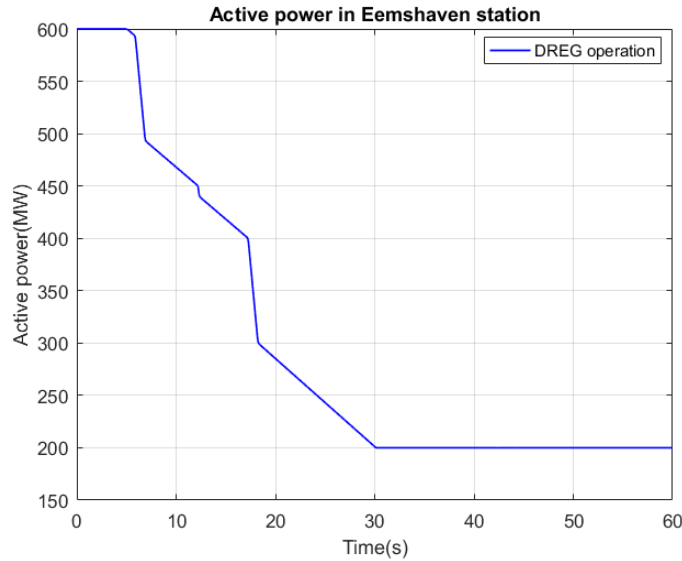
*Figure 62 - Multiple applications of DREG*

Regarding the reactive power controller, the controller is capable of following the changes in the reference of the reactive power stably and without oscillations. The change in the q – axis component of the current does not create any oscillations in the DC voltage. However, by increasing the reactive power injection the AC voltages of the Dutch system are increased. In more details, depending of the ramping rate that is chosen each time, the steepness of the AC voltages can be determined. Like in the active power controller, the AC voltages are kept near the steady state values.

Although the reactive power controller has been tested only for increasing the reactive power injection, the controller is also capable of reducing the reactive power injection with the same ramping rates. The results can be seen in Figure 63. The decrease in reactive power will also have an immediate impact in the AC voltages as well.
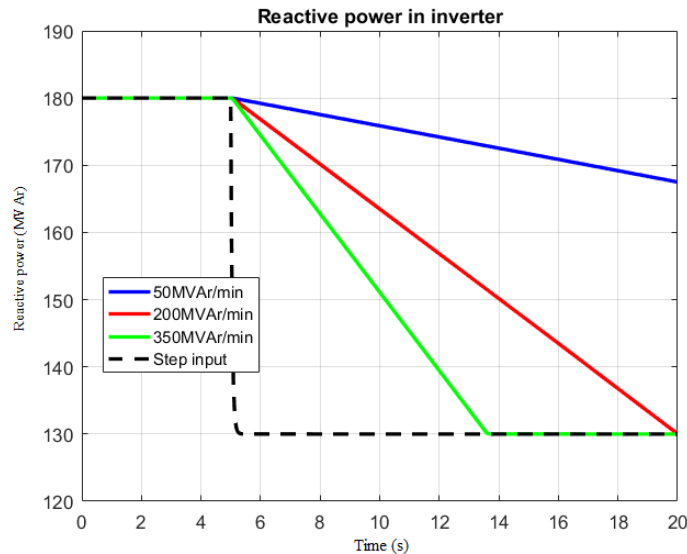


*Figure 63 - Reactive power response while decreasing reactive power from 180 MVAr to 130 MVAr*

Regarding the performance of the AC voltage controller, the investigation has shown that there are limitations in how much the AC voltage can be increased or be decreased which is associated with the reactive power capabilities of the converter station and specifically with the inverter station since this is the station where all the studies have been performed. Since the increment of the AC voltage at the PCC by 1% results in the violation of the reactive capability of the converter station, an investigation was performed to see the limits of the converter regarding the control of the AC voltage at the PCC.
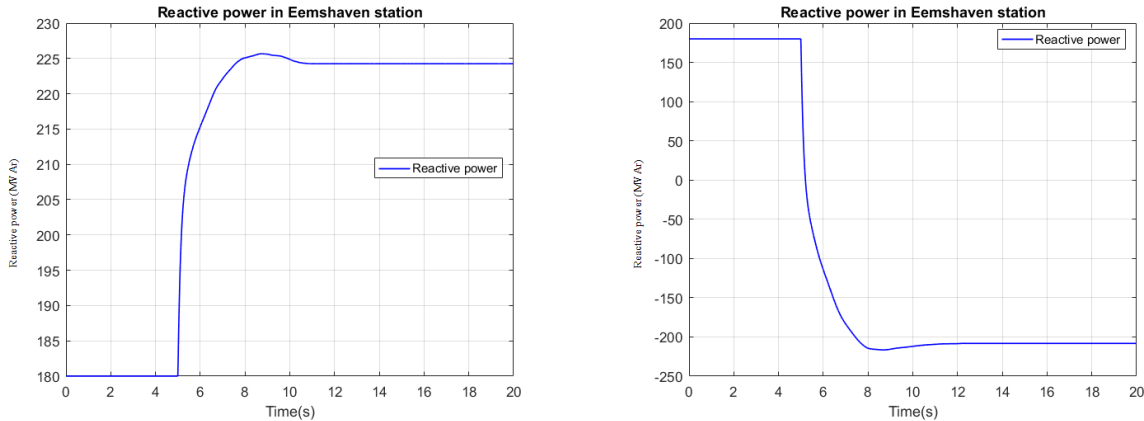


*Figure 64 - Reactive power injection. (a) AC voltage at PCC of 1.052 pu and (b) AC voltage at PCC of 1.034 pu*

Keeping in mind that in the stable operation of the station, the converter contributes is 180 MVAr, in Figure 64, the reactive power injection the increase and decrease of the voltage at the PCC can be seen. The converter station is capable to support the increase of the voltage to 1.052 pu without exceeding the upper limit of 230 MVAr as seen in Figure 64 (a). On the other hand, the converter can also support the decrease of the voltage to 1.034 without exceeding the lower limit of –230MVAr as seen in Figure 64 (b).
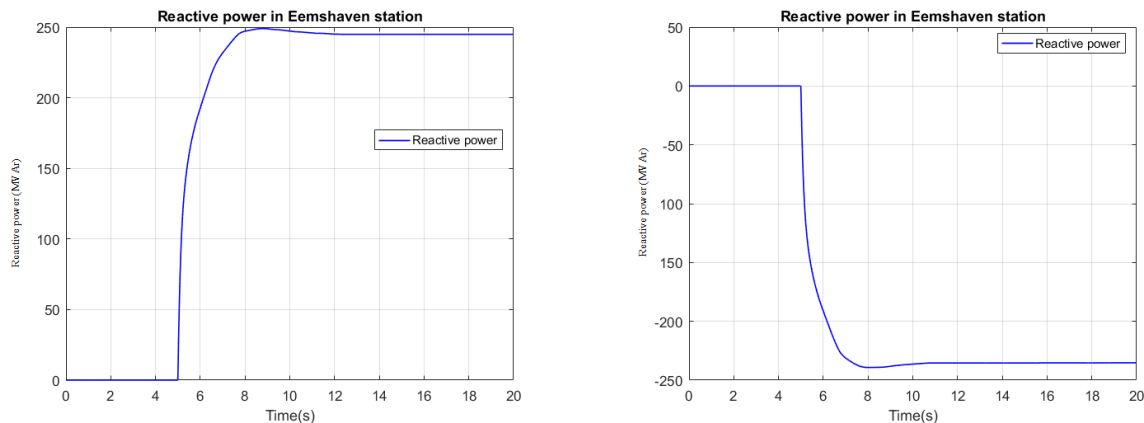


*Figure 65 - Reactive power injection. (a) AC voltage at PCC of 1.06 pu and (b) AC voltage at PCC of 1.04 pu*

An investigation was also held while the converter is contributing 0 MVAr in the stable operation. It is clear that the converter station is not capable of increasing or decreasing the AC voltage by almost 1%, since the capability of the converter has been surpassed, when the steady point of the converter at the beginning is 0 MVAr. The conclusion is that, there is a limit where the increase or decrease of the AC voltage can be compensated by the reactive power injection of the converter and the reason behind that is that the space vector theory and the power flow solutions do not agree when a dynamic event like this appears. It is certain that these kind of limitations appear also in the real converter station and might be part of the COBRA cable specifications.

Regarding the fault ride through capability, the faults that were simulated in buses 3, 4 and 5 (380 kV) resulted a DC voltage response where the DC voltage did not rise more than 10% of the nominal value and not less than 5% of the nominal value. The performance of the two equations in the reactive current injection has shown that equation (3.34) is performing better than equation (3.35). In cases where a bolted fault was simulated, the use of equation (3.34) resulted into the injection of more reactive current than equation (3.35). Due to the fact the line connecting COBRA cable, meaning bus 2 and bus 5 is too small the contribution of the converter for AC faults is small. For a high impedance fault, the contribution of equation (3.34) is again significant whereas equation (3.35) fails to perform better than the case where the FRT is not enabled.

While performing a fault at buses 6 and 7 (220 kV), the DC voltage experiences a small rise less than 5% and the same is happening for the lower value. The response of the converter regarding the contribution of reactive current is less than in the previous cases due to the fact that the fault is happening far away from the PCC. For a bolted fault, equation (3.34) is again better than equation (3.35). For a high impedance fault the FRT equations are not being activated since the voltage at the PCC has not been dropped below 0.85 pu.

# Chapter 5: Comparison of the controllers

## 5.1 Introduction

The comparison of the control structure of the VSC stations created in PSSE was one of the main purposes of this master thesis project. To compare the performance of the control structure, two models were used. One created in PSSE, with the results that were presented in the previous chapter and another model created in Powerfactory. The purpose of this comparison is to see whether the two models can provided the same set of results and if not try to find the reason behind it.

In this chapter, the analysis about the differences between these two models will be discussed as well as the results of the comparison process.

## 5.2 Differences of the models

As discussed in Chapter 3, a set of assumptions were made in order to create the model of the VSC station in FORTRAN and in PSSE software. The assumptions that were made are the following:

- Generator modules like the VSC stations that were used in this thesis are modeled as current sources. This is the typical approach that PSSE adopts for dynamic simulations.
- The model is based on [15]. The Uac, Q, Udc and P control were implemented in this version of the model.
- The inner current control structure of the VSC station is completely missing from the FORTRAN script. Instead, the inner current control structure is replaced by a proportional gain equal to 1. This means that the current references resulted by the outer controllers of the VSC station reach the current almost instantly. This, of course, has reduced the number of differential equations, which resulted in a reduced computational time.
- The phase locked loop (PLL) is also completely missing from the VSC station. It is assumed that the VSC station is able to track perfectly the changes in the bus of the point of common coupling thus no specific reason to create an additional control block was necessary.
- The energy balance of the DC link is not modeled in the PSSE. This means that the rate of change of the active power through the DC link is not properly addressed.

On the other hand, several assumptions during the creation of VSC station in Powerfactory were also considered: The assumptions are the following:

- The model is based again on the [15]. The Uac, Q, Udc, P, U/f , current control based on space vector transformation, PLL and DC voltage protection control approach, were implemented in the model.
- The internal energy balance of the MMC technology is also present in the model. For that reason the DC capacitance of the converter is included in the DC side of the HVDC link. This means that the internal regulation of the MMC is being considered by the DC voltage structure. The circulating current control of the MMC technology is not considered in this RMS model.
- The arm inductance effect of the MMC technology has been also included in the HVDC representation of the COBRA cable model.

Based on the assumptions that were discussed previously, some of the test cases that were introduced in Chapter 4 are used here as well. The comparison of the active and reactive power controller, the DC and AC voltage controller and the fault ride through capability follows.

## 5.3 Active power controller performance

Based on the information provided in Chapter 4, the comparison of the active power controller was compared while using three different cases. The cases used for the comparison can be seen in Table 5:

| First case | Active power response while increasing from 600 to 650 MW |
| --- | --- |
| Second case | Active power response while decreasing from 600 to 400 MW |
| Third case | Active power response while performing a power reversal |

*Table 5 - Active power comparison test cases*

### 5.3.1 First case: Active power response while increasing from 600 to 650 MW

At 5 seconds the active power reference has changed from 600 MW to 650 MW. The change of the active power reference will be assisted by the AREG function while changing the ramping. AREG function is being enabled at 5 seconds, with ramping rates of 100 MW/min, 500 MW/min and 999 MW/min respectively. In Figure 66, the performance of the active power controller while changing the active power reference can be seen for both models.
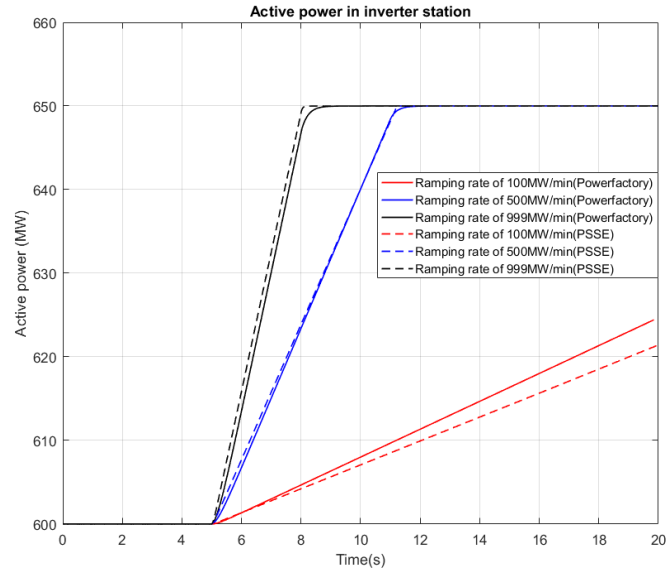
*Figure 66 - Response of the active power controller for both models*

The solid red, blue and black curves represent the performance of the active power controller for the Powerfactory model for the 100, 500 and 999 MW/min ramping rate respectively, whereas, the dashed line, with the same colors represent the performance of the active power controller that was created in PSSE. It is obvious that the model in PSSE is able to follow the response of the Powerfactory model without big differences. The major difference observed in Figure 66 is related to the ramping rate of 100 MW/min where the active power responses of the two models experience a deviation. The deviation associated with this ramping rate is around 3 MW and it is due to the false interpretation of the ramping rate value that was selected in the models.
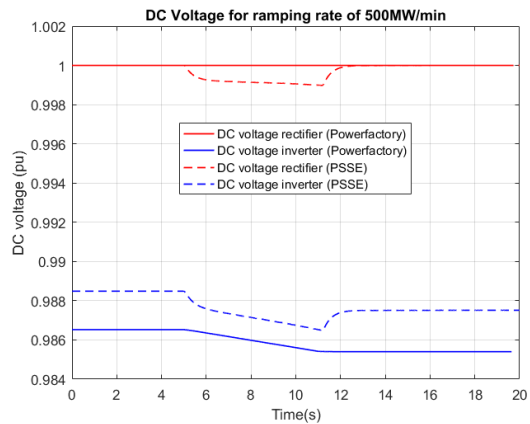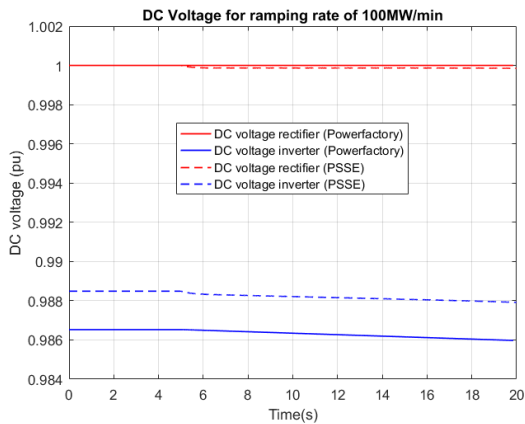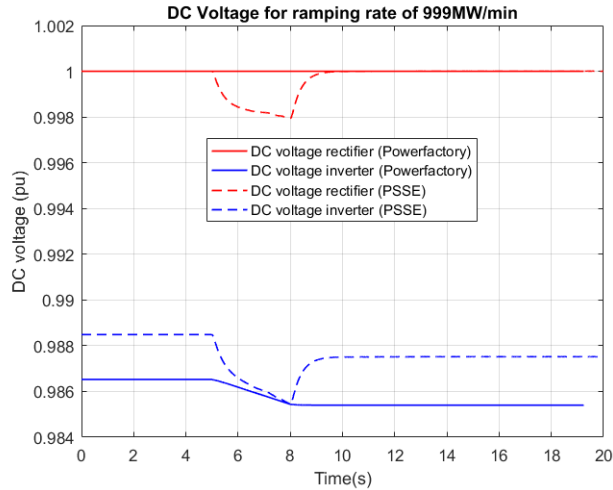
*Figure 67 - Response of the DC voltage controller for both models while using different ramping rates. (a) DC voltage response for 100MW/min, (b) DC voltage response for 500MW/min and (c) DC voltage response for 999 MW/min*

For the ramping rates that were selected, the DC voltage response was also plotted to compare the performance of the DC voltage controller. In Figure 67, the DC voltage response for each of the ramping rates can be seen. The performance of the Powerfactory model can be observed with the solid lines, whereas, the performance of the PSSE model can be seen in the dashed lines. By looking in the figures, the difference between the responses of the two models can be seen immediately. While the rectifier station (red curves) in the Powerfactory model is kept constant in Figure 67 (a), (b) and (c), the rectifier station in the PSSE model is immediately reacting to the change of the ramping rate. The reason why this happens is twofold. Firstly, the inner current controller is being replaced with a proportional gain equal to 1, which means that there is no feedback loop to correct the d – axis component of the current. Secondly, the energy balance of the DC link is not being modeled in the PSSE model. The change of rate of the active power in the rectifier station is being changed which means that there will be changes in the d – axis component of the current, whereas, in the Powerfactory model, the energy balance is modeled and the rectifier is capable of keeping the DC voltage constant at 1 pu. The behavior of the inverter station is completely normal for both models due to the fact that this is the station where the change of active power is happening and it should be the only station reacting to that change while in the rectifier station, the DC voltage should remain constant.

### 5.3.2 Second case: Active power response while decreasing from 600 to 400 MW

In the second case, in order to compare the performance of the combination of AREG and DREG functions, the active power reference has changed from 600 to 400 MW. Again as in the previous case, at 5 seconds, the active power reference has been changed to 400 MW. After 1 second, the DREG function is enabled, resulting a reduction of the active power by 100 MW with a very fast ramping rate. In Figure 68 (a), the reduction of the active power controller can be observed for both models. With the solid line, the performance of the Powerfactory model can be observed, whereas, with the dashed line, the performance of the PSSE model can be observed. It is clear that the performance of the PSSE model is similar to the performance of the Powerfactory model. The PSSE model is able to follow the changes in the ramping rate, which at first is dictated by the AREG function (500MW/min) and then by the DREG function. The differences between the two lines is of the order of 5 to 10 MW.
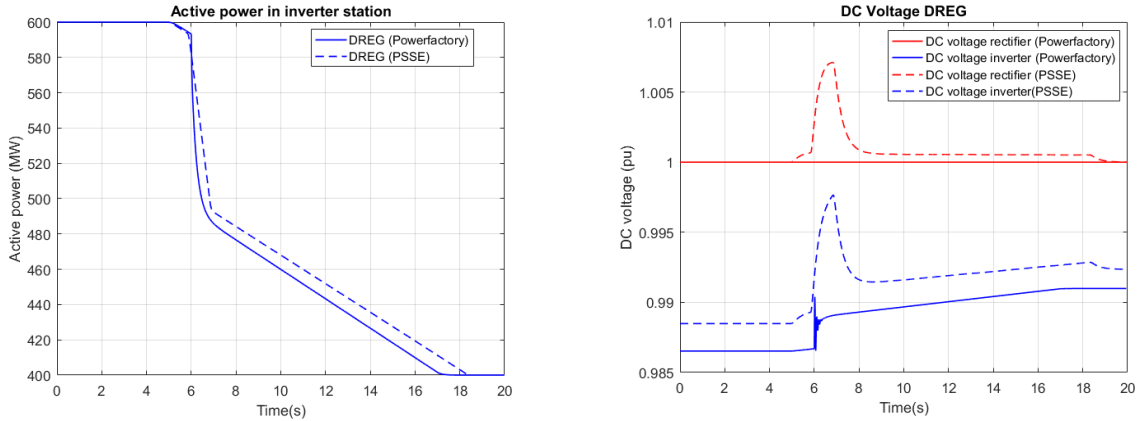
*Figure 68 - (a) Response for the active power controller for AREG and DREG cooperation and (b) DC voltage response for AREG and DREG cooperation*

In Figure 68 (b), the response of the DC voltage, when the AREG and DREG functions are enabled can be seen. As discussed in the first case, the solid lines represent the Powerfactory model whereas the dashed line represent the PSSE model. Since there is absence of the inner current control structure and the energy balance of the DC link, the rectifier station in the PSSE model reacts to the changes of the active power. On the other hand, the rectifier station in the Powerfactory model remains constant at 1 pu.

### 5.3.3 Third case: Active power response while performing a power reversal

The last case of the comparison of the active power controller will be while performing a power reversal. The change of the active power reference has been issued at 2 seconds to – 600 MW with a ramping rate of 999 MW/min.
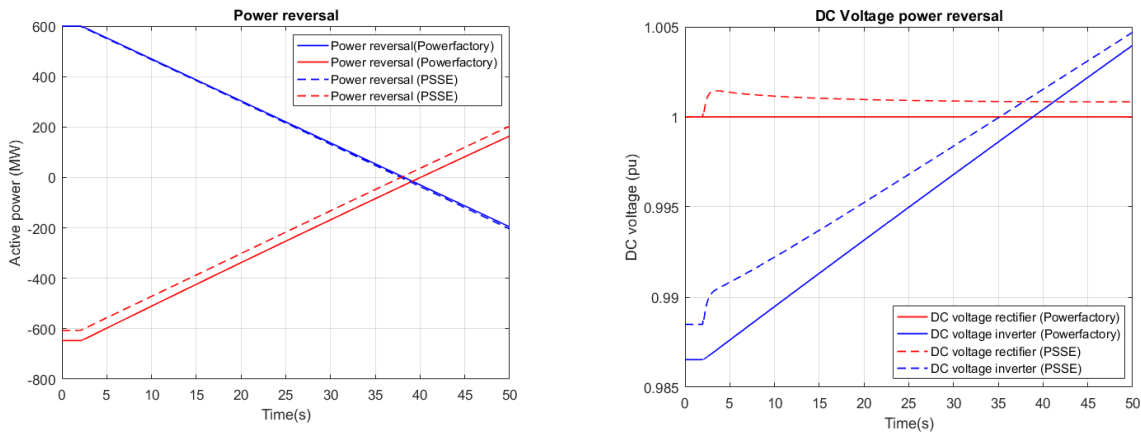


*Figure 69 - (a) Response for the active power controller for a power reversal and (b) DC voltage response for a power reversal*

Again, the performance of the PSSE model is similar to the performance of the Powerfactory model in terms of the active power, as it can be observed in Figure 69 (a). There is a difference between the rectifier stations of the two models but this is due to the fact that the losses of the station of the Powerfactory model is more than the ones in the PSSE model. In Figure 69 (b), the response of the DC voltage can be observed.

The rectifier station again has the big difference between the two models since the same reasoning regarding the previous case can be also used here.

## 5.4 Reactive power controller performance

The comparison of the reactive power controller was performed when the reactive power has been increased from 180 MVAr to 230 MVAr while using three different ramping rates of 50 MVAr/min, 200 MVAr/min and 350 MVAr/min respectively. The reactive performance has been changed at 5 seconds and the results can be observed in Figure 70.
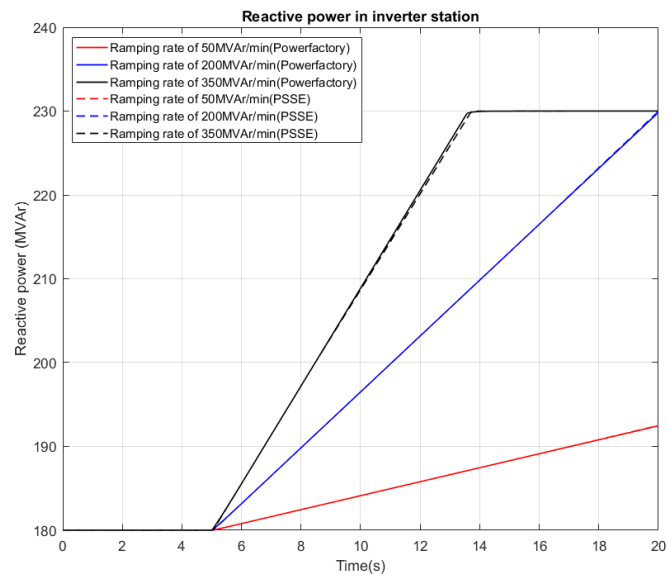


*Figure 70 - Reactive power response for different ramping rates for both models*

The solid line represents the results in the Powerfactory model whereas the dashed line represents the results in the PSSE model. From the above figure, it is obvious, that both models obtain the exact same result for all the different ramping rates.

## 5.5 AC voltage controller performance

The comparison of the AC voltage controller in both models lead to some significant findings. As mentioned in paragraph 4.5, the adjustment of the AC voltage at the point of common coupling is limited. The change of the voltage at the PCC bus must follow the converter's reactive power capability. That is due to the fact that while increasing the voltage at the PCC bus, the reactive power injection of the converter must increase thus the q – axis component of the current must increase. The opposite effect is happening when the voltage is being decreased.

The comparison has shown that the increase or decrease of the voltage by 1% at the PCC bus cannot be satisfied. In the following figures, the reactive power response of the converter while performing the aforementioned cases is evaluated.
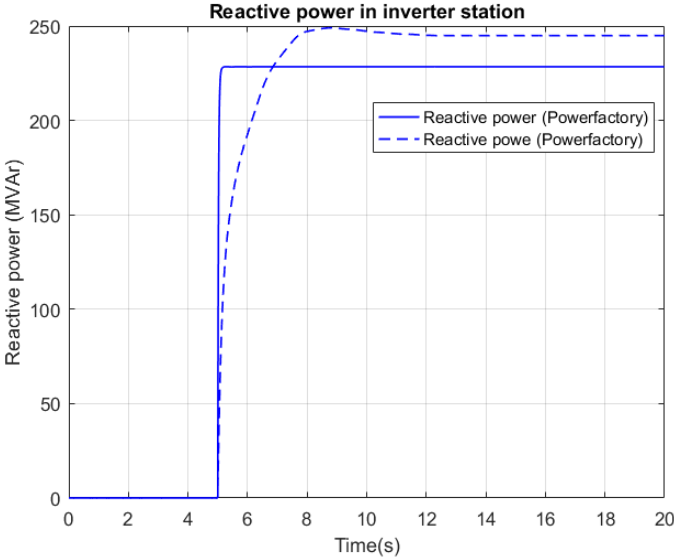


*Figure 71 - Reactive power response while the voltage at the point of common coupling has been increased by 1%*

Despite the fact that the models settle at a different time point, which is a matter of different gains used for the AC voltage controller, the increase of the voltage at the PCC in Figure 71, cannot be satisfied. The dashed line representing the results from the PSSE model, indicate that in order to increase the voltage by 1%, the reactive power capability must be violated, stabilizing around 245 MVAr. On the other hand, the solid line representing the results of the Powerfactory model limits the increment of the voltage until the moment the 230MVAr point has been reached.
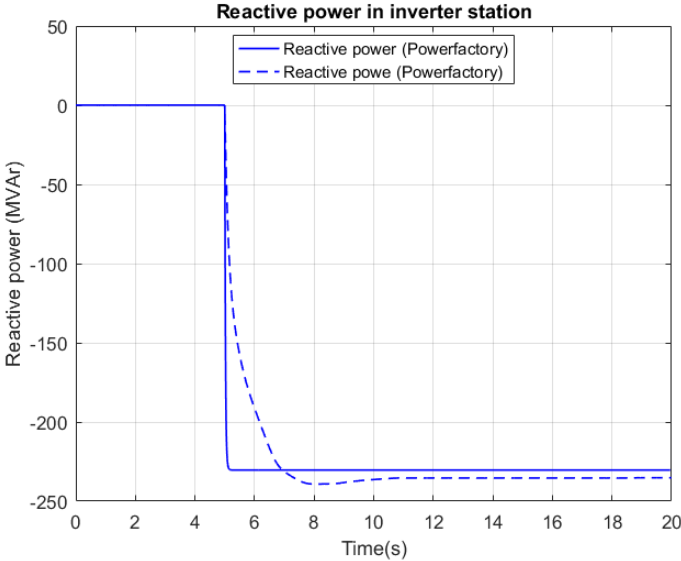


*Figure 72 - Reactive power response while the voltage at the point of common coupling has been decreased by 1%*

The same behavior is being experienced when the voltage at the PCC is being decreased by 1%. The dashed line representing the results from the PSSE model, illustrate that the decrease of the voltage by 1%, results in violating the capabilities of the converter. On the other hand, the solid line representing the results from the Powerfactory model, limit the decrease of the voltage until the point where the 230MVAr limit has been reached. Thus, it can be concluded that both models offer the same information regarding the state of the voltage at the PCC.

## 5.6 Fault ride through capability

Based on the information that was provided in paragraph 3.5.7, the comparison regarding the fault ride through capability of the converter was performed while using equation (3.34), which is the equation suggested by the TSO.
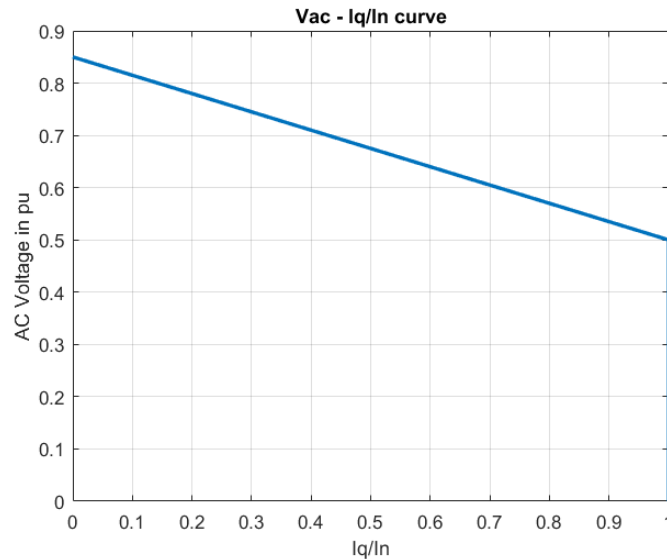


*Figure 73 - FRT equation*

In Figure 73, the behavior of the equation can be observed. It is important to note here that the fault ride through capability is being enabled when the voltage at the PCC is dropped below 0.85 pu. To evaluate the performance of the two models, three phase faults were simulated in three bus located at the 380 kV level. For these cases, the AC voltage at the PCC and the DC voltage response were plotted.
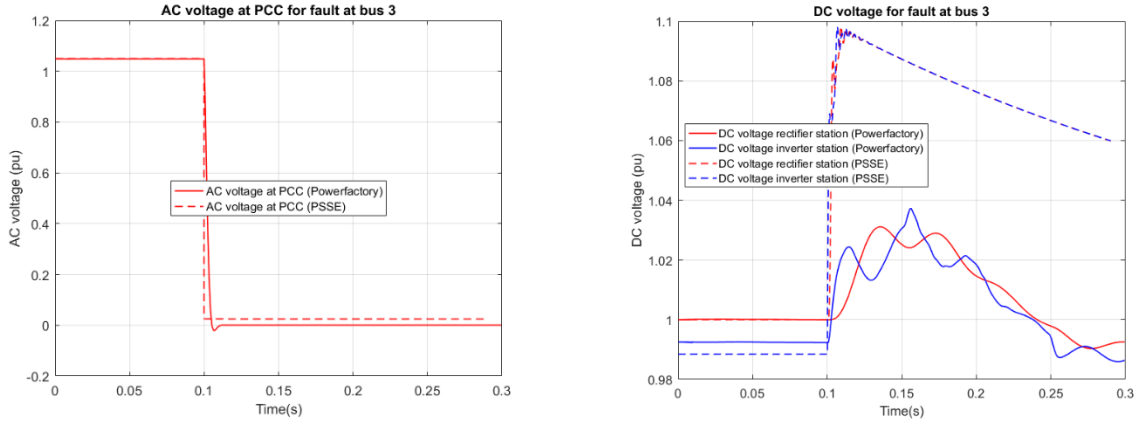
*Figure 74 - Three phase fault at bus 3. (a) AC voltage at PCC and (b) DC voltage response*

The duration of the faults was 200 ms whereas the total simulation time was 0.3 seconds. For a fault at bus 3 (Figure 74), the responses of the two models can be observed. The solid line represents the results of the Powerfactory model whereas the dashed line represents the results of the PSSE model. In Figure 74 (a), the AC voltage at the point of common coupling can be seen. It is clear that the voltage of the PCC bus is almost zero and the contribution of the converter for a fault at bus 3 slightly boosts the voltage. In Figure 74 (b), the DC voltage response of the two models can be observed. The differences can immediately be observed. The response of the Powerfactory model does not create high peaks as the PSSE model which is close to the limits of the DC cable.
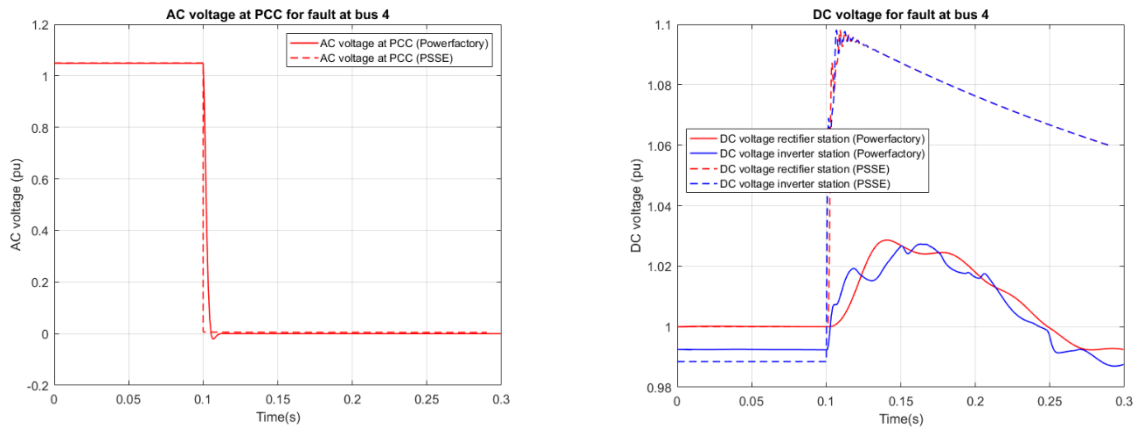


*Figure 75 - Three phase fault at bus 4. (a) AC voltage at PCC and (b) DC voltage response*
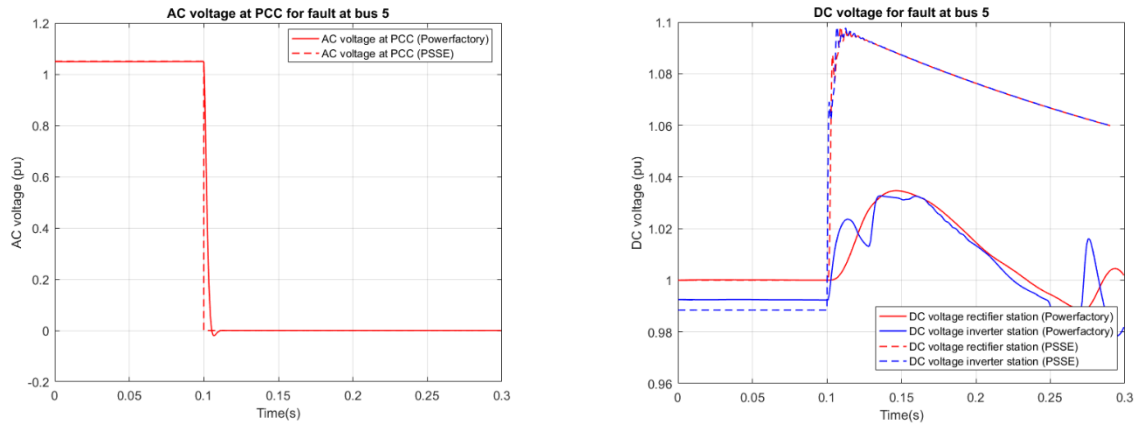
*Figure 76 - Three phase fault at bus 5. (a) AC voltage at PCC and (b) DC voltage response*

The same responses can be observed for faults at buses 4 and 5 respectively. In Figure 75 and Figure 76, the response of the AC voltage at the PCC and DC voltage response of the two models can be seen. The contribution of the converter in both cases is zero to none whereas the DC voltage of the two models have great differences. The response in the Powerfactory model does not create large overvoltages while the model in PSSE is close to the 1.1 pu limit. The reason that the models have these discrepancies in the DC voltage response lies within the performance of the DC voltage controller. The incorrect tuning of the controller plus the reasons that were described previously regarding the inner current control structure and the absence of the energy balance of the DC link create these deviations.

# Chapter 6: General Conclusions and Future Work

## 6.1 General Conclusions

This master thesis project is concerned with two major topics. Firstly, a working RMS model of the COBRA cable project was created in the PSSE software package and the special features regarding the active and reactive power as requested by the TSO were also implemented The response of the controllers and their effect on the AC system in the Dutch region was evaluated. The results were based on a version of the dynamic model of TenneT for the Eemshaven region and upgraded in order to fit the Danish power system as well. The results were obtained in PSSE software package. Changes in operating points of the active power and the reactive power in the inverter station were performed to study the influence in the AC voltages of the buses located in the Dutch power system. Changes in the AC voltage at the point of common coupling were also evaluated. Furthermore, the fault ride through capability, when faults exist in the network was also analyzed.

In addition, a comparison process was initiated to determine whether the two average models, one in Powerfactory and the one in PSSE, will obtain the same results. For that reason the controllers of both models were tested with the same test conditions and the results were compared. The purpose of it was to see if the two models will in the end provide comparable results and if not find the reasons why this is not happening. The main conclusions are presented in this Chapter.

**Conclusions regarding the performance of the controllers**

Concerning the performance of the controllers the main conclusions drawn in this thesis are:

- The active power controller is able to follow the changes of the active power reference with all the ramping rates that are within the COBRA cable project specifications.
- Increasing the active power reference in the inverter station will result in an increase of the AC voltages in the Dutch power system, whereas, a decrease in the active power reference will create the opposite effect.
- The changes in the active power result in changes in d – axis component of the current which again creates a change in the DC voltage. Increasing the active power reference results in a decrease of the DC voltage whereas the decrease of the active power reference results an increase in the DC voltage.
- The changes of the AC voltages and also the changes in the DC voltage depend on the ramping rate that is used each time. A steeper ramping rate can result in steeper effects on the AC and DC voltage values.
- The DREG function can be used on top of the AREG function and can lead into a further increase or decrease of the active power with the maximum possible ramping rate. The use of the DREG function can result in a steeper behavior of the AC voltages and the DC voltage in the DC link.

- As mentioned in Chapter 4, the DREG function can be extend and can be used for multiple applications.
- The differences between the two control modes used to obtain the reference for the q – axis component of the current can be seen from the figures in Chapter 4. The Q control mode, which controls the angle, cannot maintain the voltages of the Dutch system stable. The AC control mode on the other hand is able to control the magnitude of the AC voltage which leads to stable voltages spread across the system regardless the changes in the active power reference.
- The reactive power controller is able to follow the changes of the reactive power reference with all the ramping rates that are within the COBRA cable project specifications.
- The increase or decrease of the reactive power results an increase or decrease of the AC voltages in the Dutch system. An exception can be seen for the buses that they have generators with excitation systems that cannot correctly follow the increase or decrease of the voltage due to lack of the integral part of the excitation system.
- The increase or decrease of the AC voltage at the point of common coupling can lead to the violation of the reactive power capability of the converter and thus there is a limit on how much the AC voltage can be increased or decreased.
- The investigation regarding the fault ride through capability has shown that the use of the equation (3.34) imposed by the TSO performs better than equation (3.35) and thus the converter is able to boost the voltage by increasing its reactive power injection for three faults in the 380 kV buses (3, 4 and 5). The contribution is less when the faults are simulated in the 220 kV buses (6 and 7).

**Conclusions regarding the comparison process**

Concerning the comparison of the two models, the main conclusions drawn are:

- There a lot of differences regarding the modelling approach of the two models. Although, they are both based on [15] for the creation of the P, Q, Uac and Udc control, the inner current control is missing from the PSSE model. Also, the internal energy balance is not modelled in the PSSE model.
- Both models produce almost compatible results regarding the active power controller performance.
- The biggest difference can be observed in the response of the DC voltage controller. Although the rectifier station in the Powerfactory remains constant at 1 pu, the behavior of the rectifier station in the PSSE model is different. When the active power has changed, this change is also depicted in the DC voltage of the rectifier station. The reasons as described above are the absence of the inner current control and also the missing internal energy balance model.
- For the reactive power controller the models offer identical results as it can be seen in Chapter 5.
- Both models, regarding the AC voltage control mode offer the same conclusions. The AC voltage can be increased until a certain point without exceeding the capabilities of the converter.
- The response of the DC voltage during faults is quite different between the two models. In more details, the response of the DC voltage for the Powerfactory model resulted in lower peaks than the ones obtained from the PSSE model.
- Regarding the equation (3.34) suggested by the TSO, the contribution of the converter during three phase faults is minimal.

**Conclusions regarding the implementation of the model**

The implementation of the COBRA cable project in PSSE is the major contribution of this master thesis project. The translation of the control structure of the VSC station from the Powerfactory model in the PSSE model was essential for the creation of the model. Some of the main conclusions regarding the creation of the user – written model in PSSE are the following:

- The block diagrams associated with the control structure of the VSC station are replaced with FORTRAN coding. This means that each block diagram with their respective signals need to be translated and implemented in the FORTRAN code.
- Different time steps add different limitations while using user – written models in PSSE. In this master thesis project, the use of a small time step resulted in having files with enormous data size that cannot be used, whereas the use of a big time step created numerical instabilities that led to unsuccessful simulations.
- Overall, the creation of user – written models requires good knowledge of the software as well as the differential and algebraic equations associated with the model that needs to be created. A lot of time needs to be spent learning about the different modes that are introduced in PSSE modelling and the libraries to be added while creating a FORTRAN based model.
- As mentioned in Chapter 3, there is an interaction between the FORTRAN scripts and the PYTHON scripts that were used in the master thesis project. The PYTHON interface, which is the manager of the simulation process, is responsible for the correct input of the variables, which are essential for the initialization of the VSC script and the DC model script. It can be seen that the use of multiple software was needed to obtain the results presented in Chapter 4 and 5.

## 6.2 Recommendation for future work

In this paragraph, recommendations regarding the continuation of the present thesis are done:

- Special attention can be given in the calculation of the gains for the PI controllers of the converter, since in this master thesis project the gains that were used were obtained through a trial and error process.
- The absence of the inner current control structure and missing model of the internal energy balance creates a huge deviation regarding the DC voltage. Since the inner current control in the current model in PSSE is just a proportional gain that is equal 1, a suggestion would be that the same or a more sophisticated control structure could be modeled for the future iteration of this model. Also, the inclusion of the internal energy balance, by implementing a DC capacitance in the DC side of the VSC station will help erase the deviations created.
- A phase locked loop control structure could also create some added value in the current model. For all the simulations created in the present thesis, the assumption was that the converter station is able to track the voltage at the point of common coupling perfectly. This means that whatever the case might be the converter station is always in synchronization with the grid. For the creation of a frequency controller, the creation of the PLL control structure in PSSE would be of a major importance in order to study frequency deviations.
- Further work is also needed, regarding the extension of the current model for the case of the multi – terminal operation. As stated in Chapter 1, the COBRA cable can be extended in the future for the connection of offshore wind farms in the link. The current model is operational for a point – to

– point connection between the Dutch and Danish side. An investigation regarding the extension of the DC model FORTRAN script that was used in the current thesis is important for the multi – terminal investigation.

- Finally, in the Danish part a simple representation of the system was used in order to simulate the Danish side. A better and bigger representation of the power system of Denmark will also be important in order to improve the accuracy of the results. This will also help expand the current study for the influence of the rectifier station in the power system.

# References

[1]     COBRACABLE, Business Case Description, online available: https://www.tennet.eu/fileadmin/user_upload/Our_Grid/Interconnections/CobraCable/DCI-13-059_-_COBRAcable_Business_Case_-_03-12-2103_-_publieksversie.pdf

[2]     Paulo Chainho, Arjen A. Van der Meer, Madeleine Gibescu and Mart A.M.M. Van der Meijden, "General Modeling of Multi-Terminal VSC-HVDC Systems for Transient Stability Studies," , 2012.

[3]     Dennis A. Woodford. Hvdc transmission. Technical report, Manitoba HVDC Research Centre, 1998.

[4]     Roberto Rudervall, J.P. Charpentier, and Raghuveer Sharma. High voltage direct current (HVDC) transmission systems technology review paper. In Energy Week 2000, 2000.

[5]     L. R. Malesani, L. Tenti, P. Tomasin, P., "AC/DC/AC PWM converter with minimum energy storage in the DC link," in Applied Power Electronics Conference and Exposition, 1993. APEC '93. Conference Proceedings 1993, Eighth Annual, 1993, pp. 306-311.

[6]     N. M. T. Undeland, W. Robbins, Power Electronics: Converters, Applications, and Design, 2003.

[7]     Du, Cuiqing. The control of VSC-HVDC and its use for large industrial power systems. Goteborg :Chalmers University of Technology, 2003. ISSN 1651-4998.

[8]     "High-voltage direct current (HVDC) power transmission using voltage sourced converter (VSC)". IEC/TR 62543:2011.

[9]     Mulugeta, Temesgen. "Control, Dynamics and Operation of Multi-terminal VSC-HVDC Transmission Systems". s.l.: NTNU, 2012. ISSN 1503-8181.

[10]    A. A. van der Meer, J. Rueda-Torres, F. F. da Silva, M. Gibescu and M. A. A. M. van der Meijden, "Computationally efficient transient stability modeling of multi-terminal VSC-HVDC," 2016 IEEE Power and Energy Society General Meeting (PESGM), Boston, MA, 2016, pp. 1-5.

[11]    F.Schettler, H.Huang, and N.Christl. Hvdc transmission systems using voltage sourced converters-design and applications. In IEEE power Engineering Society Summer Meeting, 2000.

[12]    S. Cole and R. Belmans, "A proposal for standard VSC HVDC dynamic models in power system stability studies," Electric Power system Research - Science Direct, 2011.

[13] Nilanjan Ray Chaudhuri, Rajat Majumber, Balarco Chaudhuri and Jiuping Pan , "Stability Analysis of VSC MTDC Grids Connected to Multimachine AC systems," IEEE Transactions on Power Delivery, Vol. 26, NO. 4, October, 2011.

[14] Drik Van Herten and Ronnie Belmans Jef Berteen, "VSC MTDC Systems with a Distributed DC Voltage Conrol - A power Flow Approach," in PowerTech, 2011 IEEE Trondheim , vol., no., pp.1-6, 19-23 June 2011.

[15] CIGRE, "Guide for the Development of Models for HVDC Converters in a HVDC Grid", December 2014

[16] Ndreko, Mario V., Offshore Wind Power Connected to the Dutch Transmission System by VSC-HVDC Networks: Modeling and Stability Analysis, Delft University of Technology, October 2012.

[17] Eduardo Prieto-Araujo, Fernando D, Bianchi, Adria Junyent-Ferre and Oriol Gomis-Bellmunt, "Methodology for Droop Control Dynamic Analysis of Multi-terminal VSC-HVDC Grids for Offshore Wind Farms," *IEEE Transactions on Power delivery, Vol.26, NO 4, October*, 2011.

[18] Paulo Chainho, Arjen A. Van der Meer, Madeleine Gibescu and Mart A.M.M. Van der Meijden, "General Modeling of Multi-Terminal VSC-HVDC Systems for Transient Stability Studies," , 2012.

[19] Siemens PTI, PSSE Operational Manual.

[20] Jef Berteen, Stijn Cole and Ronnie Belmans, "A sequential AC/DC Power Flow Algorithm for Networks containing Multi-terminal VSC- HVDC Systems," in Power and Energy Society General Meeting, 2010 IEEE , vol., no., pp.1-7, 25-29 July 2010.

[21] C. Ismunandur, "Control of Multiterminal VSC-HVDC for Wind Power Intergration ," MSc thesis at TU delft.

[22] ENTSO – E , Network Code on HVDC connections – August 2016, online available: http://eur-lex.europa.eu/legal-content/EN/TXT/PDF/?uri=CELEX:32016R1447&from=EN

[23] T. Kalitjuka, "Control of Voltage Source Converters for Power System Applications", Department of Electric Power Engineering, Norwegian University of Science and Technology, July 2011, Norway.

[24] G. Pinares, L. Bertling-Tjernberg, L. Anh-Tuan, C. Breitholtz, "On the analysis of the dc dynamics of multi-terminal VSC-HVDC systems using small signal modeling", PowerTech, 16–20 Jun. 2013.

[25] Prabha Kundur, *Power System Stability and Control*.: McGraw-Hill Inc.

[26] R. H. Park, "Two-reaction theory of synchronous machines generalized method of analysis-part I," in Transactions of the American Institute of Electrical Engineers, vol. 48, no. 3, pp. 716-727, July 1929.

[27] E. Clarke, Circuit Analysis of AC Power Systems, vol. I, Wiley, New York, 1950.

[28] Imhof, Markus. Voltage Source Converter Based HVDC-Modelling and Coordinated Control to Enhance Power System Stability. Diss. ETH Zurich, 2015.

[29] C. L. Fortescue, "Method of the symmetrical coordinates applied to the solution of poly phase networks," Trans. AIEE, vol. 37, pp. 1027–1140.

[30] J. M. Aller, A. Bueno and T. Paga, "Power system analysis using space-vector transformation," in IEEE Transactions on Power Systems, vol. 17, no. 4, pp. 957-965, Nov 2002.

[31] M. Tsili and S. Papathanassiou, A review of grid code technical requirements for wind farms," IET Renewable Power Generation, vol. 3, no. 3, pp. 308-332, 2009.

[32] L. Zhang, L. Harnefors and H. P. Nee, "Modeling and Control of VSC-HVDC Links Connected to Island Systems," in IEEE Transactions on Power Systems, vol. 26, no. 2, pp. 783-793, May 2011.

# Appendix A: Space vector theory

The approach in space vector theory is dealing with the instantaneous values of the electrical circuit. The basic idea in space vector theory is that the one complex vector y can be represented by three phase variables, if the zero components are disregarded. A complex vector y can be defined as:

$$y^s = \frac{2}{3}(y_a + y_b e^{j\frac{2\pi}{3}} + y_c e^{j\frac{4\pi}{3}}) \quad (A.1)$$

At any moment, the complex vector y has two variables corresponding to the αβ axes, $y_\alpha$ and $y_\beta$ as shown in Figure 77. To perform the transformation of the rotating vector to a non-rotating one, a rotating dq reference frame is introduced. The dq frame rotates in the same direction as the rotating vector y with speed equal to the angular frequency of $\omega_1$ of the AC system. Furthermore, the vector y in the dq reference frame is related to the vector y in the stationary frame by:

$$y^s = e^{j\omega_1 t} y \quad (A.2)$$
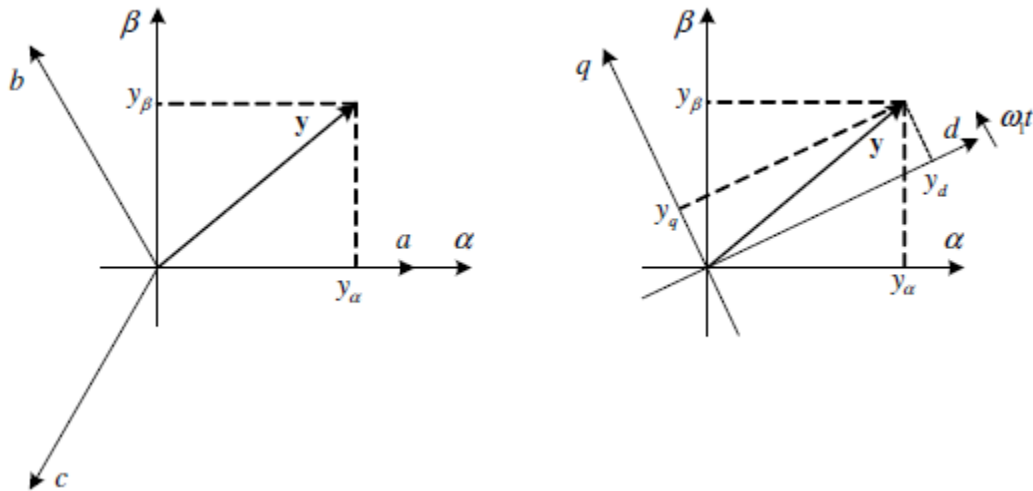


*Figure 77 - Reference frame transformations. (a) abc to αβ and (b) αβ to dq [32]*

To initiate the transformation from the three phase quantities to the dq rotating reference frame a tool was created by Park, called Park's transformation. It is used in the model of the VSC and the VSC controllers in this thesis.

Park's transformation is given by [26]:

$$\begin{bmatrix} x_a \\ x_b \\ x_c \end{bmatrix} = \sqrt{\frac{2}{3}} \begin{bmatrix} \cos\theta & -\sin\theta & \frac{1}{\sqrt{2}} \\ \cos(\theta - \frac{2\pi}{3}) & -\sin(\theta - \frac{2\pi}{3}) & \frac{1}{\sqrt{2}} \\ \cos(\theta + \frac{2\pi}{3}) & -\sin(\theta + \frac{2\pi}{3}) & \frac{1}{\sqrt{2}} \end{bmatrix} \begin{bmatrix} x_d \\ x_q \\ x_0 \end{bmatrix}$$

$$\text{where } P(\theta) = \begin{bmatrix} \cos\theta & -\sin\theta & \frac{1}{\sqrt{2}} \\ \cos(\theta - \frac{2\pi}{3}) & -\sin(\theta - \frac{2\pi}{3}) & \frac{1}{\sqrt{2}} \\ \cos(\theta + \frac{2\pi}{3}) & -\sin(\theta + \frac{2\pi}{3}) & \frac{1}{\sqrt{2}} \end{bmatrix}$$

Or the inverse Park's transformation given by the following matrix [26]:

$$\begin{bmatrix} x_d \\ x_q \\ x_0 \end{bmatrix} = \sqrt{\frac{2}{3}} \begin{bmatrix} \cos\theta & -\sin\theta & \cos(\theta + \frac{2\pi}{3}) \\ -\sin\theta & -\sin(\theta - \frac{2\pi}{3}) & -\sin(\theta + \frac{2\pi}{3}) \\ \frac{1}{\sqrt{2}} & \frac{1}{\sqrt{2}} & \frac{1}{\sqrt{2}} \end{bmatrix} \begin{bmatrix} x_a \\ x_b \\ x_c \end{bmatrix}$$

$$\text{where } P(\theta)^{-1} = \begin{bmatrix} \cos\theta & -\sin\theta & \cos(\theta + \frac{2\pi}{3}) \\ -\sin\theta & -\sin(\theta - \frac{2\pi}{3}) & -\sin(\theta + \frac{2\pi}{3}) \\ \frac{1}{\sqrt{2}} & \frac{1}{\sqrt{2}} & \frac{1}{\sqrt{2}} \end{bmatrix}$$

The equations responsible for the transformation are given below [28]:

$$x_{abc} = P(\theta)x_{dq0}, \ x_{dq0} = P(\theta)^{-1}x_{abc}$$

$$\text{where } P(\theta)^{-1}\frac{d}{dt}P(\theta) = -\omega_s J, \ J = \begin{bmatrix} 0 & 1 & 0 \\ -1 & 0 & 0 \\ 0 & 0 & 0 \end{bmatrix}.$$

# Appendix B: Simulation process

The purpose behind dynamic simulations is to accurately represent the response of a physical system to some event. This means that each component that affects the response of the system must be modelled over the time frame of interest. In PSSE, for each equipment that is being represented in a system, an equivalent model describing the dynamic behavior through the differential equations is supplied.

The model library of PSSE contains a wide variety of models which will satisfy the requirements for a vast majority of equipment. However, there are certain occasions where there is no model library and thus differential equations that can represent a specific equipment. For that reason, PSSE is encouraging user to create their own models in order to accurately represent them into the system.

The purpose of this appendix is to give a better insight on how a user can create models in PSSE and better represent the models that the user desires in each case. This does not mean that a detailed list on how generators, exciters, turbine governors, etc. are created will be given. As it have been mentioned in the previous chapters of this master thesis report, the following software were used: FORTRAN, to create the control functions of VSC stations that are present in the system, PYTHON, which is responsible for the whole simulation process and finally PSSE software itself.

**FORTRAN**

As mentioned, PSSE encourages the users to create user – written models. This can be done by using FORTRAN programming language and creating the user – written models required for specific studies. It is important to note here that no prior knowledge of the FORTRAN language is essential however knowledge regarding how to program is a must.

As explained, each model contained in the PSSE model library is consisted of differential and algebraic equations that actually represent the behavior of the model. In order to create a user – written model it is imperative to know the behavior of the model that needs to be created thus the equations that follow the model. For that reason, PSSE modelling distinguishes different modes that can be used in order to represent the equations of the model. The most important modes are the first three modes that PSSE uses and these will be described here:

- In MODE=1, the initial conditions of the model are being calculated. Depending on the information given by the creator for the model, the initial conditions are being calculated. This mode is only called once during the entire simulation and its outputs are used as inputs for the other MODES.
- In MODE=2, computations required for the differential equations are performed and stored in the DSTATE array. The DSTATE array contains all the information regarding the rate of changes of the STATE variables.
- In MODE=3, the calculation of the STATE variables is performed.

In our case the, the VSC station is modeled as a generator model and takes advantage of several variable associated with the generator model. Variables such as the terminal voltage of the generator, mechanical output of the generator and such are being used in order to store information regarding the VSC station. Moreover, the VSC station script is composed by three MODES, where MODE=1 is being called to calculate the initial conditions of the converter regarding the active power controller and reactive power controller as well as the initial values of the DC and AC voltage controller. Moreover, the initial value of

the DC voltage and the current injection of the converter is being inserted to the script from a different FORTRAN script that contains the information regarding the DC network and cable. When the simulation starts, MODE=2 takes place. In this MODE, the differential equations regarding the calculation of the d – axis and q – axis components of the current. This means that the integral part of the PI controller used in each converter controller is being calculated there and the value is stored in the DSTATE array. Following MODE=2 is MODE=3, which the values of the STATE array are being calculated. In MODE=3, the subroutines that contain the operation of the controllers are being called and the proportional part of the PI controller is being calculated. In the end, the sum of the integral and proportional part of the PI controller of each controller of the converter is being added and the result is the total active and reactive current. The script ends with the calculation of the current injection of the VSC station which is then fed to DC network script which then calculates the DC voltage of the DC grid which is fed to the VSC station script. It is clear that there is a connection between the two FORTRAN scripts.

It is essential that before starting writing the scripts for the models, to install Microsoft Visual Studio 2010, Intel Visual FORTRAN Compiler version 12.1.258 and all the linkers essential for these software (C/C++). Moreover, PSSE version 33, should be installed in the same computer as the previous software. In these case the program that is responsible for the creation of the dynamic link library, the PSSE environment manager, which contains the information regarding the VSC station and the DC network model can be implemented in the PSSE software.


**PYTHON**

For the simulation to start, parameters regarding the VSC stations need to be defined. For that purpose an excel file called *dcNetList.xls* was created. Inside the excel file variables regarding the structure of the DC system, for example, the DC voltage, the number of buses inside the DC grid and also the resistance, impedance and capacitance of the system. Moreover, this file contains all the dynamic data for the VSC stations that are used inside the FORTRAN scrips. However, in order to appropriately use this excel file a PYTHON script called *excelIO.py* containing the required information of how each cell is associated with each variable is created. If there is something that needs to be added regarding the parameters of the VSC station three things must be done: firstly, add the new variable in *dcNetList.xls*, secondly, update the *excelIO.py* script and lastly update the *dyrWriter.py* script. The *dyrWriter.py* script, contains the information regarding the number of variables that will be used from the PSSE software associated with the user – written model. This script is also responsible for the creation of the .dyr file which contains all the required dynamic information about the user – written models of the VSC station and the DC network model.

Moreover, a script that is responsible for the dynamic events that are taking place in the system called *PSSEprocess.py* is created. The operation of the extra features like AREG, DREG or the change in reference of the active or reactive power can be done by manipulating the variables associated with these values. Finally, the script called *excel2dyr.py*, contains the information regarding the whole simulation process that is from the creation of the .dyr file containing the dynamic data for the user – written models, running the dynamic events and in the end storing the simulation data.

The PYTHON software is the most crucial part for this simulation process. In order to use the PYTHON scripts discussed here, the PYTHON software needs to be installed in the computer that will be used.

Additionally, the packages related to the use of several functions located in the PYTHON scripts need to be installed.


**MATLAB**

As mentioned in the previous paragraph, the PYTHON script *excel2dyr.py* is responsible for the creation of the files that contain the simulation data. These files are then processed through the MATLAB simulation software with a script called *plot_results.m,* so that the results can be plotted in a more manageable environment. The use of these three software alongside PSSE simulation software that was used to create the case study, were utilized throughout this master thesis project. The results can be observed in Chapter 4 and Chapter 5.